Higher Order Corrections to Vector Boson Scattering at Small Scattering Angles

Dissertation
zur Erlangung des Doktorgrades
des Fachbereichs Physik
der Universität Hamburg

vorgelegt von
Krisztian Peters
aus Budapest

Hamburg
2004

Gutachter der Dissertation:	Prof. Dr. J. Bartels Prof. Dr. B. Kniehl
Gutachter der Disputation:	Prof. Dr. J. Bartels Prof. Dr. P. Zerwas
Datum der Disputation:	6. Juli 2004
Vorsitzender des Prüfungsausschusses:	Prof. Dr. G. Mack
Vorsitzender des Promotionsausschusses:	Prof. Dr. R. Wiesendanger
Dekan des Fachbereichs Physik:	Prof. Dr. G. Huber

Abstract

In the following thesis we investigate higher order corrections to electroweak vector boson scattering. These are resummed QCD and electroweak corrections at small scattering angles. QCD corrections are present since, from the perturbative analysis, the vector bosons may dissociate into quark-antiquark pairs giving rise to colour dipoles. These dipoles interact through gluon exchanges. This investigation involves the computation of the nonforward impact factors and wave functions in the dipole formalism, where we give a physical interpretation as well. We present expressions for the lowest order QCD scattering amplitude and for the leading logarithmic BFKL amplitude. Particularly we discuss numerical results for the process $\gamma\gamma \to ZZ$. We estimate QCD corrections to the cross section resulting from the interference with the electroweak ones. These are from the leading log BFKL amplitude of the order of a few percent close to the forward region already at the 1 TeV energy range and rise with the scattering energy. We also consider the helicity non-conserving cases in which the QCD corrections relative to the electroweak part of the amplitude strongly rise with energy. In the second part of the thesis we start a resummation programme for leading logarithms in the electroweak sector at small scattering angles. The first step is the decomposition of leading log electroweak contributions in terms of t-channel isospin states up to the two loop level. We establish an integral equation which resums the neutral isospin-1 contributions to all orders and fulfil a certain bootstrap relation showing the self-consistency of our investigations. We found three Regge trajectories accounting for the theory, beside the W boson trajectories a third one for the neutral channel emerging due to an appropriate mixing of photon and Z boson states.

Zusammenfassung

In der vorliegenden Arbeit werden Korrekturen höherer Ordnung für Vektorboson Streuung untersucht. Diese sind resummierte QCD und elektroschwache Korrekturen bei kleinen Streuwinkeln. QDC Beiträge entstehen indem Vektorbosonen in ein Quark-Antiquark Paar dissoziieren. Diese Dipole wechselwirken anschliessend durch Austausch von Gluonen. Diese Untersuchung beinhaltet die Berechnung der Impact-Faktoren und Wellenfunktionen in nicht-forwärts Richtung im Dipolformalismus. Ausdrücke für den Beitrag niedrigster Ordnung und für die Leading-Log-BFKL-Amplitude werden präsentiert. Insbesondere werden numerische Resultate für den Prozess $\gamma\gamma \to ZZ$ diskutiert. Korrekturen resultierend aus der Leading-Log-BFKL-Amplitude sind bereits bei Energien von 1 TeV im Prozentbereich zu finden und sie steigen mit der Energie. Im zweiten Teil der Arbeit beginnen wir ein Resummationsprogramm führender Logarithmen im elektroschwachen Sektor bei kleinen Streuwinkeln. Der erste Schritt war die Zerlegung der Leading-Log elektroschwachen Beiträge nach t-Kanal Isospin Zuständen bis zur Zwei-Loop-Ordnung. Wir leiteten eine Integralgleichung her, die die neutralen Isospin-1 Beiträge zu allen Ordnungen aufsummiert und einem Bootstrap Schema genügt. Diese Bootstrap Gleichung zeigt die Selbstkonsistenz unserer Rechnung. Wir haben drei Regge Trajektorien gefunden, neben dem W-Boson Trajektorien eine dritte im neutralen Kanal, die aufgrund der richtigen Mischung von Photon und Z-Boson Zuständen entsteht.

Contents

Introduction **7**

1 Z-pair production via photon fusion **15**

1.1 Born contribution 15

1.2 Two loop corrections in the high-energy approximation 22

1.2.1 Virtual corrections 22

1.2.2 Real corrections 24

1.2.3 Summary of section 1.2 29

2 QCD corrections **30**

2.1 Dipole picture in the nonforward direction 30

2.1.1 Nonforward impact factors 30

2.1.2 Formulation in the coordinate space 35

2.1.3 Impact parameter 38

2.1.4 Nonforward dipole-proton scattering amplitude 41

2.1.5 Open quark-antiquark production 42

2.1.6 Summary of section 2.1 44

2.2 Leading log (BFKL) contribution 45

2.2.1 Review of the LO BFKL equation 45

2.2.2 The LO BFKL amplitude 48

2.2.3 Summary of section 2.2 52

2.3 QCD corrections to $\gamma\gamma \to ZZ$ 53

2.3.1 Impact factors 53

2.3.2 Numerical results 57

2.3.3 Summary of section 2.3 69

3 Electroweak amplitudes to all orders **70**

3.1 Elastic amplitudes in order g^2 and g^4 71

3.2 Elastic amplitudes in order g^6 73

3.2.1 The two particle intermediate state 73

3.2.2 The three particle intermediate state 74

3.3 Decomposition into t-channel isospin states 77

3.3.1 Isospin-1 t-channel states 77

3.3.2 Bootstrap condition for the neutral isospin-1 channel . . . 84

3.3.3 The isospin-2 t-channel states 87

3.3.4 The t-channel exchange of vacuum quantum numbers . . 90

3.4 Summary of chapter 3 91

Summary and outlook **92**

Bibliography **97**

Introduction

The search for physics beyond the Standard Model (SM) and the determination of the crucial and still not understood mechanism of the electroweak symmetry breaking in the SM itself are major subjects of investigation in particle physics. It is hoped to increase the understanding with the help of the next generation of supercolliders, and major efforts in this direction are currently being made. Experimentally, we expect the first data and insights concerning these questions after the run of the Large Hadron Collider (LHC). Complementary, high precision measurements will come from the Next Linear Collider (NLC) e.g. TESLA, which are considered to be of great importance. Next Linear Collider is a generic name for a e^+e^- machine operating in the energy regime up to 1 TeV, providing a very clean environment, and making observables available for many processes at an accuracy better than the percent level. In addition one may have the capability of running the NLC in a $\gamma\gamma$ collision mode via Compton backscattering of laser photons off the linear collider electrons. Apart from the advantage of the higher luminosity, the energy of the initial photons can be determined more accurately than the energy of photons radiated in the e^+e^- collider mode.

The NLC may not cover the energy region where the properties of a new, more fundamental theory are directly measurable. However, through precision measurements it provides a window to non-accessible energy regimes in the sense that derivations from precision measurement can be interpreted as signals of new physics. This is the main reason, why we have to know the Standard Model cross sections also from the theoretical side as precisely as possible. The new supercolliders access energy regimes, where perturbative calculations to finite loop orders may not be adequate enough anymore. In this case one needs a certain procedure to resum the main contributions to all orders of perturbation theory.

One of the important processes one will consider in a linear collider is the scattering of vector bosons. Indeed, at the NLC the electron and positron bunches can radiate vector bosons which interact thereafter. Diverse scenarios are considered also in the Compton collider mode. Each incoming photon may turn into a virtual WW pair, followed by the scattering of one W of each pair to end with WW or ZZ states [1]. There are also the processes where initial photons scatter directly into arbitrary vector bosons.

One of the important questions one may pose while searching for new physics is the existence of anomalous triple and quartic vector boson couplings [2] or vector boson Higgs couplings [3]. These anomalous couplings affect vector boson scattering and appear in the corresponding cross sections. Contact interactions are regarded as a possible extension of the SM, which can be well investigated with vector boson scattering [2]. The natural order of magnitude of the anomalous couplings [4], however, is small and, in order to extract them, one needs to both measure and compute theoretically the SM cross sections with a precision better than 1%. In order to get a detailed understanding of the spin structure of anomalous couplings, it is important to investigate the different helicity states of the incoming and outgoing bosons as well.

Concerning the search of physics beyond the Standard Model, the fact that the first perturbative contribution starts at one loop makes especially the process $\gamma\gamma \to ZZ$ sensitive to a number of investigations. Apart from the search for anomalous couplings this process is sensitive also to particles and new physics phenomena contributing through radiative corrections [5], because of the absence of the tree level contribution. This leads to a method independent of and complementary to the direct production of new particles. Again, high precision of the Standard Model cross section is needed. In addition, the production of $Z_L Z_L$ pairs is well suited for the study of a hypothetical ultra heavy fourth fermion generation [6]. Furthermore, the detection of CP violating phases [7] or effects due to the exchange of Kaluza-Klein gravitons in large extra dimension scenarios [8] have been discussed.

Open questions about the nature of the symmetry breaking mechanism can be studied with quasi-elastic scattering of longitudinal vector bosons. Since the longitudinal modes of the massive vector bosons reflect the nature of the Goldstone modes of the unbroken theory, these will give important informations about the nature of electroweak symmetry breaking. In order to preserve partial wave unitarity two possible scenarios can occur. Either the symmetry is broken via the Higgs mechanism and the corresponding scalar particle will be discovered, or the vector bosons have to interact strongly at TeV scales, in the sense that perturbation theory will fail to be a reliable representation of these physics phenomena [9]. Attributes of a strongly coupled theory would emerge, such as resonances of intermediate vector bosons, multiple production of vector bosons, etc. In the latter scenario the vector boson scattering will be one of the key processes to be studied in the nearest future.

Processes where the s-channel helicity is not conserved, for example $\gamma\gamma \to ZZ$, are also sensitive to the Higgs sector. At high energies the biggest contribution to the cross section comes from the production of transverse polarised Z bosons in the kinematical limit of small scattering angles (helicity conserving channel). The dominant contribution to the scattering amplitudes is due to boson loops and grows proportionally to the scattering energy s. Compared to these leading contributions, the diagrams containing the Higgs contribution are suppressed by s^2. In contrast to this, in the production of longitudinal Z bosons the Higgs plays a crucial role. In this channel, both the Higgs contribution and

the W loop are constant in s (up to powers of logarithms). For large Higgs masses the s-channel Higgs exchange in the scattering amplitude of $\gamma\gamma \to Z_L Z_L$ violates partial-wave unitarity [10, 11] and makes this helicity non-conserving case sensitive to the Higgs sector. Therefore we need to know the SM cross section with a high precision in order to disentangle different symmetry breaking scenarios.

In summary, vector boson scattering processes may be seen as a central tool to probe physics beyond the SM and to reveal the nature of symmetry breaking. In order to exploit these features, high precision is needed, both on experimental and on theoretical side. Calculations of these processes at the lowest available order may not be accurate enough. One loop corrections have been calculated for all those vector bosonic processes [12] where a tree level contribution is present. For the $\gamma\gamma \to ZZ$ process, which starts at one loop in α_{EW}, no higher order corrections are available yet. The question naturally arises, if this accuracy is high enough to disentangle new physics from the SM, providing a window to non-accessible energy regimes.

The goal of this thesis is the computation of resummed higher-order corrections to vector boson scattering at small scattering angles. The main contribution to the electroweak cross section of $VV \to VV$ (with $V = W, Z, \gamma$) comes from the helicity conserving part of the amplitude at small scattering angles. With rising scattering energy the helicity conserving Born cross sections approach a constant. This contribution comes from diagrams where only spin-1 particles are exchanged in the t-channel. At leading order and $O(\alpha_{EW}^2)$ these exchanged particles are electroweak vector bosons.

At the one loop level as well as for higher orders the main contribution still comes from the t-channel exchange of spin-1 particles. These higher loop corrections in the high-energy approximation can be obtained by taking into account only this t-channel spin-1 exchange. Using s-channel unitarity conditions further simplifies the calculation. In this thesis we will compute higher order corrections to $\gamma\gamma \to ZZ$ at small scattering angles. The calculation of two loop electroweak corrections in the leading logarithmic approximation is giving corrections of the order of 10% in the 1 TeV energy regime.

Because of the stronger coupling of α_s it is natural to ask if QCD could play a role in vector boson scattering processes. For the QCD corrections a configuration arises which is similar to the above described leading order electroweak corrections. The spin-1 t-channel exchanged particles are now gluons instead of the electroweak bosons. The first gluonic contributions, which arise at the two loop level, are suppressed since these gluons are always accompanied by fermions in the t-channel. The non-suppressed QCD contributions occur at the three loop level. These emerge when the vector bosons fluctuate into a quark-antiquark pair and these dipoles interact through gluons. At the lowest order, when two gluons are exchanged in the t-channel, one obtains a contribution constant in energy. However, at higher energies more and more soft gluons are emitted, thus generating large logarithms in the energy making the QCD ampli-

tude rising with the scattering energy. These contributions cannot be neglected at large energies. The extreme attitude is to consider a resummation described by the leading order BFKL equation [13] which gives an upper bound estimate of these effects. The processes of electroweak vector boson scattering receive their biggest contribution from the same kinematical regime where these QCD effects emerge, thus these corrections have to be estimated.

In this perturbative picture, where the vector boson fluctuates into a colour dipole, the electroweak vector bosons become strongly interacting particles through a gluonic interaction of the quark-antiquark pairs. The first step of the calculation of the QCD corrections is thus the calculation of these dipoles. This colour dipole picture [14,15] is well known from deep inelastic scattering at small x and has turned out to be very useful in describing the transition from pQCD to nonperturbative strong interactions at low Q^2. In a first sequence of attempts models for the dipole cross section have been formulated in order to describe the interaction between the quark-antiquark pair and the proton in the forward direction [16–20]. Equivalently, in these models the interaction is integrated over the full region of impact parameter b. It seems natural to understand the dipole picture at nonzero momentum transfer as well, and then to search for models for the dipole cross section which depend upon the impact parameter b. Thus an investigation of the non-forward boson impact factors is important for many aspects.

First calculations of the photon impact factor for real photons in the non-forward direction have been presented rather long time ago [21,22]. The results have been obtained in momentum space, but at that time no attempt has been made to find an interpretation in terms of the photon wave function and a dipole cross section. More recently, the non-forward photon impact factor to an off-shell incoming and real outgoing photon with massless quarks has been given in [23, 24], and in [25, 26] the non-forward diffractive production of a vector particle has been analysed. Finally, in [27] the non-forward diffractive production of a (massive) quark-antiquark pair has been studied, but the result has not been presented in a form which is convenient for the colour dipole picture analysis mentioned above.

In this thesis an analysis of the non-forward boson impact factor is presented for all boson helicities and virtualities, using massive quarks and the general kinematic $V(Q_+^2) \to V(Q_-^2)$. The result is written in the form of the colour dipole picture: (boson wave function)·(colour dipole cross section)·(boson wave function). We find the form of the (non-forward) boson wave function and of the dipole cross section, and we give a physical interpretation in the infinite momentum frame. Transforming to impact parameter, the dipole cross section will be shown to depend upon the distance between one of the quarks of the colour dipole and the target. For open quark antiquark production we show that the integrated diffractive cross section can be expressed in terms of the same non-forward dipole cross section as the elastic $V \to V$ scattering amplitude.

After the calculation of the non-forward impact factors we investigate the two

gluon exchange amplitude, which is the first non-suppressed QCD correction to electroweak vector boson scattering. Next we consider the resummed contributions. A resummation of leading logarithms to all orders was calculated in [13] for quark-quark scattering, and due to the high-energy factorisation one can make use of this result. The quark impact factors have to be replaced by the boson impact factors. By integrating the BFKL kernel with the boson impact factors one obtains the resummed amplitude in the leading logarithmic approximation.

In order to give numerical estimates, we concentrate on the definite process of $\gamma\gamma \to ZZ$. At the gamma collider it will be measurable with a higher accuracy than the processes where the bosons are radiated from the electrons. We calculate leading log QCD corrections to this process at small scattering angles. For the helicity conserving case it turns out that QCD corrections in the region of about 1 TeV are at the percent level and grow moderately with energy. For the helicity breaking channel the QCD corrections to the differential cross section are of the same order at about 1 TeV, but they grow much faster with increasing energy. This growth is due to the fact that the electroweak part of the helicity breaking cross sections is (up to logarithms) suppressed by one power of s compared with the QCD ones. Our result suggests that particularly in the small angle region, possible deviations from EW calculations cannot be interpreted as signals of new physics without taking into account the QCD corrections.

Of course a similar resummation of leading logarithmic contributions to all orders can be done for the electroweak sector as well. We expect that most of the characteristics of the QCD result will be recovered, especially the rise of the cross section with energy, due to the radiation of soft electroweak bosons. Clearly, this rise will be less distinctive, since the magnitude of the weak coupling is smaller than the magnitude of the strong one and the effect of the resummation to all orders will be hardly visible at the NLC. However once it is obtained, one can easily expand the result to a given order needed for a certain energy. Finally, at energies of several TeV, e.g. at CLIC or ultrahigh-energy neutrino interactions, such a resummation will play a similar role like it does in the QCD sector at present collider energies.

A resummation of leading logarithms in a spontaneously broken $SU(2)$ theory has been calculated in [13, 28]. These resummed contributions are obtained from diagrams with ladder-like topology built with reggeized (non-elementary) vector bosons. Consequently, the reggeization of particles is a crucial point for the resummation of the theory. A particle it is said to reggeize when, if its quantum numbers are exchanged in the t-channel, the propagator in the high-energy limit behaves like the center–of–mass energy to some t dependent power. The exchange of an elementary particle would correspond to a special term in scattering amplitudes describing scattering at its particular value of angular momentum. However, it was shown that radiative corrections to the exchange of the particle quantum numbers can turn fixed singularities into moving Regge trajectories [29]. This is equivalent to the description of manifestly composite

systems, thus particles lying on Regge trajectories are made up of one another with dynamically calculable ratios and coupling constants.

In the electroweak sector the gauge group is a direct product of the abelian and non-abelian groups $SU(2) \times U(1)$. It was shown that in an abelian gauge theory like Quantum Electrodynamics the vector particle remains elementary [30]. On the other hand the $SU(2)$ Yang-Mills vector meson reggeizes [13, 28] in non-abelian gauge theories with spontaneously broken symmetries mediated by the Higgs mechanism. The according mechanism of reggeization in the electroweak sector is not a priori clear. Based on a tree level investigation it was suggested that there should be a trajectory in the charge-zero sector of the theory which does not pass through the photon or Z boson states [31]. This suggestion was confirmed up to sixth perturbative order for general gauge groups in the case of broken symmetries with abelian content [32]. It was concluded that in the case of trajectories which cannot be associated with physical particles simultaneously fixed pole terms appear which cancel the contribution of such trajectories at $J = 1$ [32].

In the second part of this thesis we start a resummation program for the electroweak sector of the Standard Model. The first step is the perturbative calculation of leading electroweak amplitudes up to the sixth order of perturbation theory. We decompose these amplitudes to all possible t-channel isospin states. Projections to the quantum numbers of the vector bosons embedded in the theory are equivalent to the projections of the isospin-1 t-channel states. The results of our calculation to sixth order of perturbation theory of the isospin-1 channels confirm the finding of [32]. We worked out the reggeization in the Standard Model explicitly. From this it can be concluded that the charged $W^{\pm}$ bosons are reggeizing, and the combination of the photon and Z boson also leads to a reggeized particle, reflecting the quantum numbers of the neutral boson W^3 of $SU(2)$ theory before the electroweak mixing. The theory contains three Regge trajectories merging at the W mass. Two are due to reggeized W bosons and the third one corresponds to the neutral channel and cannot be associated with a neutral physical vector boson in agreement with [31,32]. This trajectory emerges only with the appropriate mixing between the Z boson and photon.

The exsistence of a Regge trajectory, suggested by calculations of sixth order, can be proved to all orders with the use of a certain bootstrap scheme. This bootstrap scheme is a non-linear relation which follows from S-matrix unitarity. It was shown in $SU(2)$ theory that, with the implementation of reggeized t-channel propagators and a Bethe-Salpeter equation, contributions can be resummed to all orders [13]. Following this result we formulate an integral equation for the neutral isospin-1 t-channel state of the elctroweak sector. The solution of this equation, i.e. the infinite sum of the corresponding isospin-1 amplitudes, gives the propagator of the neutral reggeized particle itself. With this result we proved the reggeization in the neutral channel to all orders in perturbation theory in a non-trivial way. This bootstrap scheme shows the self-consistency of the perturbative calculation and confirm the conjecture of the

resummation to all orders.

In our perturbative calculation we computed the projections to the vacuum and the isospin-2 t-channels up to the sixth order as well. The former will be particularly important, since the main contribution in the high-energy asymptotics will come from the vacuum channel. Based on this calculation it will be possible to iterate the result of every isospin t-channel state up to any orders of perturbation theory in the leading logarithmic approximation. In order to do this, one has to derive the integral equations for all t-channel isospin states. Our two loop calculations provide the kernel of these integral equations. In this way the whole resummation program, which is well known for QCD, is formulated for the electroweak theory as well. For example deriving the integral equation in the vacuum channel will lead to the electroweak analogue of the famous BFKL equation [13], which has been the subject of an intense study with its various applications in QCD over many years.

The thesis will be organised as follows. We first calculate the exact one loop contribution of $\gamma\gamma \to ZZ$. The electroweak part of the amplitude was first computed in a full one loop calculation by Jikia [33] for Higgs masses over 300 GeV. In order to compute the interference term with the QCD contributions, we reproduce the results of [33], however, in this thesis we use an up to date value of the top quark mass and a Higgs mass of $m_H = 115$ GeV. We compare this one loop calculation with the one which we compute in the high-energy approximation. The result shows that the high-energy approximation is quite accurate. We compute the electroweak two loop corrections in the high-energy approximation as well. We present a numerical analysis of this two loop correction.

In Chapter 2 we calculate the QCD corrections to electroweak vector boson scattering at small angles. We first (Section 2.1.1) calculate, in momentum space, the high energy behaviour of the elastic scattering process $V+V \to V+V$ in lowest order QCD. This calculation contains mainly the computation of the non-forward boson impact factors. Next (Section 2.2) the cross section of the resummed gluonic contribution is presented, i.e. the BFKL amplitude. The impact factors are further evaluated for the process $\gamma\gamma \to ZZ$ and integrated with the BFKL kernel. This Chapter concludes with a detailed numerical study of the QCD corrections.

As a sideline of the computations we discuss the dipol cross section formula in the non-forward direction. The resulting formula on the non-forward boson impact factor which, when transformed to transverse coordinate space, leads to the photon wave function and to the non-forward dipole scattering amplitude (Section 2.1.2). The transformation to impact parameter is done in Section 2.1.3, and a physical interpretation is given in the infinite momentum frame. Section 2.1.4 briefly describes the non-forward dipole formula for Vp scattering, and in Section 2.1.6 we present the formula for open quark-antiquark production.

In Chapter 3 we begin with the resummation program for the electroweak sector. First we calculate general expressions, the ingredients for further investigations, to the order of g^4 (Section 3.1) and g^6 (Section 3.2). The higher order contributions can be divided into real and virtual corrections. Next, we decompose the electroweak contributions into t-channel isospin states (Section 3.3). For the isospin-1 channels the result begins to exponentiate and we make a conjecture how the result develops to any order. We formulate an intagral equation for the neutral isospin-1 channel and investigate the corresponding bootstrap scheme. Finally we give a brief summary and an outlook to future research work that is related or is based on the results of this thesis.

Chapter 1

Z-pair production via photon fusion

We tried to keep the expressions about higher order corrections in the following thesis as general as possible, but in order to make numerical estimates we need to concentrate on a definite process. This will be Z-pair production via photon fusion. Since the biggest part for the corrections comes from the interference term, we need to compute also the electroweak amplitude. The result of this pure electroweak contribution contains some general features of vector boson scattering which we will discuss as well.

1.1 Born contribution

The perturbative expansion of the process:

$$\gamma(p_1) + \gamma(p_2) \to Z(p_3) + Z(p_4) \tag{1.1}$$

starts at one loop. The Born amplitude was first computed in a full one loop calculation by Jikia [33] for Higgs masses over 300 GeV. In order to compute the interference with the QCD part of the amplitude we reproduce the results of [33], however, we used in this thesis an up to date value of the top quark mass and a Higgs mass of $m_H = 115$ GeV.

The imaginary parts of the helicity conserving amplitudes in the high-energy limit at $\theta = 0$ can be calculated via unitarity relations from the helicity amplitudes of $\gamma\gamma \to WW$ [34]:

$$\operatorname{Im} A_{++++}(\theta = 0) = \operatorname{Im} A_{+-+-}(\theta = 0) = s\,\frac{g^4 c_w^2 s_w^2}{2\pi M_W^2}\,, \tag{1.2}$$

where we introduced the weak coupling as: $g^2 = 4\pi\alpha_{em}/s_w^2$. This rising amplitudes lead to nondecreasing helicity conserving cross sections in the limit

$s \to \infty$ and t fixed (Regge limit). Later it will become clear that the corresponding real parts have no contributions proportional to s, because the leading s contribution from the s-channel discontinuity is completely cancelled by the u-channel discontinuity in the high-energy approximation. At small scattering angles this main contribution to the amplitude comes from the bosonic loop of the helicity conserving channel. For the helicity flip channels no contributions proportional to s survive, thus these amplitudes are suppressed by one power of s compared to the helicity conserving cases. If one of the Z bosons has transverse and the other longitudinal polarisation, the amplitude vanishes at the forward point (exchanged transverse momenta $p_T = 0$) due to angular momentum conservation.

The momenta and polarisation vectors for different helicities in the CMS of the initial photons are given by:

$$
\begin{aligned}
k_1 &= E\,(1;0,0,1) & \qquad k_2 &= E\,(1;0,0,-1)\\
\epsilon_1^{\pm} &= \frac{1}{\sqrt{2}}\,(0;1,\pm i,0) & \qquad \epsilon_2^{\pm} &= \frac{1}{\sqrt{2}}\,(0;1,\mp i,0)\\
k_3 &= E\,(1;\beta\sin\theta,0,\beta\cos\theta) & \qquad k_4 &= E\,(1;-\beta\sin\theta,0,-\beta\cos\theta)\\
\epsilon_3^{0*} &= \frac{E}{M_Z^2}\,(\beta;\sin\theta,0,\cos\theta) & \qquad \epsilon_4^{0*} &= \frac{E}{M_Z^2}\,(\beta;-\sin\theta,0,-\cos\theta)\\
\epsilon_3^{\pm *} &= \frac{1}{\sqrt{2}}\,(0,\cos\theta,\mp i,-\sin\theta) & \qquad \epsilon_4^{\pm *} &= \frac{1}{\sqrt{2}}\,(0,\cos\theta,\pm i,-\sin\theta)
\end{aligned}
$$

where β is defined as $\beta = \sqrt{1-4M_Z^2/s}$ with s being the square of the centre of mass energy E and θ is the scattering angle in the s-channel. The Feynman diagrams were generated with *FeynArts* [35] and the resulting amplitudes were algebraically simplified using *FormCalc* [36]. To evaluate the one-loop integrals the package *LoopTools* [36, 37] was used. Explicit expressions for the bosonic and fermionic helicity amplitudes can be found in [33] and [38] respectively.

The result of the numerical computations for the integrated cross section is displayed in Fig. 1.1. The cross sections are plotted for the extreme cases when both of the incoming photons have full circular polarisations $\lambda_{\gamma 1} = \lambda_{\gamma 2} = +1$. The mass of the Higgs boson was set to $m_H = 115$ GeV unless a different value is stated and the parameters $\alpha_W = \alpha/s_W^2$, $\alpha = 1/128$, $m_Z = 91.2$ GeV, $m_t = 174.3$ GeV and $\alpha_s(M_Z)$ have been used in the numerical computations. Fig. 1.1(a) is the integrated cross section for the production of two longitudinal Z bosons. This part of the cross section is sensitive to the mass of the Higgs boson. With rising Higgs mass the cross section for the production of longitudinal Z bosons is rising, until a critical value of the Higgs mass about 1.2 TeV is reached. Above this critical value of the Higgs mass we expect a breakdown of perturbation theory, in order to preserve partial wave unitarity [9]. The upper curves correspond to the results with $M_H = 800$ GeV and in the lower curves

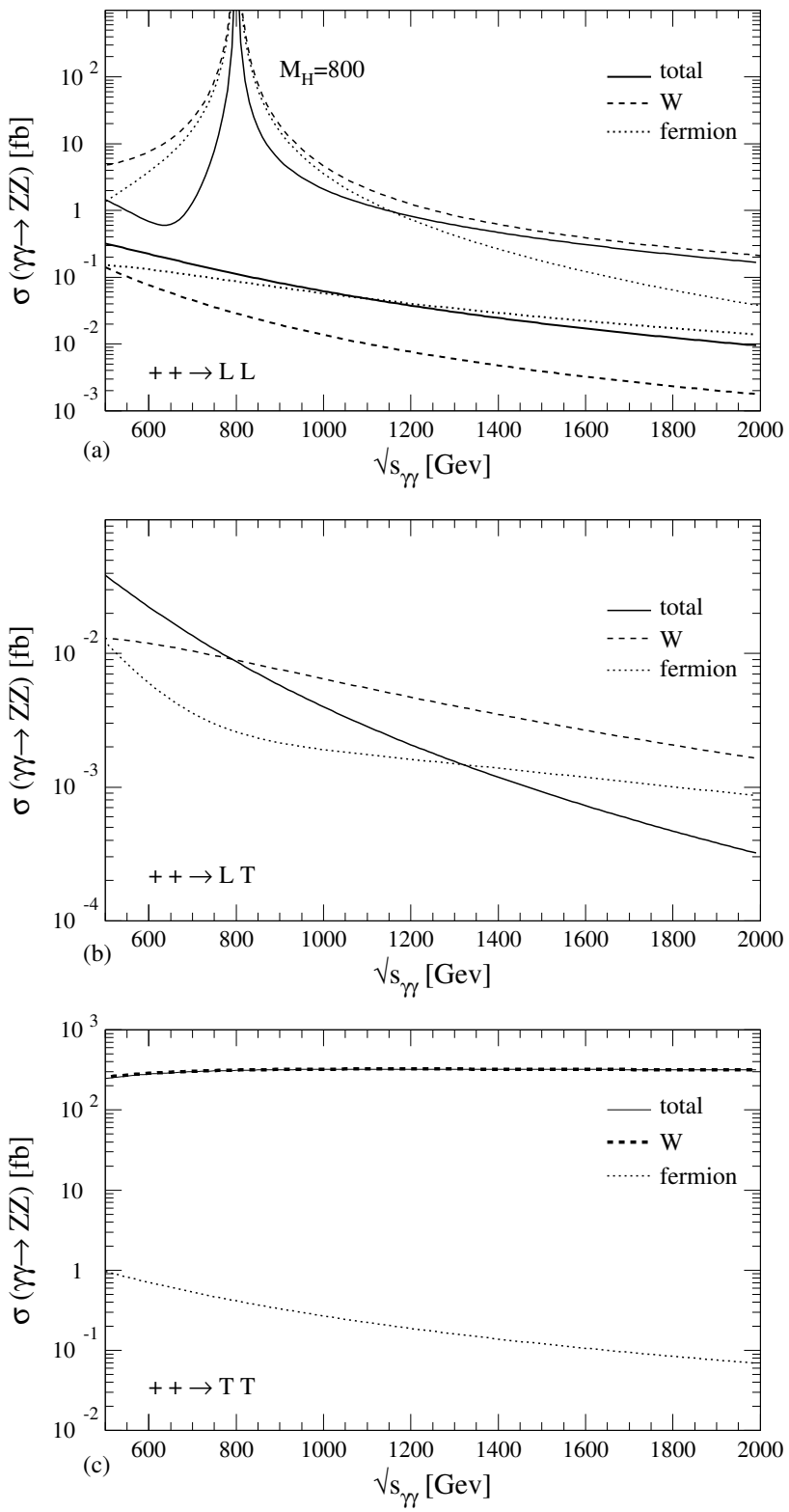

Figure 1.1: The integrated cross sections for different Z boson helicities. The dotted lines are the fermion contributions, the dashed lines are the W boson contributions and the solid lines are the total contributions. The Higgs mass is 115 GeV except a different value is stated and the Higgs decay width has been set to zero.

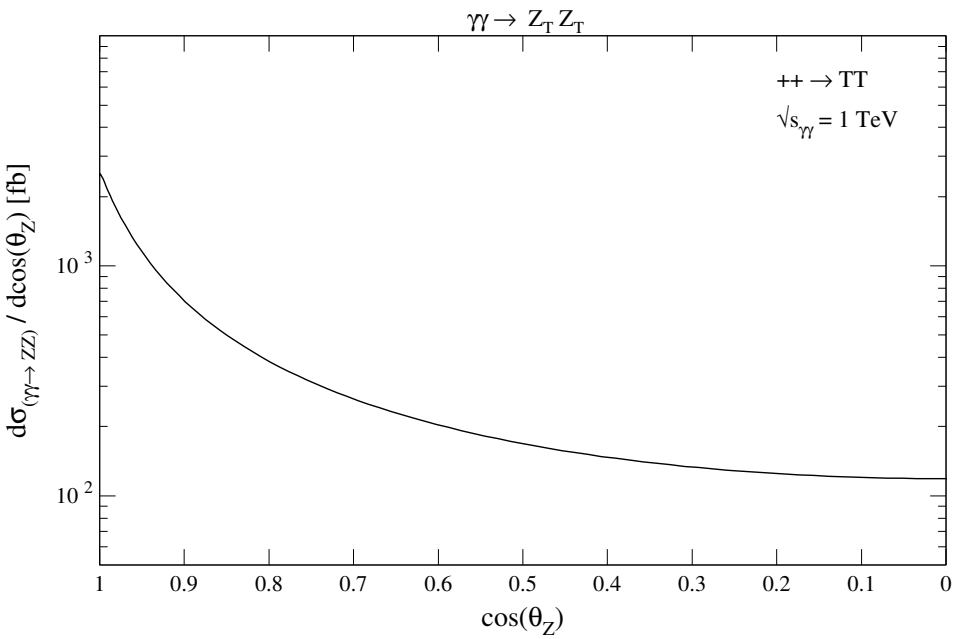

Figure 1.2: Differential cross section for the production of transverse Z bosons at $\sqrt{s} = 1$ TeV.

the Higgs mass is $M_H = 115$ GeV. The decay width of the Higgs has been set to zero, which will be not relevant to our discussion. The dotted lines in the figure are the fermion contributions, the dashed lines are the W boson contributions and the solid lines are the total contributions. In both helicity breaking cross sections Fig. 1.1(a) and 1.1(b) the fermion and W boson contributions are of the same order of magnitude and the cross sections decrease with rising energy.

The integrated cross section for the production of transverse Z bosons is plotted in Fig. 1.1(c). Here the fermion contribution is suppressed and decreases with the scattering energy, while the W boson contribution approaches a constant, overlapping with the total contribution. The helicity breaking parts of the cross section are suppressed by orders of magnitude and decrease further with rising scattering energy, thus the helicity conserving part dominates the process $\gamma\gamma \to ZZ$ completely. In Fig. 1.2 the differential cross section for the production of transverse Z bosons at the scattering energy of 1 TeV is plotted. The main contribution comes from scattering at small angles, which corresponds to the Regge limit where the scattering energy is much larger than any other momentum scales. This behaviour comes from spin-1 W boson exchange in the t-channel giving (1.2) in the forward limit. The property, that the main contribution to the cross section is due to spin-1 boson exchange at small scattering angles and leads to a non-decreasing cross section for the helicity conserving parts, belongs to all vector boson scattering processes.

Figure 1.3: The surviving contributions to the leading electroweak amplitude in the Regge limit for real γ and transverse polarised Z. The solid line represents the W boson.

If we are interested in the main contribution, which is coming from the Regge region, where

$$\begin{aligned} s &\gg |t| \\ |t| &\sim M_W^2 \,, \end{aligned} \tag{1.3}$$

we can do the calculation in the high-energy approximation. In this procedure contributions which are suppressed by powers of t/s can be neglected, which leads to a significant simplification in the computation. Furhter, ur computational method is based on the reconstruction of the asymptotic behaviour of the amplitudes by means of unitarity conditions in the s-channel.

For the calculation we introduce Sudakov parametrisation of the momenta, thus any 4-momentum is parametrised as:

$$k = \alpha p_1 + \beta p_2 + k_\perp \,. \tag{1.4}$$

The CMS we work in is defined by the momenta of the incoming photons which are given by the light cone vectors p_1 and p_2, thus the c.m. energy squared is

$$s = 2p_1 \cdot p_2 \tag{1.5}$$

and the momentum transfer squared is

$$t = q^2 = \alpha\beta s + q_\perp^2 \,. \tag{1.6}$$

The surviving graphs of the helicity conserving amplitude are the W box and cross diagrams, depicted in Fig. 1.3. In order to simplify the calculation we compute first the s-channel discontinuity i.e. the s-channel W internal lines are taken on-shell. In this case the s-channel discontinuity coincides with the imaginary part of the amplitude. For example the imaginary part of the box contribution reads:

$$\mathrm{Im}\, A^{(1)}_{\mathrm{Box}\,\gamma\gamma\to zz} = \frac{1}{2}\int d\Pi_2 A^{(0)}_{\gamma\gamma\to ww}(k^2) A^{(0)\dagger}_{ww\to zz}((k-q)^2) \,, \tag{1.7}$$

where a summation over the W boson helicities has been done by means of:

$$\sum_{\lambda} \epsilon_{\lambda}^{\mu}(k)\epsilon_{\lambda}^{\nu}(k) = -g^{\mu\nu} + \frac{k^{\mu}k^{\nu}}{M_W^2} \tag{1.8}$$

and the two-body phase space is

$$\int d\Pi_2 = \int \frac{d^4k}{(2\pi)^2}\, \delta\left((p_1-k)^2 - M_W^2\right)\, \delta\left((p_2+k)^2 - M_W^2\right)\,. \tag{1.9}$$

The on-shell conditions of the outgoing bosons imply

$$\alpha = |\beta| \simeq \frac{-k_\perp^2}{s} \ll 1 \quad \text{and} \quad k^2 \simeq k_\perp^2\,,\; q^2 \simeq q_\perp^2 \tag{1.10}$$

with all transverse momenta being of the same order of magnitude. Thus rewriting (1.9) in Sudakov variables, it simplifies to:

$$\int d\Pi_2 = \frac{1}{8\pi^2 s}\int d^2k_\perp\,. \tag{1.11}$$

Retaining only the leading power of s the one boson exchange amplitude gives:

$$iA^{(0)}(k^2) = -ig_{vv}^2 \delta_{\lambda_1\lambda_3}\delta_{\lambda_2\lambda_4}\frac{2s}{k_\perp^2 - M_W^2}\,. \tag{1.12}$$

With (1.7) and (1.11) and (1.12), and taking into account the W^+ and W^- contributions, one gets for the imaginary part of the box contribution:

$$\mathrm{Im}\, A_{\mathrm{Box}} = s\, 2\, s_w^2 c_w^2 g^4\, \delta_{\lambda_1\lambda_3}\delta_{\lambda_2\lambda_4}\int \frac{d^2k_\perp}{(2\pi)^2}\frac{1}{k_\perp^2 - M_W^2}\,\frac{1}{(k-q)_\perp^2 - M_W^2}\,. \tag{1.13}$$

Equation (1.13) yields immediately the real part by just noting that $\ln(-s) = \ln s - i\pi$. Thus the reconstructed (leading) amplitude for the Box contribution reads:

$$\begin{aligned} A_{\mathrm{Box}} &= \frac{-s}{\pi}\ln\left(\frac{s}{t-M_W^2}\right)\; 2\, s_w^2 c_w^2 g^4 \\ &\times \quad \delta_{\lambda_1\lambda_3}\delta_{\lambda_2\lambda_4}\int \frac{d^2k_\perp}{(2\pi)^2}\frac{1}{k_\perp^2 - M_W^2}\,\frac{1}{(k-q)_\perp^2 - M_W^2}\,. \end{aligned} \tag{1.14}$$

Performing the loop integration we end up with:

$$\begin{aligned} A_{\mathrm{Box}} &= \frac{-s}{\pi}\ln\left(\frac{s}{t-M_W^2}\right)\; \frac{c_w^2}{s_w^2}\,\alpha_{em}^2\,\delta_{\lambda_1\lambda_3}\delta_{\lambda_2\lambda_4} \\ &\times \quad \frac{8\pi}{\sqrt{t^2 - 4tM_W^2}}\;\ln\left[\left(\frac{-t+\sqrt{t^2-4tM_W^2}}{-t-\sqrt{t^2-4tM_W^2}}\right)^2\right]. \end{aligned} \tag{1.15}$$

The amplitude of the crossed diagram is obtained from the box contribution (1.14) by replacing s by $u \approx -s$. Adding the box and crossed contributions, the

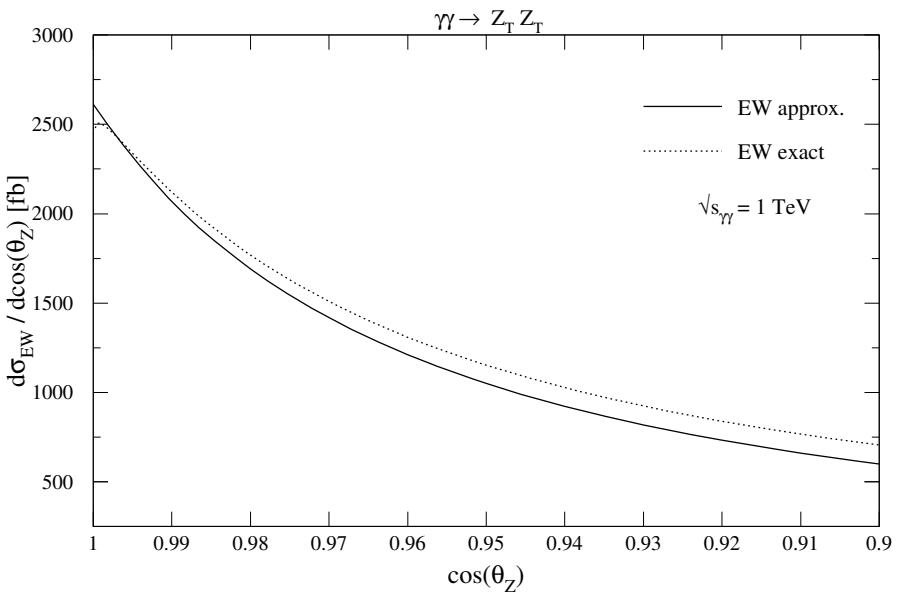

Figure 1.4: Angular distribution of the leading electroweak contribution for transverse Z pair production in polarised $\gamma\gamma$ collision at $\sqrt{s} = 1$ TeV. The solid line is the result of the high-energy approximation, the dotted line is the result of the exact calculation.

leading logarithmic contribution is cancelled and we are left with the imaginary part of the helicity conserving box contribution:

$$\begin{aligned} A^{(1)++++}_{\gamma\gamma\to zz} &= A^{(1)+-+-}_{\gamma\gamma\to zz} \\ &= is\,\alpha^2_{em}\,\frac{c_w^2}{s_w^2}\,\frac{8\pi}{\sqrt{t^2-4tM_W^2}}\,\ln\left[\left(\frac{-t+\sqrt{t^2-4tM_W^2}}{-t-\sqrt{t^2-4tM_W^2}}\right)^2\right]. \end{aligned} \tag{1.16}$$

This result justifies our previous statement that the leading order electroweak contribution is purely imaginary and the cross section is constant in s.

In Fig. 1.4 the angular distribution obtained in the high-energy approximation (1.16) is plotted and compared with the exact result for the scattering energy of 1 TeV. The solid line is the result of the calculation in the high-energy approximation, in which all Feynman diagrams have been neglected apart from the two of Fig. 1.3. The dotted line is the result of the exact calculation, taking into account all contributions. For $\cos\theta \approx 0.9$ the result of the high-energy approximation has a deviation of about 15% from the exact calculation, for smaller scattering angles the deviation decrease. With rising centre of mass energy the accuracy of the Regge calculation will continuously increase.

1.2 Two loop corrections in the high-energy approximation

We calculate two loop corrections to $\gamma\gamma \to Z_T Z_T$ in the Regge limit with the techniques presented in the last section, i.e. reconstructing the asymptotic behaviour by means of unitarity relations and neglecting contributions suppressed by s. Corrections in the high-energy approximation come only from Feynman graphs where a Z boson, a photon or a Higgs particle is exchanged within the W-loop of Fig. 1.3. Contributions from other Feynman diagrams, having for example fermions or scalars in the t-channel, are suppressed by powers of s. For the same reason QCD corrections do not contribute in this limit. Due to the strong coupling they seem to be important, however, they are suppressed since the gluons are always accompanied by a fermion in the t-channel. Thus Feynman graphs including leptons or ghost will be discarded. In respect of the helicities, the only non-suppressed contribution in the Regge limit is the helicity conserving part of the amplitude. From now on we will omit to write the helicity conserving factor $\delta_{\lambda_1\lambda_3}\delta_{\lambda_2\lambda_4}$ explicitly in the expressions, and remind that the following results are valid only for the production of transverse Z bosons.

For the two loop corrections the momenta of the exchanged W bosons are parametrised as:

$$\begin{aligned} k_1 &= \alpha_1 p_1 + \beta_1 p_2 + k_{1\perp} \\ k_2 &= \alpha_2 p_1 + \beta_2 p_2 + k_{2\perp} \end{aligned} \tag{1.17}$$

and leading $\ln s$ contributions come from the kinematical regime where

$$\begin{aligned} 1 &\gg \alpha_1 \gg \alpha_2, \\ 1 &\gg |\beta_2| \gg |\beta_1|. \end{aligned} \tag{1.18}$$

Since we use unitarity relations in the calculation, we have to cut the above mentioned diagrams in all possible ways. One loop graphs with self-energy or vertex corrections to the left or to the right of the cut are sub-dominant in $\ln s$. With respect to the s-channel discontinuity the contributions can be divided into to groups: the two-particle intermediate state or virtual corrections and the three-particle intermediate state or real corrections.

1.2.1 Virtual corrections

First we consider the contributions to the amplitude where a Z boson is exchanged within the W-loop. For the virtual radiative corrections, the imaginary part of the s-channel amplitude is given by

$$\begin{aligned} \mathrm{Im}_s A^Z_{virt}(s,t) &= \frac{1}{2}\int d\Pi_2 A^{(1)}_{\gamma\gamma\to ww}(k_2^2) A^{(0)\dagger}_{ww\to zz}((k_2-q)^2) \\ &+ \frac{1}{2}\int d\Pi_2 A^{(0)}_{\gamma\gamma\to ww}(k_1^2) A^{(1)\dagger}_{ww\to zz}((k_1-q)^2) \end{aligned} \tag{1.19}$$

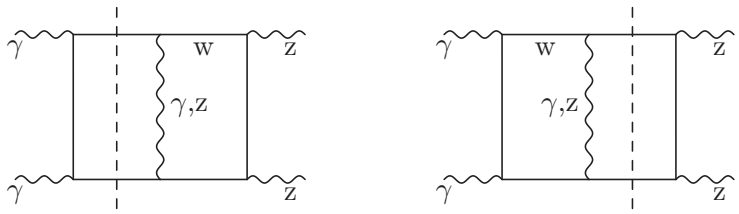

Figure 1.5: Contributions to the two-particle intermediate state of the two loop corrections to $\gamma\gamma \to Z_T Z_T$. The W boson is marked by a solid line.

and the corresponding diagrams are depicted in Fig.1.5. In general, there are contributions with a crossed diagram to the right and to the left of the cut as well. However, for the amplitudes $A^{(1)}_{\gamma\gamma\to ww}$ and $A^{(1)}_{ww\to zz}$ in (1.19) the crossed contribution is absent, thus contrary to $A^{(1)}_{\gamma\gamma\to zz}$, these amplitudes are predominantly real, resulting in an equation similar to (1.14). They are enhanced by a factor $\ln s$ compared to $A^{(1)}_{\gamma\gamma\to zz}$. With the use of the results previously obtained (1.8), (1.11), (1.12) and (1.14) we get:

$$\begin{aligned}
\mathrm{Im_s} A^Z_{virt}(s,t) &= s \ln\left(\frac{s}{M_W^2 - t}\right) g^2_{\gamma w} g^4_{zw} \frac{1}{(2\pi)^5} \int d^2k_{1\perp} d^2k_{2\perp} \qquad (1.20)\\
&\times \left\{ \frac{2}{((k_1-k_2)^2_\perp - M_Z^2)(k^2_{2\perp} - M_W^2)((q-k_1)^2_\perp - M_W^2)} \right.\\
&+ \left. \frac{2}{((k_1-k_2)^2_\perp - M_Z^2)(k^2_{1\perp} - M_W^2)((q-k_2)^2_\perp - M_W^2)} \right\}
\end{aligned}$$

for the imaginary part of the s-channel contribution to the amplitude. The u-channel contribution is obtained in the same manner, in fact, we just need to do again the replacement s by u. The full amplitude is obtained via the subtracted dispersion relation:

$$\begin{aligned}
A(s,t) = A(s_0,t) &+ A(u_0,t) + \frac{(s-s_0)}{\pi} \int_{th}^{\infty} \frac{ds'}{(s'-s)(s'-s_0)} \,\mathrm{Im}_s A\\
&+ \frac{(u-u_0)}{\pi} \int_{th}^{\infty} \frac{du'}{(u'-u)(u'-u_0)} \,\mathrm{Im}_u A\,. \qquad (1.21)
\end{aligned}$$

Computing this amplitude, the leading logarithmic contribution (double logarithm in the energy) is cancelled and the result is, like the one loop contribution, purely imaginary:

$$A^Z_{virt}(s,t) = i\,\mathrm{Im_s} A^Z_{virt}(s,t)\,. \qquad (1.22)$$

If we put $M_Z^2 = 0$ and change the couplings in an appropriate way, we get the corresponding result which comes from the photon contribution.

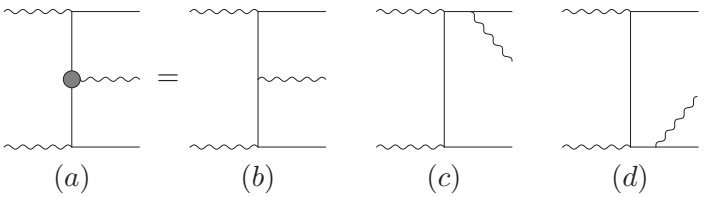

Figure 1.6: Vector boson contribution to the three-particle intermediate state. The wavy lines represents either a photon or a Z boson, while the solid line is a W boson. The t-channel W bosons carry the momenta k_1 and k_2.

1.2.2 Real corrections

Now we consider the three-particle intermediate state to the s-channel discontinuity. The surviving diagrams with bosons in the final state are depicted in Fig.1.6(b-d), where the intermediate particle V (wavy line) can be either a Z boson or a photon. In the kinematical region of (1.18), the on-shellness of this particle implies:

$$\alpha_1\beta_2 s = (k_1 - k_2)_\perp^2 - M_V^2, \tag{1.23}$$

and M_V is the mass of the emitted particle. From this is follows that:

$$k_1^2 \simeq k_{1\perp}^2, \quad k_2^2 \simeq k_{2\perp}^2, \tag{1.24}$$

with all transverse momenta being also here of the same order of magnitude.

First we consider the emission of a Z boson. With the kinematics (1.17), (1.18), (1.23), (1.24) and retaining only the leading power of s the diagram of Fig.1.6(b) becomes:

$$iA_{2\to3,b}^{\rho,\,Z} = -is\ 2\ g_{\gamma w}^2 g_{zw}\ \frac{(-\alpha_1 p_1 - \beta_1 p_2 + (k_1+k_2)_\perp)^\rho}{(k_{1\perp}^2 - M_W^2)(k_{2\perp}^2 - M_W^2)}. \tag{1.25}$$

The diagram of Fig.1.6(c) with the Z emitted from the upper W boson gives:

$$iA_{2\to3,c}^{\rho,\,Z} = -is\ 4\ g_{\gamma w}^2 g_{zw}\ \frac{p_1^\rho}{\beta_2 s(k_{2\perp}^2 - M_W^2)}, \tag{1.26}$$

and the one where the Z is emitted from the lower W boson, Fig.1.6(d), gives:

$$iA_{2\to3,d}^{\rho,\,Z} = -is\ 4\ g_{\gamma w}^2 g_{zw}\ \frac{p_2^\rho}{\alpha_1 s(k_{1\perp}^2 - M_W^2)}. \tag{1.27}$$

The overall sign of these expressions changes depending on the charge flow of the W boson. In the calculation of the discontinuity this dependence cancels. Putting (1.25), (1.26) and (1.27) together gives the full $O(g^3)$ contribution in the high-energy approximation for the emission of a Z boson:

$$iA_{2\to3}^{\rho,\,Z} = i4\ g_{\gamma w}^2 g_{zw}\ \frac{p_1^\nu}{k_{1\perp}^2 - M_W^2}\Gamma_{\nu\mu}^{\rho,\,Z}\frac{p_2^\mu}{k_{2\perp}^2 - M_W^2}\ . \tag{1.28}$$

where $\Gamma^{\rho,\,Z}_{\nu\mu}$ is the effective WZ-vertex defined analogue to [22]:

$$\Gamma^{\rho,\,Z}_{\nu\mu} = \frac{2\,p_1^\nu p_2^\mu}{s}\,C^{\rho,\,Z} \tag{1.29}$$

with

$$C^{\rho,\,Z} = \left(\alpha_1 - \frac{2(k_{1\perp}^2 - M_W^2)}{\beta_2 s}\right) p_1^\rho + \left(\beta_2 - \frac{2(k_{2\perp}^2 - M_W^2)}{\alpha_1 s}\right) p_2^\rho - (k_1+k_2)_\perp^\rho . \tag{1.30}$$

The sum of the three Feynman diagrams of Fig.1.6(b-d) equals the Feynman diagram of Fig.1.6(a), where the gauge coupling to the t-channel W boson is replaced with the effective vertex (1.29).

Having calculated the three-particle production amplitude, the imaginary part of the amplitude for the real corrections reads:

$$\mathrm{Im}_s\, A^Z_{real}(s,t) = \frac{-g^{\rho\sigma}}{2}\int d\Pi_3\, A^{\rho,\,Z}_{2\to3}(k_1,k_2) A^{\sigma\dagger,\,Z}_{2\to3}(q-k_1,q-k_2)\,. \tag{1.31}$$

The $k^\rho k^\sigma/M_Z^2$ contribution emerging with the summation of the Z boson helicities, cf. (1.8), gives a vanishing contribution in the case of equal t-channel particles in Fig.1.6(a), in this case W bosons. Using (1.17), (1.18), (1.23) and (1.24), the three-body phase space can be written as:

$$\begin{aligned}\int d\Pi_3 &= \int d^4k_1 d^4k_2 \\ &\times\ \delta[(p_1-k_1)^2 - M_W^2]\;\delta[(k_1-k_2)^2 - M_Z^2]\;\delta[(p_2+k_2)^2 - M_W^2] \\ &= \frac{1}{4(2\pi)^5 s}\,\ln\left(\frac{s}{M_W^2-t}\right)\int d^2k_{1\perp} d^2k_{2\perp}\,.\end{aligned} \tag{1.32}$$

In calculating the real corrections to the imaginary part of the amplitude (1.31) it is necessary to know the scalar product of the vectors (1.30) with different momenta. In the case of the Z boson contribution we have:

$$\begin{aligned}-g^{\rho\sigma} C^{\rho,\,Z}(k_1,k_2) C^{\sigma\dagger,\,Z}(k_1-q,k_2-q) \;&=\; -2q_\perp^2 - M_Z^2 + 4M_W^2 \\ &+ \frac{2(k_{1\perp}^2 - M_W^2)((q-k_2)_\perp^2 - M_W^2)}{(k_1-k_2)_\perp^2 - M_Z^2} + \frac{2(k_{2\perp}^2 - M_W^2)((q-k_1)_\perp^2 - M_W^2)}{(k_1-k_2)_\perp^2 - M_Z^2}\end{aligned} \tag{1.33}$$

and we have made use of the relation (1.23). Substituting (1.28) and (1.33) into (1.31) and making use of the product (1.33) we get

$$\begin{aligned}\mathrm{Im}\, A^Z_{real}(s,t) &= s\ln\left(\frac{s}{M_W^2-t}\right) g_{\gamma w}^2 g_{zw}^4 \frac{1}{(2\pi)^5}\int d^2k_{1\perp} d^2k_{2\perp} \\ &\times \left\{\frac{2q_\perp^2 + M_Z^2 - 4M_W^2}{(k_{1\perp}^2 - M_W^2)(k_{2\perp}^2 - M_W^2)((q-k_1)_\perp^2 - M_W^2)((q-k_2)_\perp^2 - M_W^2)}\right. \\ &- \frac{2}{((k_1-k_2)_\perp^2 - M_Z^2)(k_{2\perp}^2 - M_W^2)((q-k_1)_\perp^2 - M_W^2)} \\ &- \left.\frac{2}{((k_1-k_2)_\perp^2 - M_Z^2)(k_{1\perp}^2 - M_W^2)((q-k_2)_\perp^2 - M_W^2)}\right\}\end{aligned} \tag{1.34}$$

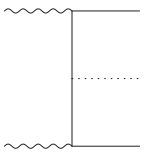

Figure 1.7: The Higgs contribution. Wavy lines can be either a photon or a Z boson, the solid line is the W boson and the dotted line corresponds to the Higgs.

for the Z boson contribution of the real corrections to the s-channel discontinuity. Adding the u-channel part and reconstruct the full amplitude via (1.21), we have similar to the virtual contribution,

$$A^Z_{real}(s,t) = i\,\mathrm{Im}_s A^Z_{real}(s,t)\,. \tag{1.35}$$

Summing the real (1.35) and virtual (1.22) corrections to the amplitude with a Z boson exchanged in the W loop we get the result:

$$\begin{aligned} A^Z(s,t) &= is\ln\left(\frac{s}{M_W^2-t}\right) g^2_{\gamma w} g^4_{zw} \frac{1}{(2\pi)^5}\int d^2k_{1\perp} d^2k_{2\perp} \\ &\times \frac{2q_\perp^2 + M_Z^2 - 4M_W^2}{(k_{1\perp}^2 - M_W^2)(k_{2\perp}^2 - M_W^2)((q-k_1)_\perp^2 - M_W^2)((q-k_2)_\perp^2 - M_W^2)} \end{aligned} \tag{1.36}$$

for the Z boson contribution to the amplitude. The virtual part of the amplitude (1.21) was completely cancelled by the last two terms of the real corrections (1.35). The absence of the crossed contributions in (1.19) was significant for this cancellation.

For a vanishing Z mass and an appropriate modification of the couplings, we get the similar expression for the part of the amplitude where a photon is exchanged in the W loop:

$$\begin{aligned} A^\gamma(s,t) &= is\ln\left(\frac{s}{M_W^2-t}\right) g^4_{\gamma w} g^2_{zw} \frac{1}{(2\pi)^5}\int d^2k_{1\perp} d^2k_{2\perp} \\ &\times \frac{2q_\perp^2 - 4M_W^2}{(k_{1\perp}^2 - M_W^2)(k_{2\perp}^2 - M_W^2)((q-k_1)_\perp^2 - M_W^2)((q-k_2)_\perp^2 - M_W^2)}\,. \end{aligned} \tag{1.37}$$

For the real corrections we also have to take into account the exchange of a Higgs boson. To the virtual corrections the Higgs exchange is not contributing, since it would lead to a spin-0 exchange in the t-channel. In the real corrections the amplitudes corresponding to (1.26) and (1.27) are suppressed as well. The only non-suppressed Feynman graph is the one where the Higgs boson is radiated from the t-channel W boson Fig.1.7, thus in the product

$$\mathrm{Im}\, A^H_{real}(s,t) = \frac{1}{2}\int d\Pi_3\, A^H_{2\to3}(k_1,k_2) A^H_{2\to3}(k_1-q,k_2-q)\,, \tag{1.38}$$

the spin-0 Higgs will be in the s-channel. Taking into account the introduced kinematics and retaining only the leading power of s, the amplitude of Fig.1.7 gives:

$$iA^H_{2\to 3} = -is\ 2\ g^2_{\gamma w} g_{hw}\ \frac{M_W}{(k^2_{1\perp} - M^2_W)(k^2_{2\perp} - M^2_W)}. \tag{1.39}$$

Writing this result in a similar way as (1.28), but now for the case of the emission of the scalar particle, the effective vertex reduces to

$$\Gamma^H_{\nu\mu} = \frac{-2\, p_1^\nu p_2^\mu}{s} M_W \tag{1.40}$$

and the square of the vertex will contain in place of the product (1.33) simply the factor M^2_W. The contributions that cancel each other in the case where a Z boson or a photon is exchanged within the W loop are subleading in the case of the Higgs exchange. With (1.39) and (1.38) we get the result of the Higgs contribution to the s-channel discontinuity. Adding the u-channel contribution and reconstructing the real part, we have:

$$\begin{aligned} A^H(s,t) &= is \ln\left(\frac{s}{M^2_W - t}\right) g^2_{\gamma w} g^2_{zw} g^2_{hw} \frac{1}{(2\pi)^5} \int d^2k_{1\perp} d^2k_{2\perp} \\ &\times \frac{M^2_W}{(k^2_{1\perp} - M^2_W)(k^2_{2\perp} - M^2_W)((q-k_1)^2_\perp - M^2_W)((q-k_2)^2_\perp - M^2_W)}, \end{aligned} \tag{1.41}$$

while again a factor 2 comes from the W^+ and W^- contributions.

Summing the Z boson (1.36), photon (1.37) and Higgs contributions (1.41) one arrives at the full two loop amplitude in the high-energy approximation:

$$\begin{aligned} A^{(2)}(s,t) &= is \ln\left(\frac{s}{M^2_W - t}\right) g^2_{\gamma w} g^2_{zw} \frac{1}{(2\pi)^5} \int d^2k_{1\perp} d^2k_{2\perp} \\ &\times \frac{g^2_{zw}(2q^2_\perp + M^2_Z - 4M^2_W) + g^2_{\gamma w}(2q^2_\perp - 4M^2_W) + g^2_{hw} M^2_W}{(k^2_{1\perp} - M^2_W)(k^2_{2\perp} - M^2_W)((q-k_1)^2_\perp - M^2_W)((q-k_2)^2_\perp - M^2_W)}. \end{aligned} \tag{1.42}$$

Here we already see that the two loop contribution is negative, yielding negative corrections, since the Born contribution is positive. At this stage we also see that the biggest contribution comes from the Z boson exchange in the W loop. The Higgs contribution is cancelling part of the photon and Z boson contribution. The numerator can be written in a more compact way with the electroweak couplings previously introduced:

$$\begin{aligned} A^{(2)}(s,t) &= is \ln\left(\frac{s}{M^2_W - t}\right) 2\, s^2_w c^2_w\, g^6 \frac{1}{(2\pi)^5} \int d^2k_{1\perp} d^2k_{2\perp} \\ &\times \frac{q^2_\perp - M^2_W}{(k^2_{1\perp} - M^2_W)(k^2_{2\perp} - M^2_W)((q-k_1)^2_\perp - M^2_W)((q-k_2)^2_\perp - M^2_W)}. \end{aligned} \tag{1.43}$$

Finally, performing the remaining four integrals with the help of Feynman

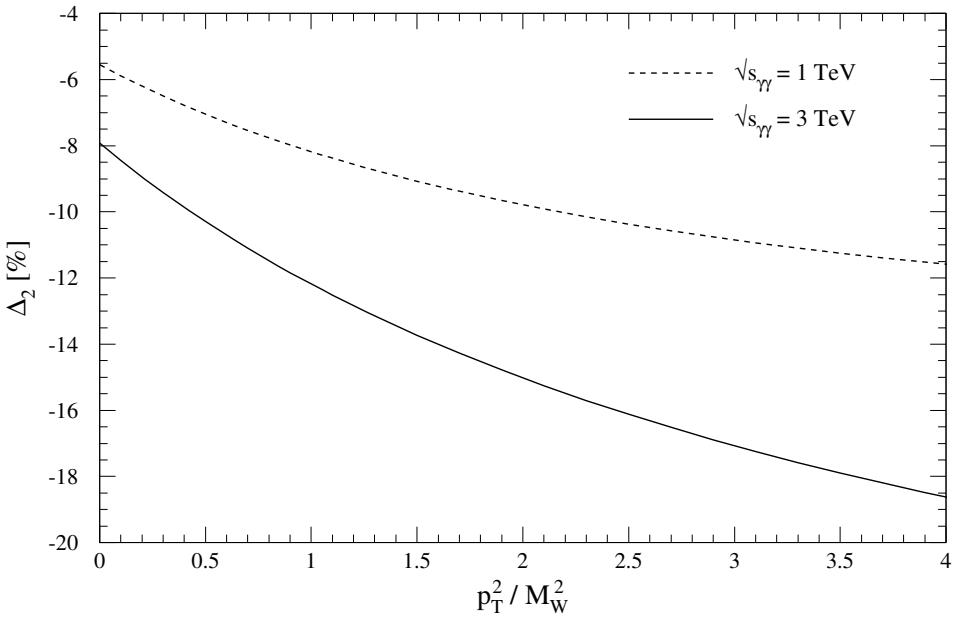

Figure 1.8: Two loop corrections in the high-energy approximation to the differential cross section relative to the Born contribution for different centre of mass energies $\sqrt{s}$. The relative correction is defined as $\Delta_2 = \left(\frac{d\sigma^{(1+2)}}{dp_T^2} - \frac{d\sigma^{(1)}}{dp_T^2}\right) / \frac{d\sigma^{(1)}}{dp_T^2}$

parametrisation, one ends up with:

$$\begin{aligned} A^{(2)}(s,t) &= i\,4s \ln\left(\frac{s}{M_W^2 - t}\right) \alpha_{em}^3 \frac{c_w^2}{s_w^4} \\ &\times \frac{t - M_W^2}{t^2 - 4t\,M_W^2} \ln^2\left[\left(\frac{-t + \sqrt{t^2 - 4tM_W^2}}{-t - \sqrt{t^2 - 4tM_W^2}}\right)^2\right] \end{aligned} \tag{1.44}$$

for the two-loop contributions of $\gamma\gamma \to ZZ$ in the Regge limit. As in the case of the Born contribution, the leading logarithm of the real part was cancelled and the amplitude is imaginary and subleading in $\ln s$.

In Fig.1.8 two-loop corrections to the differential cross section relative to the Born contributions are plotted. These relative corrections are defined as:

$$\Delta_2 = \left(\frac{d\sigma^{(1+2)}}{dp_T^2} - \frac{d\sigma^{(1)}}{dp_T^2}\right) / \frac{d\sigma^{(1)}}{dp_T^2} \tag{1.45}$$

and are displayed as functions of the exchanged transverse momenta p_T^2 for centre of mass energies of 1 TeV and 3 TeV. The corrections are negative and at the

10% level for 1 TeV. Further, the magnitude of the corrections rise logarithmically with the scattering energy, due to the logarithm gained in the additional loop integration. For small p_T both, one loop and two loop contributions approach a constant. For higher p_T the two loop contribution decrease slower due to the square of the logarithm in (1.44). This results indicates, that for the achievement of percent level corrections a more accurate calculation has to be done and also higher corrections have to be taken into account. For energies of a few TeV a calculation by loop orders will not be sufficient enough. One has to do rather a resummation of logarithms in the energy for which the presented results are the first two terms of such an expansion at the leading logarithmic accuracy.

1.2.3 Summary of section 1.2

The process $\gamma\gamma \to ZZ$ starts at one loop. The main contribution comes from the helicity conserving part and from scattering at small angles, due to spin-1 exchange in the t-channel. These part of the amplitude are proportional to the scattering energy leading to a nondecreasing cross section with rising energy. Whereas the helicity breaking parts are suppressed with s. Apart from the fact that the Born contribution starts at one loop, the above mentioned properties are appropriate for any process of quasi-elastic vector boson scattering. We found that leading logarithmic 2 loop corrections to $\gamma\gamma \to ZZ$ are at the order of 10% at 1 TeV.

Chapter 2

QCD corrections

Contributions to vector boson scattering which do not decrease with the scattering energy are due to the QCD sector as well. In this contributions the spin-1 particles exchanged in the t-channel are strongly interacting gluons. If these gluons are exchanged in a quark box the corresponding contributions are decreasing, since the spin-1 particle is always accompanied by quarks in the t-channel. The first non-decreasing contributions emerge at three loop. Bosons fluctuate into a colour dipole and these dipoles interact through gluons.

2.1 Dipole picture in the nonforward direction

In order to investigate higher order QCD corrections to vector boson scattering at small scattering angles we have to start with the calculation of the non-forward vector boson impact factors. It is intuitive to present and discuss the result in the colour dipole picture. In this picture the impact factors are the product of two wave functions, which describe the probability of the boson fluctuation into a colour dipole. At the lowest, non-suppressed order, two gluons are exchanged in the t-channel giving a contribution constant in energy.

2.1.1 Nonforward impact factors

To be definitive, let us consider quasi-elastic boson scattering at high energies and small (but nonzero) momentum transfer. In order to have a non-falling cross section we consider the lowest order QCD diagrams with two-gluon exchange, pictured in Fig.2.1. The vector boson fluctuation into a quark anti-quark pair is described by the product of the two boson wave functions. This quantity is called the (non-forward) vector boson impact factor. Due to the high-energy factorisation one can compute first the impact factors and then integrate these with the gluon propagators. In the high-energy limit, corresponding to s going

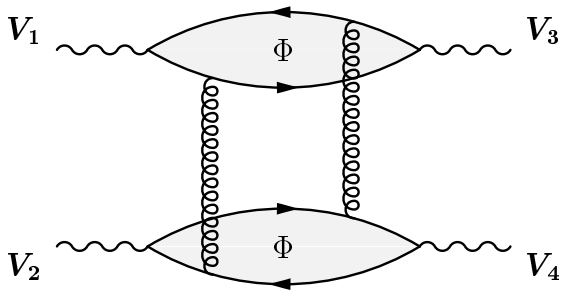

Figure 2.1: The two gluon exchange of the $VV \to VV$ elastic cross section.

to infinity and t fixed (Regge limit), we calculate first the s-channel discontinuity and restore after the amplitude through dispersion relations. Thus the intermediate quark lines inside the impact factors are taken on-shell. This procedure and the high-energy factorisation simplifies the calculation significantly. The scattering amplitude takes the form:

$$A(s,\mathbf{l}) = \frac{is}{2}\int \frac{d^2\mathbf{k}}{(2\pi)^3}\,\frac{\Phi(q,k,l)}{(\mathbf{k}+\mathbf{l})^2}\,\frac{\Phi(p,-k,-l)}{(\mathbf{k}-\mathbf{l})^2}\,, \tag{2.1}$$

where Φ is the impact factor and the boldface marked letters are the transverse part of the Euclidean momenta. As usual, the integration of the two longitudinal components of the loop momenta are absorbed into the definition of the impact factors. The remaining integrals may be computed numerically. The four diagrams which contribute to the boson impact factor Φ are shown in Fig. 2.2. Our task here is the calculation of the boson impact factor, and its interpretation in transverse coordinate space.

We first do the calculation in momentum space, and we compute the discontinuity of the scattering amplitude. The assignment of the loop momentum is illustrated in Fig. 2.2; in all four graphs, the momenta of the cut quark lines are identical, e.g. $u-q$ for the upper quark line. The momenta of the incoming bosons are $q+l$ and $p-l$, while the outgoing bosons have momenta $q-l$ and $p+l$. We use Sudakov variable with the light cone vectors $p' = p + yq$, $y \simeq -p^2/2p\cdot q$ and $q' = q + xp$, $x \simeq -q^2/2p\cdot q$. For the incoming and outgoing bosons we introduce the invariants

$$Q_\pm^2 \;=\; -(q\pm l)^2, \qquad s \equiv (p+q)^2 \;\simeq\; 2\,p'\cdot q', \qquad t \;=\; (2\,l)^2. \tag{2.2}$$

The other bosons involved in the process have similar expressions with the momentum p instead of q. In the case of on-shell bosons the virtuality reduces to the boson mass, i.e. $Q^2 = -M_V^2$. We write the momenta:

$$\begin{aligned} u &= \alpha\, q' + \beta\, p' + u_\perp \\ k &= \alpha_k\, q' + \beta_k\, p' + k_\perp \\ l &= \alpha_l\, q' + \beta_l\, p' + l_\perp\,. \end{aligned} \tag{2.3}$$

In terms of these parameters the boson virtualities are

$$Q_\pm^2 \simeq (x \mp \beta_l)s - l_\perp^2. \tag{2.4}$$

where we used the fact that $\alpha_l \sim |t|/s \ll 1$ in the high energy limit. In the following we use the Euclidean form of the transverse momenta marked in boldface, i.e. $k_\perp^2 = -\mathbf{k}^2 < 0$. In the high energy limit, we also approximate the numerator of the exchanged gluons by the first term in the decomposition

$$g_{\mu\nu} = \frac{2}{s}(p'_\mu q'_\nu + p'_\nu q'_\mu) + g^\perp_{\mu\nu}. \tag{2.5}$$

With these simplifications, the integral of the first diagram takes the following form:

$$\alpha_s \sum_f C_f \frac{s}{2} \int \frac{d\beta_k}{2\pi} \int \frac{d\alpha\, d\beta\, d^2u_\perp}{(2\pi)^4} \times \tag{2.6}$$
$$\frac{\delta[(\alpha-1)(\beta-x)s + u_\perp^2 - m_f^2]\;\delta[\alpha(\beta-\beta_k)s + (u-k)_\perp^2 - m_f^2]}{[\alpha(\beta-\beta_l)s + (u-l)_\perp^2 - m_f^2][(\alpha-1)(\beta-\beta_k+x-\beta_l)s + (u-k-l)_\perp^2 - m_f^2]}$$
$$\times \mathrm{Tr}[\not{p}'(q+l)(\not{u}-\not{k}-\not{q}'-\not{l}+m_f^2)\not{p}'(\not{u}-\not{q}'+m_f^2)\times$$
$$\times \not{q}(q-l)(\not{u}-\not{l}+m_f^2)\not{p}'(\not{u}-\not{k}+m_f^2)]\,.$$

Performing the two β-integration with the delta functions leads to the following relations

$$\beta_k = \frac{(u-k)_\perp^2 - m_f^2}{\alpha s} + \frac{u_\perp^2 - m_f^2}{(1-\alpha)s} - x \tag{2.7}$$
$$\beta = \frac{u_\perp^2 - m_f^2}{(1-\alpha)s} - x\,.$$

A difference between the photon and the other bosons is given by the chiral coupling to the quarks of the latters. Consequently extra terms in the traces appear and the ones proportional to odd powers of γ^5 do not contribute because of charge conjugation invariance. Thus, regarding the impact factors, the W and Z bosons behave both in the same way as the photon, only the magnitude of the coupling to the quarks depends on the nature of the boson.

For longitudinally polarised bosons, the polarisation vectors in terms of Sudakov variables read:

$$\epsilon_L(q \pm l) = \frac{1}{|Q_\pm|}\left[(1 \pm \alpha_l)\,q' + \left(x \mp \beta_l - \frac{2l_\perp^2}{s}\right)p' \pm l_\perp\right]. \tag{2.8}$$

For the bosons appearing in lower impact factor the same expression holds with an exchange of q and p and $l \to -l$.

The calculation of the trace in (2.6) greatly simplifies if we make use of the Ward identity, i.e. the addition of a vector proportional to $q \pm l$ to the polarisation vector does not change the result. In this way the q' dependence of ϵ_L can

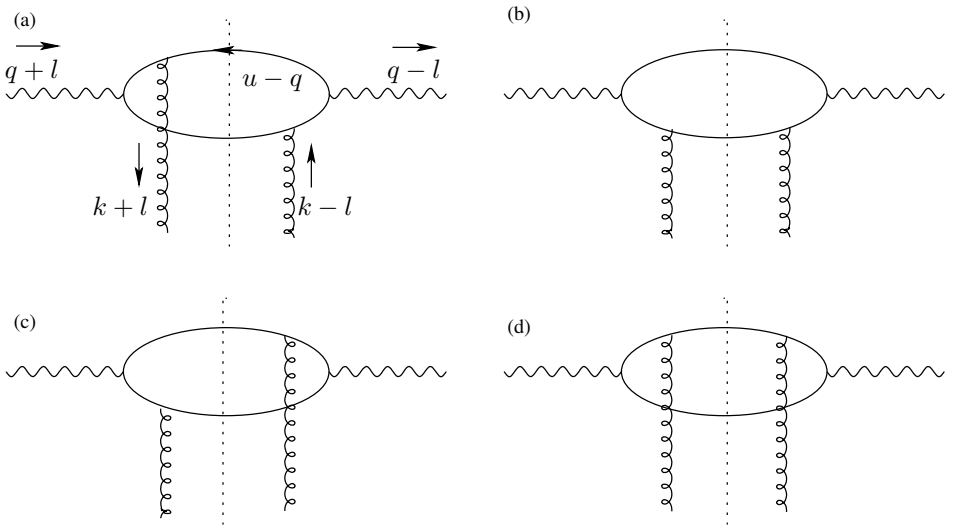

Figure 2.2: The diagrams contributing to the impact factor

be eliminated. The trace is computed in terms of Sudakov variables using the fact that p' and q' are light cone vectors. After summing the contributions corresponding to the four diagrams in Fig. 2.2, given by the integrals of the type (2.6), the impact factor for the longitudinally polarised bosons takes the form:

$$\Phi_{LL}(q,k,l) \;=\; \alpha_s\sqrt{N_c^2-1}\,\sum_f C_f\,4\sqrt{4\pi}\,|Q_+||Q_-|\int_0^1 d\alpha\int\frac{d^2\mathbf{u}}{(2\pi)^2}$$
$$\times\;\alpha^2(1-\alpha)^2\left(\frac{1}{D_1^+}-\frac{1}{D_2^+}\right)\left(\frac{1}{D_1^-}-\frac{1}{D_2^-}\right). \tag{2.9}$$

The four terms have been written in a factorised form, each of them corresponds to one Feynman graph in Fig. 2.2, where we have used:

$$D_1^\pm \;=\; (\mathbf{u}\pm(1-\alpha)\mathbf{l})^2 \;+\; \alpha(1-\alpha)\,Q_\pm^2 \;+\; m_f^2 \tag{2.10}$$

$$D_2^\pm \;=\; (\mathbf{u}-\mathbf{k}\mp\alpha\mathbf{l})^2 \;+\alpha(1-\alpha)\,Q_\pm^2 \;+\; m_f^2\,. \tag{2.11}$$

The constant C_f is the product of the coupling of the incoming and outgoing boson to the quarks of flavour f. Setting $t = 0$ one gets the well known expression in the forward direction.

In the same way we calculate the transverse impact factor where the transverse polarisation vector reads:

$$\epsilon_T^{(h)}(q\pm l) \;=\; \epsilon_\perp^{(h)} \;\pm\; \frac{2l_\perp\cdot\epsilon_\perp^{(h)}}{s}\;(q'-p'\pm l_\perp)\,, \tag{2.12}$$

where $h=\pm$ denotes two helicity states and

$$\epsilon_\perp^{(h)} \;=\; \frac{1}{\sqrt{2}}\,(0,1,\pm i,0)\,. \tag{2.13}$$

After some algebra and the use of the Ward identity, the expression for the transverse impact factor becomes:

$$\begin{aligned}\Phi_{TT}^{(ij)}(q,k,l) \;=\;& \alpha_s\sqrt{N_c^2-1}\sum_f C_f\sqrt{4\pi}\int_0^1 d\alpha\int\frac{d^2\mathbf{u}}{(2\pi)^2}\\ &\times\left\{-4\alpha(1-\alpha)\;\boldsymbol{\epsilon}_i\cdot\left(\frac{\mathbf{N_1^+}}{D_1^+}-\frac{\mathbf{N_2^+}}{D_2^+}\right)\left(\frac{\mathbf{N_1^-}}{D_1^-}-\frac{\mathbf{N_2^-}}{D_2^-}\right)\cdot\boldsymbol{\epsilon}_j^*\right.\\ &+\boldsymbol{\epsilon}_i\cdot\boldsymbol{\epsilon}_j^*\left[\left(\frac{\mathbf{N_1^+}}{D_1^+}-\frac{\mathbf{N_2^+}}{D_2^+}\right)\cdot\left(\frac{\mathbf{N_1^-}}{D_1^-}-\frac{\mathbf{N_2^-}}{D_2^-}\right)\right.\\ &\left.\left.+m_f^2\;\left(\frac{1}{D_1^+}-\frac{1}{D_2^+}\right)\left(\frac{1}{D_1^-}-\frac{1}{D_2^-}\right)\right]\right\}. \qquad (2.14)\end{aligned}$$

where

$$\boldsymbol{\epsilon}_j = 1/\sqrt{2}(1,\pm i) \qquad (2.15)$$

are two-dimensional polarisation vectors corresponding to the two transverse polarisations $j=\pm$. Again, it was possible to write the result in a factorised form where we used the following definitions:

$$\mathbf{N_1^\pm} \;=\; \mathbf{u}\pm(1-\alpha)\mathbf{l} \qquad\qquad \mathbf{N_2^\pm} \;=\; \mathbf{u}-\mathbf{k}\mp\alpha\mathbf{l}\,. \qquad (2.16)$$

Setting $t=0$ and summing over the two helicity states, one gets the well-known expressions in the forward direction, see e.g. [39]. This result also agrees with the one for real photons obtained in [21].

Finally, with the same procedure one can study the impact factor for the incoming boson longitudinally polarised while the outgoing boson is transversely polarised.

$$\begin{aligned}\Phi_{LT}^{(j)}(q,k,l) \;=\;& \alpha_s\sqrt{N_c^2-1}\sum_f C_f\,2\,|Q_+|\sqrt{4\pi}\int_0^1 d\alpha\int\frac{d^2\mathbf{u}}{(2\pi)^2} \qquad (2.17)\\ &\times\;\alpha(1-\alpha)(1-2\alpha)\left(\frac{1}{D_1^+}-\frac{1}{D_2^+}\right)\left(\frac{\mathbf{N_1^-}}{D_1^-}-\frac{\mathbf{N_2^-}}{D_2^-}\right)\cdot\boldsymbol{\epsilon}_j^*\,,\end{aligned}$$

and vice versa for the incoming boson longitudinal and the outgoing one transverse, one has

$$\begin{aligned}\Phi_{TL}^{(i)}(q,k,l) =\;& \alpha_s\sqrt{N_c^2-1}\sum_f C_f\,2\sqrt{4\pi}\,|Q_-|\int_0^1 d\alpha\int\frac{d^2\mathbf{u}}{(2\pi)^2} \qquad (2.18)\\ &\times\;\alpha(1-\alpha)(1-2\alpha)\;\boldsymbol{\epsilon}_\mathbf{i}\cdot\left(\frac{\mathbf{N_1^+}}{D_1^+}-\frac{\mathbf{N_2^+}}{D_2^+}\right)\left(\frac{1}{D_1^-}-\frac{1}{D_2^-}\right)\,.\end{aligned}$$

where $\boldsymbol{\epsilon}_j = 1/\sqrt{2}(1,\pm i)$ are two-dimensional polarisation vectors corresponding to the two transverse polarisations $j=\pm$. The impact factors have been written in a factorised form where the two parts correspond to the boson wave functions,

describing the probability that a boson dissociates into a quark-antiquark pair. In order to obtain the lowest order QCD amplitude, one has to substitute these impact factors into (2.1) and integrate over the gluon momenta.

It is important to realize that the impact factor Φ_{LT} is nonzero in the nonforward direction in contrast to the forward case. This corrects the statement made in the analysis [24] in which $\Phi_{LT} = 0$ in the nonforward case was claimed. The reason for $\Phi_{LT} \neq 0$ is the different symmetry behaviour of the transverse and longitudinal boson wave functions. This property is more transparent in the coordinate space formulation and will be explained in the next chapter.

2.1.2 Formulation in the coordinate space

In view of further discussion, it is instructive to transform these results to coordinate space. As an example, we will discuss these for virtual photons. Of course, the same results hold for other electroweak bosons with the appropriate change in the couplings. We start from the general formulae:

$$\begin{aligned}\frac{1}{\mathbf{k}^2+\delta^2} &= \int \frac{d^2\mathbf{r}}{2\pi}\, e^{i\mathbf{k}\cdot\mathbf{r}}\, K_0(\delta r) \\ \frac{\mathbf{k}}{\mathbf{k}^2+\delta^2} &= \int \frac{d^2\mathbf{r}}{2\pi}\, e^{i\mathbf{k}\cdot\mathbf{r}}\, i\,\delta\,\frac{\mathbf{r}}{r}\, K_1(\delta r)\,. \end{aligned} \tag{2.19}$$

where $K_{0,1}(z)$ are modified Bessel functions. Let us concentrate first on the longitudinal impact factor. After using the first relation from the above, (2.9) takes the form

$$\begin{aligned}\Phi_{LL}(q,k,l) \;=\; & \alpha_s\,\sqrt{N_c^2-1}\,e^2\sum_f q_f^2\, 4\sqrt{4\pi}\,|Q_+||Q_-|\int_0^1 d\alpha\,\alpha^2(1-\alpha)^2 \\ & \times\int\frac{d^2\mathbf{u}}{(2\pi)^2}\int\frac{d^2\mathbf{r}}{2\pi}\, e^{i\mathbf{u}\cdot\mathbf{r}}\left(e^{i(1-\alpha)\mathbf{l}\cdot\mathbf{r}}-e^{-i(\mathbf{k}+\alpha\mathbf{l})\cdot\mathbf{r}}\right)K_0(\delta_+ r) \\ & \times\left(\int\frac{d^2\mathbf{r}'}{2\pi}\, e^{i\mathbf{u}\cdot\mathbf{r}'}\left(e^{-i(1-\alpha)\mathbf{l}\cdot\mathbf{r}'}-e^{-i(\mathbf{k}-\alpha\mathbf{l})\cdot\mathbf{r}'}\right)K_0(\delta_- r')\right)^* \end{aligned} \tag{2.20}$$

where $\delta_\pm^2 = \alpha(1-\alpha)Q_\pm^2 + m_f^2$. The integration over $\mathbf{u}$ leads to the delta function,

$$\int\frac{d^2\mathbf{u}}{(2\pi)^2}\, e^{i\mathbf{u}\cdot(\mathbf{r}-\mathbf{r}')} \;=\; \delta^2(\mathbf{r}-\mathbf{r}')\,,$$

which allows to perform the integration over $\mathbf{r}'$. Thus we obtain

$$\begin{aligned}\Phi_{LL}(q,k,l) \;=\; & \alpha_s\,\sqrt{N_c^2-1}\,e^2\sum_f q_f^2\, 4\sqrt{4\pi}\,|Q_+||Q_-| \\ & \times\int_0^1 d\alpha\int\frac{d^2\mathbf{r}}{(2\pi)^2}\,\alpha^2(1-\alpha)^2 \\ \times\;\underbrace{e^{i(1-\alpha)\mathbf{l}\cdot\mathbf{r}}\,K_0(\delta_- r)}\left(1-e^{-i(\mathbf{k}+\mathbf{l})\cdot\mathbf{r}}\right)&\left(1-e^{i(\mathbf{k}-\mathbf{l})\cdot\mathbf{r}}\right)\underbrace{e^{i(1-\alpha)\mathbf{l}\cdot\mathbf{r}}\,K_0(\delta_+ r)}\,. \end{aligned} \tag{2.21}$$

It is important to note that the integrand (the second line) in (2.21) is invariant under the transformation: $\alpha \to 1-\alpha$ and $\mathbf{r} \to -\mathbf{r}$. This reflects the symmetry of the dipole formula under the interchange of quark and antiquark.

The underlined elements in (2.21) are proportional to the light-cone wave functions of the longitudinal incoming and outgoing photons. To be precise, in the nonforward case the *longitudinal* photon wave function $\Psi^0_{\lambda'\lambda}$ (where $\lambda'(\lambda) = \pm$ denotes the helicity of the (anti)quark) for a given flavour f is given by

$$\Psi^0_{+-}(q \pm l, \mathbf{r}, \alpha) \;=\; \Psi^0_{-+} \;=\; \frac{e\, q_f}{2\,\pi^{3/2}}\,\sqrt{N_c}\,\alpha(1-\alpha)\,|Q_\pm|\,K_0(\delta_\pm r)\,e^{\pm i(1-\alpha)\mathbf{l}\cdot\mathbf{r}}$$

$$\Psi^0_{++} \;=\; \Psi^0_{--} \;=\; 0\,. \tag{2.22}$$

The above wave function differs from the photon wave function with only longitudinal momentum, known from the total cross section for the $\gamma^*\gamma^*$ scattering [14], by the exponential factor involving transverse momentum $\mathbf{l}$ and the longitudinal momentum fraction α (this factor has also been found in [23,25]). It has important consequences for the discussion of the impact parameter representation presented in the next section. Summarising, the impact factor (2.21) in the coordinate space becomes

$$\Phi_{LL}(q,k,l) \;=\; 4\pi^{3/2}\,\alpha_s\,\frac{\sqrt{N_c^2-1}}{N_c}\,\int_0^1 d\alpha\,\int d^2\mathbf{r}$$

$$\times\left(1-e^{-i(\mathbf{k}+\mathbf{l})\cdot\mathbf{r}}\right)\left(1-e^{i(\mathbf{k}-\mathbf{l})\cdot\mathbf{r}}\right)\sum_f\sum_{\lambda'\lambda}\left\{\overline{\Psi}^0_{\lambda'\lambda}(q-l,\mathbf{r},\alpha)\,\Psi^0_{\lambda'\lambda}(q+l,\mathbf{r},\alpha)\right\}$$

where $\overline{\Psi}$ is complex conjugate to Ψ. Inserting this relation into the formula (2.1) for the scattering amplitude, we find for the longitudinally polarised external photons

$$\begin{aligned} A_{LL}(s,\mathbf{l}) \;=\; & is\int d^2\mathbf{r}_1\int d^2\mathbf{r}_1\int_0^1 d\alpha_1\int_0^1 d\alpha_2 \\ & \times\sum_{f_1}\sum_{\lambda'\lambda}\left\{\overline{\Psi}^0_{\lambda'\lambda}(q-l,\mathbf{r}_1,\alpha_1)\,\Psi^0_{\lambda'\lambda}(q+l,\mathbf{r}_1,\alpha_1)\right\} \\ & \times\, N(\mathbf{r}_1,\mathbf{r}_2,\mathbf{l}) \\ & \times\sum_{f_2}\sum_{\lambda'\lambda}\left\{\overline{\Psi}^0_{\lambda'\lambda}(p+l,\mathbf{r}_2,\alpha_2)\,\Psi^0_{\lambda'\lambda}(p-l,\mathbf{r}_2,\alpha_2)\right\}\,, \end{aligned} \tag{2.23}$$

where $N(\mathbf{r}_1,\mathbf{r}_2,\mathbf{l})$ is the scattering amplitude of two dipoles of the transverse size $\mathbf{r}_1$ and $\mathbf{r}_2$ with the momentum transfer $2\mathbf{l}$, in the two gluon exchange approximation

$$\begin{aligned} N(\mathbf{r}_1,\mathbf{r}_2,\mathbf{l}) \;=\; & \alpha_s^2\,\frac{(N_c^2-1)}{N_c^2}\int\frac{d^2\mathbf{k}}{(\mathbf{k}+\mathbf{l})^2(\mathbf{k}-\mathbf{l})^2} \\ & \times\left(1-e^{-i(\mathbf{k}+\mathbf{l})\cdot\mathbf{r}_1}\right)\left(1-e^{i(\mathbf{k}-\mathbf{l})\cdot\mathbf{r}_1}\right)\left(1-e^{i(\mathbf{k}+\mathbf{l})\cdot\mathbf{r}_2}\right)\left(1-e^{-i(\mathbf{k}-\mathbf{l})\cdot\mathbf{r}_2}\right)\,. \end{aligned} \tag{2.24}$$

Let us concentrate now on the impact factor for *transverse* photons $\Phi_{TT}^{(ij)}$, (2.14). Using formulas (2.19) and repeating the steps presented in the longitudinal case, we obtain

$$\begin{aligned}\Phi_{TT}^{(ij)}(q,k,l) \;=\; & \alpha_s\,\sqrt{N_c^2-1}\,e^2\sum_f q_f^2\;\sqrt{4\pi} \\ & \times\int_0^1 d\alpha\int\frac{d^2\mathbf{r}}{(2\pi)^2}\;\left(1-e^{-i(\mathbf{k}+\mathbf{l})\cdot\mathbf{r}}\right)\left(1-e^{i(\mathbf{k}-\mathbf{l})\cdot\mathbf{r}}\right) \\ \times\Bigg\{ & -4\alpha(1-\alpha)\left(\frac{\boldsymbol{\epsilon}_j\cdot\mathbf{r}}{r}\delta_- K_1(\delta_- r)\,e^{-i(1-\alpha)\mathbf{l}\cdot\mathbf{r}}\right)^*\left(\frac{\boldsymbol{\epsilon}_i\cdot\mathbf{r}}{r}\delta_+ K_1(\delta_+ r)\,e^{i(1-\alpha)\mathbf{l}\cdot\mathbf{r}}\right) \\ & +\,\delta_{ij}\,\left(\delta_-\,K_1(\delta_- r)\,e^{-i(1-\alpha)\mathbf{l}\cdot\mathbf{r}}\right)^*\left(\delta_+\,K_1(\delta_+ r)\,e^{i(1-\alpha)\mathbf{l}\cdot\mathbf{r}}\right) \\ & +\,\delta_{ij}\,m_f^2\left(K_0(\delta_- r)\,e^{-i(1-\alpha)\mathbf{l}\cdot\mathbf{r}}\right)^*\left(K_0(\delta_+ r)\,e^{i(1-\alpha)\mathbf{l}\cdot\mathbf{r}}\right)\Bigg\}\end{aligned} \tag{2.25}$$

where we used the fact that $\boldsymbol{\epsilon}_i\cdot\boldsymbol{\epsilon}_j^* = \delta_{ij}$. The above formula can be written in a similar form as (2.23) using helicity wave functions

$$\begin{aligned}\Phi_{TT}^{(ij)}(q,k,l) = {} & 4\,\pi^{3/2}\,\alpha_s\,\frac{\sqrt{N_c^2-1}}{N_c}\int_0^1 d\alpha\int d^2\mathbf{r} \\ \times\left(1-e^{-i(\mathbf{k}+\mathbf{l})\cdot\mathbf{r}}\right)\left(1-e^{i(\mathbf{k}-\mathbf{l})\cdot\mathbf{r}}\right) & \sum_f\sum_{\lambda'\lambda}\left\{\overline{\Psi^j_{\lambda'\lambda}}(q-l,\mathbf{r},\alpha)\,\Psi^i_{\lambda'\lambda}(q+l,\mathbf{r},\alpha)\right\}\end{aligned} \tag{2.26}$$

where i,j are the helicities of the incoming and outgoing photon, respectively, and $\lambda'(\lambda)$ denotes the helicity of the (anti)quark. The photon wave functions are defined in terms of these helicities as:

$$\Psi^+_{+-}(q\pm l,\mathbf{r},\alpha) \;=\; \frac{i\,e\,q_f}{2\,\pi^{3/2}}\,\sqrt{N_c}\,\alpha\,\frac{\boldsymbol{\epsilon}_+\cdot\mathbf{r}}{r}\,\delta_\pm\,K_1(\delta_\pm r)\,e^{\pm i(1-\alpha)\mathbf{l}\cdot\mathbf{r}} \tag{2.27}$$

$$\Psi^-_{+-}(q\pm l,\mathbf{r},\alpha) \;=\; -\frac{i\,e\,q_f}{2\,\pi^{3/2}}\,\sqrt{N_c}\,(1-\alpha)\,\frac{\boldsymbol{\epsilon}_-\cdot\mathbf{r}}{r}\,\delta_\pm\,K_1(\delta_\pm r)\,e^{\pm i(1-\alpha)\mathbf{l}\cdot\mathbf{r}} \tag{2.28}$$

$$\Psi^+_{-+}(q\pm l,\mathbf{r},\alpha) \;=\; -\frac{i\,e\,q_f}{2\,\pi^{3/2}}\,\sqrt{N_c}\,(1-\alpha)\,\frac{\boldsymbol{\epsilon}_+\cdot\mathbf{r}}{r}\,\delta_\pm\,K_1(\delta_\pm r)\,e^{\pm i(1-\alpha)\mathbf{l}\cdot\mathbf{r}} \tag{2.29}$$

$$\Psi^-_{-+}(q\pm l,\mathbf{r},\alpha) \;=\; \frac{i\,e\,q_f}{2\,\pi^{3/2}}\,\sqrt{N_c}\,\alpha\,\frac{\boldsymbol{\epsilon}_-\cdot\mathbf{r}}{r}\,\delta_\pm\,K_1(\delta_\pm r)\,e^{\pm i(1-\alpha)\mathbf{l}\cdot\mathbf{r}} \tag{2.30}$$

$$\Psi^+_{++} = \Psi^-_{--}(q\pm l,\mathbf{r},\alpha) \;=\; \frac{e\,q_f}{(2\pi)^{3/2}}\,\sqrt{N_c}\,m_f\,K_0(\delta_\pm r)\,e^{\pm i(1-\alpha)\mathbf{l}\cdot\mathbf{r}} \tag{2.31}$$

$$\Psi^+_{--} = \Psi^-_{++} \;=\; 0\,. \tag{2.32}$$

Again, the exponentials in the above are due to the transverse momentum of the photons. Similar wave functions were defined in [23] and [27]. The difference between reference [23] and our results lies in the minus sign in (2.28) and (2.29), and we found a different relative normalisation between (2.31) and the rest of the nonzero wave functions (2.27)–(2.30) compared to [27]. It is important to realize that in the forward case, when $\mathbf{l} = 0$ and $i = j$, after the summation over the two transverse polarisations, the expression in the curly brackets in (2.25) becomes a well known expression for the square of the photon wave function in forward kinematics

$$|\Psi_T(q, \mathbf{r}, \alpha)|^2 \ \sim \ \sum_f e_f^2 \left\{ [\alpha^2 + (1-\alpha)^2]\, \delta^2\, K_1^2(\delta r) \ + \ m_f^2\, K_0^2(\delta r) \right\}$$

where $\delta^2 = \alpha(1-\alpha)Q^2 + m_f^2$. The structure of the full amplitude for transverse photons is the same as in (2.23) with the wave function factors replaced by those in the curly brackets in (2.26).

For completeness we also present the formula for the impact factor with mixed polarisation (2.17)

$$\Phi_{LT}^{(j)}(k,l) = 4\,\pi^{3/2}\,\alpha_s\,\frac{\sqrt{N_c^2-1}}{N_c}\,\int_0^1 d\alpha \int d^2\mathbf{r} \tag{2.33}$$

$$\times \left(1 - e^{-i(\mathbf{k}+\mathbf{l})\cdot\mathbf{r}}\right)\left(1 - e^{i(\mathbf{k}-\mathbf{l})\cdot\mathbf{r}}\right) \sum_f \sum_{\lambda'\lambda} \left\{ \overline{\Psi_{\lambda'\lambda}^j}(q-l, \mathbf{r}, \alpha)\Psi_{\lambda'\lambda}^0(q+l, \mathbf{r}, \alpha) \right\}$$

Here the impact factor is written as a convolution of the two boson wave functions and the dipole interaction. Due to the different symmetry behaviour of the transverse and longitudinal boson wave functions, the helicity-flip impact factors are in general non-zero. They vanish only for forward scattering, where $\mathbf{l} = 0$. The dipole interaction is invariant under the transformation of the dipole size vector $\mathbf{r} \to -\mathbf{r}$, and so is the longitudinal wave function, (2.22). In contrast to this the transverse wave function, (2.27)-(2.30), is antisymmetric under this transformation, since it is proportional to $\mathbf{r}$. The convolution of two transverse wave functions is therefore symmetric under this transformation, whereas the convolution of a transverse and a longitudinal one is antisymmetric, leading to the vanishing result for $\mathbf{l} = 0$. If $\mathbf{l}$ is non-zero, this symmetry properties are broken, resulting in a non-vanishing Φ_{TL} and Φ_{TL}.

In each presented case the scattering amplitude $A(s, \mathbf{l})$ has the form of (2.23) with the wave function replacement which takes into account helicities of the external photons.

2.1.3 Impact parameter

In our notation, the four-momentum transfer squared t between the two $q\bar{q}$ systems is given by the transverse two-dimensional vector $\mathbf{\Delta} = 2\mathbf{l}$, i.e. $t = -\mathbf{\Delta}^2$.

The impact parameter $\boldsymbol{b}$ is defined as a Fourier conjugate variable to $\boldsymbol{\Delta}$, and the scattering amplitude in the impact parameter space is given by

$$\tilde{A}(s,\boldsymbol{b}) \,=\, \int \frac{d^2\boldsymbol{\Delta}}{(2\pi)^2}\, e^{i\boldsymbol{b}\,\cdot\,\boldsymbol{\Delta}}\, A(s,\boldsymbol{\Delta})\,. \tag{2.34}$$

Performing this integral, we keep the total energy $\sqrt{s}$ as well as virtualities of the external photons, $Q_\pm^2$ and $P_\pm^2$, fixed. Let us concentrate on the amplitude for longitudinal photons (2.23) with the wave function (2.22). The dependence on $\boldsymbol{\Delta}$ (or $\mathbf{l}$) resides in the exponential factors in the wave functions and the dipole-dipole scattering amplitude $N(\mathbf{r}_1,\mathbf{r}_2,\boldsymbol{\Delta})$, (2.24). Thus performing the transformation (2.34) the amplitude (2.23) we find

$$\begin{aligned}\tilde{A}(s,\boldsymbol{b}) \,=\, is \int d^2\mathbf{r}_1 \int d^2\mathbf{r}_1 \int_0^1 d\alpha_1 \int_0^1 d\alpha_2 \\ \times \sum_{f_1} \sum_{\lambda'\lambda} \left\{\overline{\Psi}_{\lambda'\lambda}(Q_-,\mathbf{r}_1,\alpha_1)\, \Psi_{\lambda'\lambda}(Q_+,\mathbf{r}_1,\alpha_1)\right\} \\ \times\, \tilde{N}(\mathbf{r}_1,\mathbf{r}_2,\boldsymbol{b}+(1-\alpha_1)\mathbf{r}_1+(1-\alpha_2)\mathbf{r}_2) \\ \times \sum_{f_2} \sum_{\lambda'\lambda} \left\{\overline{\Psi}_{\lambda'\lambda}(P_+,\mathbf{r}_2,\alpha_2)\, \Psi_{\lambda'\lambda}(P_-,\mathbf{r}_2,\alpha_2)\right\}\,.\end{aligned} \tag{2.35}$$

The wave functions above are the forward photon wave functions with the indicated photon virtualities, given by eqs. (2.27) with the exponential factors being removed. This is due to the fact that, when transforming to impact parameter, we have to include the momentum transfer dependence of these factors into the definition of the dipole-dipole scattering amplitude $\tilde{N}$:

$$\begin{aligned}&\tilde{N}(\mathbf{r}_1,\mathbf{r}_2,\boldsymbol{b}+(1-\alpha_1)\mathbf{r}_1+(1-\alpha_2)\mathbf{r}_2) \\ &= \int \frac{d^2\boldsymbol{\Delta}}{(2\pi)^2}\, e^{i\,(\boldsymbol{b}+(1-\alpha_1)\boldsymbol{r_1}+(1-\alpha_2)\boldsymbol{r_2})\,\cdot\,\boldsymbol{\Delta}}\, N(\mathbf{r}_1,\mathbf{r}_2,\boldsymbol{\Delta})\,.\end{aligned} \tag{2.36}$$

From (2.36) we see that, in the dipole-dipole scattering amplitude, the dependence upon the impact parameter contains an α-dependent shift relative to the impact parameter $\boldsymbol{b}$ which refers to the external photon (2.34): $\boldsymbol{b} \to \boldsymbol{b}+(1-\alpha_1)\mathbf{r}_1+(1-\alpha_2)\mathbf{r}_2$. Furthermore, as we have already remarked after (2.21), the dipole scattering amplitude (for fixed transverse dipole sizes and longitudinal momenta) is invariant under the interchanges $\alpha_1 \to (1-\alpha_1)$, $\mathbf{r}_1 \to -\mathbf{r}_1$ or/and $\alpha_2 \to (1-\alpha_2)$, $\mathbf{r}_2 \to -\mathbf{r}_2$.

Let us give a physical interpretation of this result. In the high energy limit, the incoming photon and the quark-antiquark pair are conveniently described in an infinite momentum frame. In this frame, as it has been shown many years ago [40,41], there exists a subgroup of the Poincare group which is isomorphic to the symmetry group of Galilei transformations in nonrelativistic two-dimensional quantum mechanics. This two dimensional motion takes place in the transverse

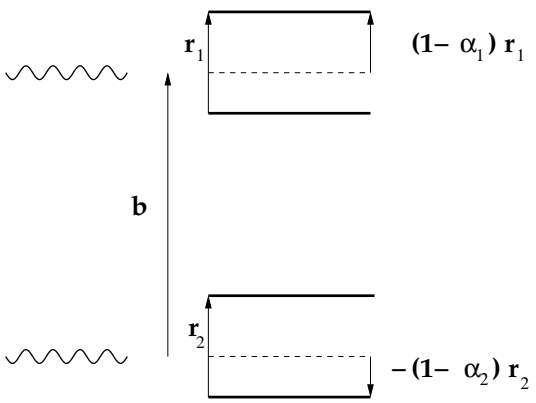

Figure 2.3: *The interpretation of relation (2.39) in the transverse coordinate plane: the wavy lines denote the incoming photons, the full lines the quark antiquarks of the upper and the lower colour dipoles.*

plane, and the longitudinal momentum plays the role of the nonrelativistic mass. In our case of dipole-dipole scattering we choose the upper incoming photon to move in the positive z-direction, i.e. in light cone variables q has a large q_+ component. Inside the upper impact factor, the upper quark line with longitudinal momentum fraction $1-\alpha_1$ carries the 'mass' $m_u = (1-\alpha_1)q_+$, whereas the lower quark line has the 'mass' $m_l = \alpha_1 q_+$. The vector $\mathbf{r}_1$ denotes the transverse distance between the upper and lower quark line, and the impact parameter $\boldsymbol{b}$ is the transverse distance between the two incoming photons. If we interpret the upper incoming photon as being in the centre of mass of the upper quark-antiquark system, see Fig. 2.3, the two vectors

$$\boldsymbol{b} + \frac{m_u}{m_u + m_l}\mathbf{r}_1 \;=\; \boldsymbol{b} + (1-\alpha_1)\mathbf{r}_1 \tag{2.37}$$

and

$$\boldsymbol{b} - \frac{m_l}{m_u + m_l}\mathbf{r}_1 \;=\; \boldsymbol{b} - \alpha_1\mathbf{r}_1 \tag{2.38}$$

denote the position of the upper and lower quark, respectively. A similar argument holds for the lower dipole, i.e. the vector

$$\boldsymbol{b} + (1-\alpha_1)\,\mathbf{r}_1 + (1-\alpha_2)\,\mathbf{r}_2 \tag{2.39}$$

denotes the distance between the upper quark line in the upper dipole and the lower quark line in the lower dipole. The peculiar $\boldsymbol{b}$-dependence of (2.36) then says that the interaction between the upper and lower colour dipoles depends upon the distance between one of the two quarks of the upper dipole and one of the quarks in the lower dipole (and not upon the distance $\boldsymbol{b}$ between the centre of mass coordinates of the two dipoles). Moreover, because of the symmetry under $\alpha \to 1-\alpha$, $\mathbf{r} \to -\mathbf{r}$ we are free to interchange the quarks inside one of the two colour dipoles.

Finally, the appearance of the phase factors $\exp\{\pm i(1-\alpha)\mathbf{l}\cdot\mathbf{r}\}$ in (2.27) can be understood as follows. Inverting (2.19) we find, for example, for the upper

incoming longitudinal photon

$$K_0(\delta_+ r)\, e^{i(1-\alpha)\mathbf{lr}} \;=\; \int \frac{d^2\mathbf{k}}{2\pi}\, e^{-i(\mathbf{k}-(1-\alpha)\mathbf{l})\cdot\mathbf{r}}\, \frac{1}{\mathbf{k}^2+\delta_+^2}\,, \tag{2.40}$$

i.e. the momentum conjugate to the transverse distance $\mathbf{r}$ is $(\mathbf{k}-(1-\alpha)\mathbf{l})$ rather than $\mathbf{k}$. The incoming photon carries transverse momentum $\mathbf{l}$ and splits into quark and antiquark with longitudinal and transverse momenta $(1-\alpha,\, \mathbf{k})$ and $(\alpha,\, -\mathbf{k}+\mathbf{l})$, respectively. In the infinite momentum frame this corresponds to the masses $m_1 = (1-\alpha)q_+$ and $m_2 = \alpha q_+$. From nonrelativistic mechanics we know that the relative momentum of the quark-antiquark pair (i.e. the momentum conjugate to the relative coordinate $\mathbf{r}$) is given by

$$\frac{m_2}{m_1+m_2}\mathbf{p}_1 - \frac{m_1}{m_1+m_2}\mathbf{p}_2 \;=\; \alpha\mathbf{k} - (1-\alpha)(-\mathbf{k}+\mathbf{l}) = \mathbf{k} - (1-\alpha)\mathbf{l}\,. \tag{2.41}$$

So the appearance of the phase factor looks very natural.

2.1.4 Nonforward dipole-proton scattering amplitude

In a case when the lower photon is replaced by the proton, an unintegrated gluon distribution $f(x_\pm, , \mathbf{k}, \mathbf{l})$ appears [42], where $x_\pm = Q_\pm^2/s$ and the adopted notation means that f depends on both the variables. Thus, strictly speaking, f is a nondiagonal (skewed or generalised) unintegrated gluon distribution since both the longitudinal and transverse momenta of the exchanged gluons, $k \pm l$, are not equal, see Fig. 2.2. In the proton case, the amplitude (2.1) reads

$$A(s, \mathbf{l}=\boldsymbol{\Delta}/2) \;=\; \frac{is}{2}\int \frac{d^2\mathbf{k}}{(2\pi)^3}\, \frac{\Phi(q,\mathbf{k},\mathbf{l})}{(\mathbf{k}+\mathbf{l})^2}\, \frac{f(x_\pm,\mathbf{k},\mathbf{l})}{(\mathbf{k}-\mathbf{l})^2}\,. \tag{2.42}$$

Repeating the steps from section 2.1.2, we find in the coordinate space the analogue of (2.23)

$$\begin{aligned} A(s,\mathbf{l}=\boldsymbol{\Delta}/2) \;&=\; is\int d^2\mathbf{r}\int_0^1 d\alpha \qquad (2.43)\\ &\times\; \sum_f \sum_{\lambda'\lambda} \left\{\overline{\Psi}_{\lambda'\lambda}(q-l,\mathbf{r},\alpha)\, N(x_\pm,\mathbf{r},\mathbf{l})\, \Psi_{\lambda'\lambda}(q+l,\mathbf{r},\alpha)\right\} \end{aligned}$$

where now $N(x_\pm, \mathbf{r}, \mathbf{l})$ is a nonforward dipole–proton scattering amplitude

$$\begin{aligned} N(x_\pm,\mathbf{r},\mathbf{l}) \;&=\; \frac{\alpha_s}{4\pi^{3/2}}\, \frac{\sqrt{N_c^2-1}}{N_c} \int \frac{d^2\mathbf{k}}{(\mathbf{k}+\mathbf{l})^2(\mathbf{k}-\mathbf{l})^2}\\ &\times\; \left(1-e^{-i(\mathbf{k}+\mathbf{l})\cdot\mathbf{r}}\right)\left(1-e^{i(\mathbf{k}-\mathbf{l})\cdot\mathbf{r}}\right) f(x_\pm,\mathbf{k},\mathbf{l})\,. \qquad (2.44) \end{aligned}$$

In the impact parameter representation we have:

$$\begin{aligned} \tilde{A}(s,\boldsymbol{b}) \;&=\; is\int d^2\mathbf{r}\int_0^1 d\alpha \qquad (2.45)\\ &\times\; \sum_f \sum_{\lambda'\lambda} \left\{\overline{\Psi}_{\lambda'\lambda}(Q_-,\mathbf{r},\alpha)\, \tilde{N}(x_\pm,\mathbf{r},\boldsymbol{b}+(1-\alpha)\mathbf{r})\, \Psi_{\lambda'\lambda}(Q_+,\mathbf{r},\alpha)\right\} \end{aligned}$$

with

$$\tilde{N}(x_\pm, \mathbf{r}, \boldsymbol{b} + (1-\alpha)\mathbf{r}) \;=\; \int \frac{d^2\boldsymbol{\Delta}}{(2\pi)^2}\, e^{i\,(\boldsymbol{b} + (1-\alpha)\mathbf{r})\,\cdot\,\boldsymbol{\Delta}}\, N(x_\pm, \mathbf{r}, \mathbf{l} = \boldsymbol{\Delta}/2)\,. \tag{2.46}$$

Again, there are forward photon wave functions in (2.45) since the nonforward exponentials are incorporated into (2.46). As we have mentioned before, this expression is invariant under the replacement: $\alpha \to 1-\alpha$ and $\mathbf{r} \to -\mathbf{r}$, which can be easily seen by inserting (2.44) into (2.46) and performing the symmetry transformation.

For completeness we also quote the formula for diffractive vector production in the nonforward direction [25], e.g. for the production of longitudinal ρ-mesons. In our kinematics, the impact factor has the form (2.43), with the wave function for the outgoing photon, $\Psi(q-l, \mathbf{r}, \alpha)$, being replaced by the meson wave function:

$$\Psi(q-l, \mathbf{r}, \alpha) \;\;\to\;\; \Psi_\rho(\mathbf{r}, \alpha)\, e^{-i(1-\alpha)\mathbf{lr}} \tag{2.47}$$

As in the case of VV scattering, the extra phase factor accounts for the nonzero transverse momentum of the vector particle.

2.1.5 Open quark-antiquark production

In the final step of our discussion we remove, in the upper dipole system, the wave function of the outgoing photon, i.e. we consider the diffractive production of an open quark-antiquark pair in the nonforward direction, $\gamma^* + p \to (q\bar{q}) + p$. We follow our previous notation: the incoming photon carries the momentum $q+l$, and the outgoing antiquark and quark have the momenta $q-u$ and $u-l$, respectively. The scattering amplitude has the form (2.42) with the replacement: $\Phi(q,k,l) \to \Phi^{\gamma^* \to (q\bar{q})}_{\lambda'\lambda}(q,u,k,l)$. For the longitudinal photon, the new impact factor for open quark-antiquark production is given by:

$$\Phi^{0,\gamma^*\to(q\bar{q})}_{+-}(q,\mathbf{u},\mathbf{k},\mathbf{l}) \;=\; 2\,(2\pi)^{3/2}\alpha_s\sqrt{\frac{N_c^2-1}{N_c}}\, e_f\,[\alpha(1-\alpha)]^{3/2}\,|Q_+|\,\times \tag{2.48}$$

$$\left(\frac{1}{D(\mathbf{u}+(1-\alpha)\mathbf{l})} + \frac{1}{D(\mathbf{u}-(1+\alpha)\mathbf{l})} - \frac{1}{D(\mathbf{u}+\mathbf{k}-\alpha\mathbf{l})} - \frac{1}{D(\mathbf{u}-\mathbf{k}-\alpha\mathbf{l})}\right)$$

with $D(\mathbf{k}) = \mathbf{k}^2 + \alpha(1-\alpha)Q_+^2 = \mathbf{k}^2 + \delta_+^2$. Inserting (2.19), we arrive at:

$$\Phi^{0,\gamma^*\to(q\bar{q})}_{+-}(q,\mathbf{u},\mathbf{k},\mathbf{l}) \;=\; 2\,(2\pi)^{3/2}\alpha_s\sqrt{\frac{N_c^2-1}{N_c}}\, e_f\,[\alpha(1-\alpha)]^{3/2}\,|Q_+| \tag{2.49}$$

$$\times \int \frac{d^2\mathbf{r}'}{2\pi}\, e^{i\mathbf{u}\cdot\mathbf{r}'}\left(1 - e^{-i(\mathbf{k}+\mathbf{l})\cdot\mathbf{r}'}\right)\left(1 - e^{i(\mathbf{k}-\mathbf{l})\cdot\mathbf{r}'}\right) e^{i(1-\alpha)\mathbf{l}\cdot\mathbf{r}'} K_0(\delta_+ r')\,.$$

From the discussion at the end of section 2.1.2 we know that the transverse distance between the outgoing quark an antiquark, $\mathbf{r}$, is conjugate to the transverse momentum $\mathbf{u}-(1-\alpha)\mathbf{l}$. We therefore define the scattering amplitude for the production of a dipole of the size $\mathbf{r}$ by taking the Fourier transform

$$\Phi_{+-}^{0,\gamma^*\to(q\bar{q})}(q,\mathbf{r},\mathbf{k},\mathbf{l}) \equiv \int \frac{d^2\mathbf{u}}{(2\pi)^2}\, e^{-i(\mathbf{u}-(1-\alpha)\mathbf{l})\cdot\mathbf{r}}\, \Phi_{+-}^{0,\gamma^*\to(q\bar{q})}(q,\mathbf{u},\mathbf{k},\mathbf{l})\,, \tag{2.50}$$

and

$$\begin{aligned}\Phi_{+-}^{0,\gamma^*\to(q\bar{q})}(q,\mathbf{r},\mathbf{k},\mathbf{l}) &= 2\sqrt{2\pi}\,\alpha_s\sqrt{\frac{N_c^2-1}{N_c}}\,e_f\,[\alpha(1-\alpha)]^{3/2}\,|Q_+| \\ &\times e^{i(1-\alpha)\mathbf{l}\cdot\mathbf{r}}\left(1-e^{-i(\mathbf{k}+\mathbf{l})\cdot\mathbf{r}}\right)\left(1-e^{i(\mathbf{k}-\mathbf{l})\cdot\mathbf{r}}\right)e^{i(1-\alpha)\mathbf{l}\cdot\mathbf{r}}\,K_0(\delta_+ r) \\ &= \sqrt{2}\,(2\pi)^2\alpha_s\frac{\sqrt{N_c^2-1}}{N_c}\sqrt{\alpha(1-\alpha)} \\ &\times e^{i(1-\alpha)\mathbf{l}\cdot\mathbf{r}}\left(1-e^{-i(\mathbf{k}+\mathbf{l})\cdot\mathbf{r}}\right)\left(1-e^{i(\mathbf{k}-\mathbf{l})\cdot\mathbf{r}}\right)\Psi_{+-}^0(q+l,\mathbf{r},\alpha).\end{aligned} \tag{2.51}$$

Finally, the scattering amplitude of the dipole on a proton our result takes the form:

$$A_{+-}^{\gamma^*\to(q\bar{q})}(s,\alpha,\mathbf{r},\mathbf{l}) = is\sqrt{2\pi}\,\sqrt{\alpha(1-\alpha)}\,e^{i(1-\alpha)\mathbf{l}\cdot\mathbf{r}}\,N(x_\pm,\mathbf{r},\mathbf{l})\,\Psi_{+-}^0(q+l,\mathbf{r},\alpha) \tag{2.52}$$

with the dipole scattering amplitude from (2.44). When transforming to impact parameter $\boldsymbol{b}$, again the shifted variable $\boldsymbol{b}+(1-\alpha)\mathbf{l}$ appears, the distance from the target centre to the quark. For the integrated and spin summed cross section

$$\begin{aligned}\frac{d\sigma}{d^2\boldsymbol{\Delta}} &= \frac{1}{16\pi^2 s^2}\,\frac{1}{4\pi}\,\frac{1}{\alpha(1-\alpha)} \\ &\times \int_0^1 d\alpha \int \frac{d^2\mathbf{u}}{(2\pi)^2}\,\sum_{\lambda'\lambda}|A_{\lambda'\lambda}^{\gamma^*\to(q\bar{q})}(s,\alpha,\mathbf{u},\mathbf{l}=\boldsymbol{\Delta}/2)|^2\,,\end{aligned} \tag{2.53}$$

we obtain after transforming to transverse coordinates:

$$\frac{d\sigma}{d\boldsymbol{\Delta}^2} = \frac{1}{16\pi}\int_0^1 d\alpha\int d^2\mathbf{r}\,\sum_{\lambda'\lambda}\overline{\Psi_{\lambda'\lambda}^0}(q+l,\mathbf{r},\alpha)\,|N(x_\pm,\mathbf{r},\mathbf{l})|^2\,\Psi_{\lambda'\lambda}^0(q+l,\mathbf{r},\alpha). \tag{2.54}$$

This generalises the well-known formula for the diffractive quark-antiquark production in the forward direction [14]. In particular, the integrated cross section for diffractive quark-antiquark production contains the same dipole scattering amplitude as the elastic Vp process (2.44).

2.1.6 Summary of section 2.1

In this section we have discussed the generalisation of the colour dipole picture to the nonforward direction. For the elastic scattering of two colour dipoles we found that the dipole cross section depends upon the transverse distance between the ends of the two dipoles, and not between the centres of the two quark-antiquark pairs. This result also holds for diffractive vector production. For open $q\bar{q}$-production, we confirm the well-known result of the forward direction: the integrated (over the transverse size of the produced quark-antiquark pair) cross section is described by the square of the elastic dipole cross section. Results presented in this section have been published in [43].

2.2 Leading log (BFKL) contribution

With rising centre of mass energy the two quark-antiquark dipoles, calculated in the last section, radiate more gluons. This higher order corrections provide large logarithms in energy, while the strong coupling is small:

$$\alpha_s \log s \sim 1, \qquad \alpha_s \ll 1 \tag{2.55}$$

These logarithms rise with the scattering energy, thus the radiation of more gluons enhances the cross section. These contributions cannot be neglected at large energies. Diagrams of ladder topology, built with (non elementary) reggeized gluons, can contribute up to the order $\alpha_s^n \ln^n(s/s_0)$. These diagrams are scatched in Fig.2.4. The gluons in the t-channel are reggeized gluons, marked as zigzag lines while the emitted (curly) gluons are real ones. The virtualities of the bosons Q_V^2 provide the large external scale justifying a perturbative calculation. On the other hand, the boson masses or virtualities have to be at the same order of magnitude in order to prevent from additional large logarithms of transverse momenta, leading to DGLAP evolution.

One possibility to take this contribution into consideration is a resummation described by the LO BFKL equation [13] which gives an upper bound estimate of these effects. This possibility is related to the property of the factorisation of the scattering amplitude in the Regge limit, in terms of the impact factors associated to the external particles and the BFKL Green's function. We will briefly outline the derivation of the BFKL Green's function in this section.

2.2.1 Review of the LO BFKL equation

We like to review a perturbative QCD content of the Pomeron exchange, described by the BFKL equation [13], which will be computed here in the leading logarithmic approximation (LLA). One important achievement of [13] was the proof of the gluon reggeization to all orders in perturbation theory. The denotation "reggeized gluon" means a gluon with a modified propagator (in Feynman gauge) of the form:

$$D_{\mu\nu}(s, q^2) = -i \, \frac{g_{\mu\nu}}{q^2} \left(\frac{s}{s_0} \right)^{\alpha(q^2)} \tag{2.56}$$

where $1 + \alpha(q^2)$ is the Regge trajectory of the gluon and $\alpha(q^2)$ is the trajectory function. Thus any amplitude with exchange of the gluon quantum numbers reduces to an amplitude with the exchange of a single particle, called reggeon.

In the high-energy Regge limit, where the centre of mass energy of the process is much larger than any other momentum scale, every amplitude was found to obey a factorisation. This factorisation is called the Regge factorisation and was already used in the calculation of the two-gluon amplitude. This allows a separate treatment of the interaction and the couplings of the external particles.

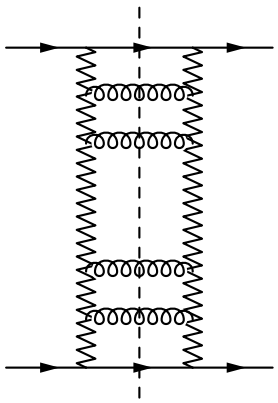

Figure 2.4: Ladder diagrams contributing to the BFKL evolution. Reggeized gluons are sketched as zigzag lines.

Every amplitude in LLA will be expressed in terms of effective vertices between external particles and reggeized gluons. Accordingly, a general ansatz for the elastic scattering of two particles A and B in the high-energy limit of small scattering angles and for the exchange of a particle with negative signature we have:

$$A_8 = \Gamma_A \frac{s}{t} \left[\left(\frac{s}{-t} \right)^{\alpha(t)} + \left(\frac{-s}{-t} \right)^{\alpha(t)} \right] \Gamma_B. \tag{2.57}$$

The vertices Γ_A and Γ_B as well as the gluon trajectory function are perturbatively calculable. Therefore one can make a loop expansion for Γ and $\alpha(t)$.

$$\Gamma_{A,B} = g\,\Gamma^{(0)}_{A,B} + g^3 \Gamma^{(1)}_{A,B} + \cdots \tag{2.58}$$

$$\alpha(t) = g^2 \alpha^{(1)}(t) + g^4 \alpha^{(2)}(t) + \cdots \tag{2.59}$$

and this expansion leads to the following Regge ansatz for (2.57):

$$\begin{aligned} A_8 &= \alpha_s \frac{s}{t} \Big\{ 2\,\Gamma^{(0)}_A \Gamma^{(0)}_B + \alpha_s \Gamma^{(0)}_A\, \alpha^{(1)} \left[\ln \frac{s}{-t} + \ln \frac{-s}{-t} \right] \Gamma^{(0)}_B \\ &+ 2\alpha_s \left(\Gamma^{(1)}_A \Gamma^{(0)}_B + \Gamma^{(0)}_A \Gamma^{(1)}_B \right) \Big\} + \cdots \end{aligned} \tag{2.60}$$

The first line of (2.60) belongs to the leading logarithmic approximation, since both terms are of the type $(\alpha_s \ln s)^n$. The second line of (2.60) is already beyond that approximation, contributing to the next-to-leading logarithmic approximation, where the additional α_s is not accompanied by a $\log s$.

In order to calculate the expression (2.60) perturbatively, we switch to the definitive process of massless quark-quark scattering. The leading order calculation in α_s is giving the first term of the expansion (2.60), with the simple quark-quark-gluon vertex in the high-energy approximation:

$$\Gamma^{(0)}_{qq} = t^a_{ij} \delta_{hh'}. \tag{2.61}$$

where h, h' is the helicity of the quarks and t^a_{ij} denotes the colour group generator. Calculating now the one loop contribution, one is left with the s- and u-channel box-contributions. There are more one-loop diagrams like self-energy and vertex corrections, but analogous to the electroweak calculation presented before, they are subleading in $\ln s$ and therefore can be ignored. The s- and u-channel box-contributions give us the second term of (2.60) and since we know $\Gamma^{(0)}_{qq}$ from the tree level calculation, we can identify the trajectory function $\alpha^{(1)}(t)$. This gluon trajectory function presents the virtual part of the LLA corrections at one-loop level to the single gluon exchange. Since gluons are massless it contains infrared singularities. In space-time dimension $D = 4 - 2\epsilon$ it reads:

$$\alpha^{(1)}(t) = \frac{2g^2 N_c}{(4\pi)^{2-\epsilon}} \frac{c_\Gamma (-t)^{-\epsilon}}{\epsilon}. \tag{2.62}$$

with $c_\Gamma = 1 - \gamma_E \epsilon + \mathcal{O}(\epsilon^2)$ and N_c being the number of colours.

Apart from the virtual corrections, there are also contributions in the LLA from real gluon emission. We expect from any gluon loop a large logarithm in the scattering energy, so we consider the case where n-gluons are emitted in the t-channel. For quark-quark scattering, using unitarity relations, we can write the amplitude

$$\mathrm{Im}_s \, A^{A'B'}_{AB}(s,t) = \sum_{n=0}^{\infty} \int d\Phi_{2+n} \, A^{A'B'+n}_{AB} (A^{A'B'+n}_{AB})^*, \tag{2.63}$$

where $A^{A'B'+n}_{AB}$ is the production amplitude of n gluons and $d\Phi_{2+n}$ is the phase space measure for the $2+n$ particle intermediate state. Assigning for the massless quarks the light cone momenta p_A and p_B, we can write the gluon momenta k_i in Sudakov decomposition as:

$$k_i = \alpha_i p_A + \beta_i p_B + k_\perp \, . \tag{2.64}$$

The leading $\ln s$ contributions come from the kinematical regime, where the Sudakov component of the emitted gluons are strongly ordered, called Multi-Regge-kinematics:

$$1 \gg \alpha_1 \gg \cdots \gg \alpha_n \gg -t/s \tag{2.65}$$

$$1 \gg |\beta_n| \gg \cdots \gg |\beta_1| \gg -t/s \tag{2.66}$$

and the transverse momenta are of fixed order. With this kinematics the amplitude $A^{A'B'+n}_{AB}$ for the production of n-gluons takes the form:

$$\begin{aligned} A^{A'B'+n}_{AB} \;=\; & 2s \, \Gamma^{c_1}_{AA'} \left[\frac{1}{t_1} \left(\frac{s}{s_0} \right)^{\alpha(t_1)} \right] \gamma^{d_1}_{c_1 c_2} \left[\frac{1}{t_2} \left(\frac{s}{s_0} \right)^{\alpha(t_2)} \right] \cdots \\ & \cdots \gamma^{d_n}_{c_n c_{n+1}} \left[\frac{1}{t_{n+1}} \left(\frac{s}{s_0} \right)^{\alpha(t_{n+1})} \right] \Gamma^{c_{n+1}}_{BB'} . \end{aligned} \tag{2.67}$$

The coupling of the external quarks to the reggeized gluon Γ was already computed in the Born case. The effective vertex $\gamma^{d_i}_{c_i c_{i+1}}$ describes the emission of a

real gluon from the t-channel reggeized gluon,

$$\gamma^{d_i}_{c_i c_{i+1}} = g f_{c_i c_{i+1} d_i} e^*_\mu C^\mu, \tag{2.68}$$

where e^*_μ is the polarisation vector and d is the colour index of the real gluon, c the colour index of the reggeized gluons, and C^μ the non-local Lipatov vertex, like in the electroweak case but now for massless gluons:

$$C^\mu(q_{i+1}, q_i) = \left(\alpha_i + \frac{2\boldsymbol{q}_i^2}{\beta_{i+1} s}\right) p_A^\mu + \left(\beta_{i+1} + \frac{2\boldsymbol{q}_{i+1}^2}{\alpha_i s}\right) p_B^\mu - (q_i + q_{i+1})^\mu_\perp \,. \tag{2.69}$$

This vertex is obtained from the calculation of $qq \to qqg$ in the Regge kinematic. The appropriate Feynman graphs are sketched in Fig.2.5, the corresponding calculation was also done for electroweak vector bosons in section 1.2. In order

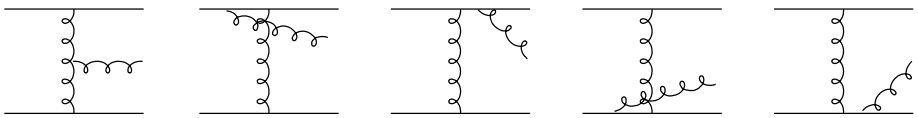

Figure 2.5: Feynman diagrams contributing to the Lipatov vertex.

to proceed one has to insert the n-gluon production amplitude (2.67) into the elastic amplitude (2.63). The phase space measure $d\Phi_{2+n}$ for the 2+n particle intermediate state contains the integration of the Sudakov parameters α_i and β_i. While the β_i integrations are straight forward, the convolution of the α_i integrals can be disentangled by taking the Mellin transform of the amplitude (2.63). The result can be written in a recursive relation, where the partial wave of the transition amplitude for two reggeons has to satisfy the integral equation:

$$\begin{aligned} &[\omega - \alpha(-\mathbf{k}^2) - \alpha(-(\mathbf{k}-\mathbf{q})^2)]\; \mathcal{G}(\omega, \boldsymbol{k}, \boldsymbol{k}', \boldsymbol{q}) \\ &\quad = \quad \delta^{(2)}(\boldsymbol{k} - \boldsymbol{k}') - \frac{N_c \alpha_s}{2\pi^2} \int d^2\boldsymbol{\kappa}\, \frac{\mathcal{K}(\boldsymbol{k}, \boldsymbol{\kappa})}{\boldsymbol{k}^2 (\boldsymbol{\kappa} - \boldsymbol{q})^2}\, \mathcal{G}(\omega, \boldsymbol{\kappa}, \boldsymbol{k}', \boldsymbol{q})\,. \end{aligned} \tag{2.70}$$

The kernel of the integral equation represents the contribution of the real radiative corrections and is resulting from the contraction of the Lipatov vertices. The α terms on the left-hand side represent the virtual radiative corrections, coming from the loop integration of the ladder rungs. The solution of this integral equation [44] can be obtained in impact parameter space, using the conformal invariance properties of the equation.

2.2.2 The LO BFKL amplitude

For the physical processes we want to study we need the BFKL Greens function in momentum space, depending on the scattering energy. The impact factors have been calculated in the preceding section and the discontinuity of the LL resummed amplitude is simply obtained by inserting the non-forward BFKL

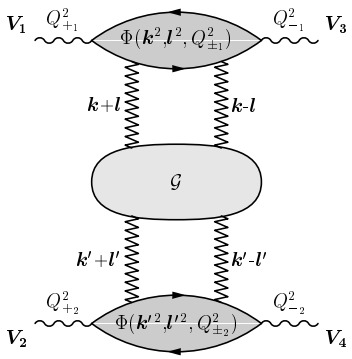

Figure 2.6: The BFKL Pomeron exchange in the $VV \to VV$ elastic cross section.

Pomeron Green's function in the place of the two gluon propagators. Indeed one has

$$Disc_s A = is \int \frac{d^2\boldsymbol{k}}{(2\pi)^3}\frac{d^2\boldsymbol{k}'}{(2\pi)^3}\Phi(q,k,l)G(y|\boldsymbol{k}+\boldsymbol{l},\boldsymbol{k}-\boldsymbol{l};\boldsymbol{k}'+\boldsymbol{l},\boldsymbol{k}'-\boldsymbol{l})\Phi(p,-k',-l), \tag{2.71}$$

where $y = \ln s/s_0$ is the rapidity variable and s_0 is a typical scale in the process. The exchanged transverse momenta is $2\boldsymbol{l}$. Clearly, for $\alpha_s \to 0$, when all rungs of the BFKL resummation decouple, the Green's function reduces to the two gluon exchange, which means that we use the following normalisation:

$$\lim_{\alpha_s\to 0} G(y|\boldsymbol{k}+\boldsymbol{l},\boldsymbol{k}-\boldsymbol{l};\boldsymbol{k}'+\boldsymbol{l},\boldsymbol{k}'-\boldsymbol{l}) = \frac{(2\pi)^3}{(\boldsymbol{k}+\boldsymbol{l})^2(\boldsymbol{k}-\boldsymbol{l})^2}\delta^{(2)}(\boldsymbol{k}-\boldsymbol{k}') \tag{2.72}$$

In the following we briefly give the ingredients needed to construct the BFKL Green's function. The eigenfunctions $E_{h,\bar{h}}$ of the BFKL kernel, which appears in the integral Bethe-Salpeter like equation resumming all the LL terms, are well known in coordinate space, wherein their form is dictated by conformal invariance. They are given by

$$E_{h,\bar{h}}(\boldsymbol{r}_{10},\boldsymbol{r}_{20}) = \left(\frac{r_{12}}{r_{10}r_{20}}\right)^h \left(\frac{r^*_{12}}{r^*_{10}r^*_{20}}\right)^{\bar{h}}, \tag{2.73}$$

with $\boldsymbol{r}_{ij} = \boldsymbol{r}_i - \boldsymbol{r}_j$ etc., $h = (1+n)/2 + i\nu$, $\bar{h} = (1-n)/2 + i\nu$ ($h^* = 1-\bar{h}$, $\bar{h}^* = 1-h$). Let us note that standard complex notation for two-dimensional vectors is used on the right-hand side, i.e. $r_i = x_i + \mathrm{i}\, y_i$. The conformal weights h, decomposed in n (integer conformal spin) and ν (real), label the principal series of unitary representations of the Möbius group. Fourier transforming to momentum space (we use the Lipatov's convention which assigns a $1/(2\pi)^2$ to any coordinate integration) one finds [45]:

$$\begin{aligned}\tilde{E}_{h\bar{h}}(\boldsymbol{k}_1,\boldsymbol{k}_2) &= \int \frac{d^2\boldsymbol{r}_1}{(2\pi)^2}\frac{d^2\boldsymbol{r}_2}{(2\pi)^2}E_{h,\bar{h}}(\boldsymbol{r}_1,\boldsymbol{r}_2)e^{i(\boldsymbol{k}_1\cdot\boldsymbol{r}_1+\boldsymbol{k}_2\cdot\boldsymbol{r}_2)} \\ &= C\Big(X(\boldsymbol{k}_1,\boldsymbol{k}_2) + (-1)^n X(\boldsymbol{k}_2,\boldsymbol{k}_1)\Big).\end{aligned} \tag{2.74}$$

The coefficient C is given by

$$C = \frac{(-i)^n}{(4\pi)^2} h\bar{h}(1-h)(1-\bar{h})\Gamma(1-h)\Gamma(1-\bar{h}). \tag{2.75}$$

The functions X in complex notation can be expressed in terms of hypergeometric functions:

$$\begin{aligned} X(\boldsymbol{k}_1, \boldsymbol{k}_2) &= \left(\frac{k_1}{2}\right)^{\bar{h}-2} \left(\frac{k_2^*}{2}\right)^{h-2} \\ &\times F\left(1-h, 2-h; 2; -\frac{k_1^*}{k_2^*}\right) F\left(1-\bar{h}, 2-\bar{h}; 2; -\frac{k_2}{k_1}\right) . \end{aligned} \tag{2.76}$$

This analytic form does not contain any term of the type $\delta^2(\boldsymbol{k}_1)$ or $\delta^2(\boldsymbol{k}_2)$ which are present in the coordinate representation (2.73). The impact factor of a colourless external particle vanishes for zero momentum of any gluon exchanged and therefore the delta-function type terms do not contribute.

The Pomeron intercept has the form $\alpha_P(0) = 1 + \chi(\nu, n)$, where

$$\begin{aligned} \chi(\nu,n) = \chi_h &= \bar{\alpha}_s \left(2\psi(1) - \psi(\frac{1+|n|}{2} + i\nu) - \psi(\frac{1+|n|}{2} - i\nu)\right) \\ \bar{\alpha}_s &= \frac{N_c \alpha_s}{\pi}, \end{aligned} \tag{2.77}$$

are the kernel eigenvalues corresponding to the eigenfunctions in equations (2.73)-(2.74). We shall use the Pomeron Green's function in the momentum representation. Starting from the form in coordinate representation [46] one can perform a Fourier transform [45] and making use of the Casimir operator properties of the Möbius group, one can chose a representation which is more convenient to perform a Fourier transform. In particular, after considering the relation

$$\begin{aligned} \frac{1}{|r_{12}|^4} E_{h,\bar{h}}(r_{10}, r_{20}) &= \frac{1}{16} |\boldsymbol{\partial}_1|^2 |\boldsymbol{\partial}_2|^2 \frac{1}{(r_{12}^2 \partial_1 \partial_2) \times (h.c.)} E_{h,\bar{h}}(r_{10}, r_{20}) \\ &= \frac{1}{16} \frac{1}{[\nu^2 + (n-1)^2/4][\nu^2 + (n+1)^2/4]} \\ &\times |\boldsymbol{\partial}_1|^2 |\boldsymbol{\partial}_2|^2 E_{h,\bar{h}}(r_{10}, r_{20}) \end{aligned} \tag{2.78}$$

one can write for the amputated Green's function

$$\begin{aligned} &G_2^{(A)}(y|r_1, r_2; r_{1'}, r_{2'}) = \\ &\int d\mu \, d^2\boldsymbol{r}_0 \, e^{y\chi(\nu,n)} \, N_h \, |\boldsymbol{\partial}_1|^2 |\boldsymbol{\partial}_2|^2 E_{h,\bar{h}}(r_{10}, r_{20}) E^*_{h,\bar{h}}(r_{1'0}, r_{2'0}) \end{aligned} \tag{2.79}$$

where we use the measure in the conformal weight space $\int d\mu = \sum_n \int d\nu$ with the following normalisation factor N_h:

$$N_h = \frac{(\nu^2 + n^2/4)}{[\nu^2 + (n-1)^2/4][\nu^2 + (n+1)^2/4]}. \tag{2.80}$$

In order to find the momentum representation we take the Fourier transform taking into account the total momentum conservation. Dividing also by $|\boldsymbol{k}_1|^2|\boldsymbol{k}_2|^2$, we obtain for the nonamputated Green's function:

$$\tilde{G}_2(y|\boldsymbol{k}_1,\boldsymbol{k}_2;\boldsymbol{k}_{1'}\boldsymbol{k}_{2'}) \tag{2.81}$$
$$= (2\pi)^3 \int d\mu(h)\, e^{y\,\chi_h}\, N_h \times (2\pi)^2\, \tilde{E}_{h,\bar{h}}(\boldsymbol{k}_1,\boldsymbol{k}_2)\tilde{E}^*_{h,\bar{h}}(\boldsymbol{k}_{1'},\boldsymbol{k}_{2'})\,.$$

The $(2\pi)^3$ factor in front of the integral comes from the normalisation (2.72); the second $(2\pi)^2$ factor results from the $\boldsymbol{\rho}_0$ integration, together with a $\delta^{(2)}(\boldsymbol{k}_1+\boldsymbol{k}_2-\boldsymbol{k}_{1'}-\boldsymbol{k}_{2'})$ related to the overall momentum conservation.

Let us finally rewrite the expression of the amplitude discontinuity in (2.71) by inserting in it the relation (2.82). On defining the conformal weight representation for the impact factors according to

$$\Phi_h(q,l) = \int \frac{d^2\boldsymbol{k}}{(2\pi)^3}\Phi(q,k,l)\tilde{E}_{h,\bar{h}}(\boldsymbol{k}+\boldsymbol{l},\boldsymbol{k}-\boldsymbol{l})\,, \tag{2.82}$$

together with the primed $\Phi'_h(q,l)$ computed with the conjugate eigenstate, one has

$$Disc_s A = is(2\pi)^5 \int d\mu(h)\, N_h\, e^{y\,\chi_h}\, \Phi_h(q,l)\Phi'_h(p,l)\,. \tag{2.83}$$

We stress that due to high energy factorisation the energy dependence is encoded in the LL BFKL Green's function and the only other dependence in the momenta of the incoming particles is through the invariant external masses on which the impact factors depend. In the last expression the dominant contribution for large y can be easily extracted with a saddle point analysis for $n=0$ around $\nu=0$ and therefore reduces to

$$Disc_s A = is(2\pi)^5 16 e^{y\,\chi_0}\frac{\sqrt{2\pi}}{(2ay)^{3/2}}\Phi_0(q,l)\Phi'_0(p,l)\,, \tag{2.84}$$

where $\chi_0 = 4\ln(2)\bar{\alpha}_s$ is the leading BFKL intercept and $a = 14\zeta(3)\bar{\alpha}_s$.

The forward limit presents a well known cusp behaviour and it must converge to the result obtained on using a forward BFKL Green's function

$$G_F(y|\boldsymbol{k},\boldsymbol{k}') = (2\pi)^3 \int d\mu(h)\, e^{y\,\chi_h}\, \tilde{E}^{(F)}_{h,\bar{h}}(\boldsymbol{k})\tilde{E}^{(F)*}_{h,\bar{h}}(\boldsymbol{k}')\,, \tag{2.85}$$

which is written in the spectral representation with the forward BFKL amputated eigenfunctions given by $\tilde{E}^{(F)}_{h,\bar{h}}(\boldsymbol{k}) = 1/(\pi\sqrt{2})k^{h-1}k^{*\,\bar{h}-1}$.

The saddle point approximations can be carried on in a way similar to the nonforward case. We shall define

$$\Phi^{(F)}_h(q) = \int \frac{d^2\boldsymbol{k}}{(2\pi)^3}\Phi(q,k,0)\frac{1}{\boldsymbol{k}^2}\tilde{E}^{(F)}_{h,\bar{h}}(\boldsymbol{k})\,, \tag{2.86}$$

as well as a $\Phi_h^{'(F)}(q)$ for the scalar product with the conjugate Pomeron state and write the discontinuity in the forward case as

$$Disc_s^{(F)} A = is(2\pi)^3 e^{y\,\chi_0} \frac{\sqrt{2\pi}}{(2ay)^{1/2}} \Phi_0^{(F)}(q) \Phi_0^{'(F)}(p)\,. \tag{2.87}$$

Let us note that in the transition from the nonforward to forward physics the perturbative QCD analysis is increasingly affected by the long distance interactions (contributions for all values of the impact parameter), since gluons are massless. This implies that some care is required to treat the general nonforward expression in this limit. The saddle point approximation for $n = 0$ around $\nu = 0$ leading to (2.84) is accurate only for l down to values of the order of one. Strictly speaking, performing the saddle point approximation of (2.83) in the region of very small l one needs to shift the saddle point which becomes l dependent. In our numerical calculation we have used (2.84) down to $|2\mathbf{l}|^2 = 1/2\, M_Z^2$, and then we have extrapolated to the forward value, (2.87).

A more precise analysis, avoiding the use of the saddle point approximation is of course possible but it is not needed for the order of magnitude estimate which is pursued here. Few checks have been done with an exact Green's function computation, confirming such an expectation.

Finally, in order to evaluate the elastic cross sections we need to obtain the amplitude from the computed discontinuity. Instead of using the full dispersion relation technique, a simple evaluation compatible with the approximation adopted is given by

$$A \sim \left(1 - i\frac{\pi}{2}\frac{\partial}{\partial y}\right) \frac{1}{2} Disc_s A\,, \tag{2.88}$$

as provided by the signature factor in the partial wave amplitude analysis.

2.2.3 Summary of section 2.2

For higher energies the radiation of gluons enhances the cross section. This higher-order corrections provide large logarithms in energy, which rise with the scattering energy. These contributions cannot be neglected at large energies. One possibility to take this into consideration is a resummation described by the LO BFKL equation [13] which gives an upper bound estimate of these effects.

We outlined in this chapter the computation of the resummed LO BFKL cross section. After calculating the n-gluon production amplitude, an integral equation can be derived [13]. The solution of this equation [22] describes the evolution in $\ln s$ of the LLA amplitudes.

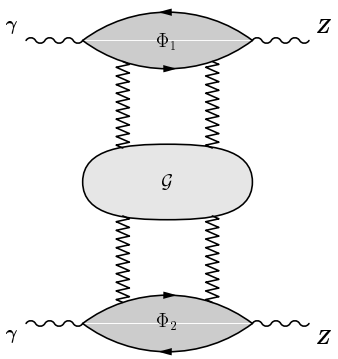

Figure 2.7: The BFKL exchange in the $\gamma\gamma \to ZZ$ elastic cross section.

2.3 QCD corrections to $\gamma\gamma \to ZZ$

In order to calculate the magnitude of QCD corrections, one has to switch to a definite process. This process will be $\gamma\gamma \to ZZ$, which was used also for the computation of the two-loop electroweak corrections. This provides a direct comparison between the two type of corrections.

2.3.1 Impact factors

The amplitude of this process in the high energy limit is illustrated in Fig. 2.7. The ingredients needed have been discussed in sections 2.1 and 2.2. To proceed with an explicit calculation we have to specify the couplings C_f, which depend on the external bosons, and the virtualities appearing in the impact factors given in equations (2.14) and (2.18). The starting expressions are for massive quarks. For practical purposes only the top quark mass has to be taken into account, since the quark masses are accompanied by the large Z mass. The integrals which correspond to the quark loop have to be performed. The last integration we compute is the convolution of the impact factors with the BFKL states (2.82) and (2.86).

We calculate this process for all external bosons on-shell. In such a case we have Q_+^2 identically zero and $Q_-^2 = -M_Z^2$. The coupling constants C_f - the product of the γ-quark and Z-quark couplings - are given by:

$$C_f = \frac{4\pi\alpha_{em}}{2\sin\theta_w\cos\theta_w}\left\{q_f T_f^3 - 2\,q_f^2\sin^2\theta_w\right\}\,. \tag{2.89}$$

First we consider the scattering of the photons into transverse Z bosons. To proceed we have to solve the remaining integrations for the impact factor Φ_{TT} in (2.14). In order to compute the integral over the two dimensional Euclidean

vector $\mathbf{u}$ we employ a standard Feynman parametrisation and rewrite (2.14) as:

$$\begin{aligned}
\Phi_{TT}^{(ij)}(q,k,l) &= \alpha_s\sqrt{N_c^2-1}\sum_f C_f\sqrt{4\pi}\int_0^1 d\alpha\int\frac{d^2\mathbf{u}}{(2\pi)^2}\int_0^1 dx \\
&\times \left\{\frac{4\alpha(1-\alpha)[\boldsymbol{\epsilon}_i\cdot\mathbf{u}\;\boldsymbol{\epsilon}_j^*\cdot\mathbf{u}-x(1-x)\boldsymbol{\epsilon}_i\cdot\mathbf{p_a}\;\boldsymbol{\epsilon}_j^*\cdot\mathbf{p_a}]}{[u^2+x(1-x)p_a^2-xm+m_f^2]^2}\right. \\
&- \frac{(u^2-x(1-x)p_a^2+m_f^2)(\boldsymbol{\epsilon}_i\cdot\boldsymbol{\epsilon}_j^*)}{[u^2+x(1-x)p_a^2-xm+m_f^2]^2} \\
&- \frac{4\alpha(1-\alpha)[\boldsymbol{\epsilon}_i\cdot\mathbf{u}\;\boldsymbol{\epsilon}_j^*\cdot\mathbf{u}-x(1-x)\boldsymbol{\epsilon}_i\cdot\mathbf{p_b}\;\boldsymbol{\epsilon}_j^*\cdot\mathbf{p_b}]}{[u^2+x(1-x)p_b^2-xm+m_f^2]^2} \\
&+ \left.\frac{(u^2-x(1-x)p_b^2+m_f^2)(\boldsymbol{\epsilon}_i\cdot\boldsymbol{\epsilon}_j^*)}{[u^2+x(1-x)p_b^2-xm+m_f^2]^2}\right\}. \qquad (2.90)
\end{aligned}$$

Here we have defined $\mathbf{p_a}=-\mathbf{k}-(1-2\alpha)\mathbf{l}$, $\mathbf{p_b}=2\alpha\mathbf{l}$ and $m=\alpha(1-\alpha)(M_Z^2+i\epsilon)$. Strictly speaking, at this stage of the calculation m is taken negative and subsequently, after having performed the integrations, analytically continued to positive values obtaining the above definition. The first fraction corresponds to the two diagrams where one of the gluons is attached to the quark and the other to the antiquark. The second fraction corresponds to the two diagrams where the two gluons are attached to the same (anti)quark. Each of them would lead to a divergent integral but, of course, the sum in (2.90) gives a finite result.

On performing the $\mathbf{u}$ integration we end up with:

$$\begin{aligned}
\Phi_{TT}^{(ij)}(q,k,l) &= \alpha_s\sqrt{N_c^2-1}\sum_f C_f\sqrt{4\pi}\int_0^1\frac{d\alpha}{2\pi}\int_0^1 dx \qquad (2.91)\\
&\times \left\{-4\alpha(1-\alpha)\,x(1-x)\right. \\
&\times \left(\frac{\boldsymbol{\epsilon}_i\cdot\mathbf{p_a}\;\boldsymbol{\epsilon}_j^*\cdot\mathbf{p_a}}{x(1-x)p_a^2-xm+m_f^2}-\frac{\boldsymbol{\epsilon}_i\cdot\mathbf{p_b}\;\boldsymbol{\epsilon}_j^*\cdot\mathbf{p_b}}{x(1-x)p_b^2-xm+m_f^2}\right) \\
&+ \boldsymbol{\epsilon}_i\cdot\boldsymbol{\epsilon}_j^*\left([\alpha^2+(1-\alpha)^2]\ln\left[\frac{x(1-x)p_a^2-xm+m_f^2}{x(1-x)p_b^2-xm+m_f^2}\right]\right. \\
&+ \left.\left.\frac{x(1-x)p_a^2-m_f^2}{x(1-x)p_a^2-xm+m_f^2}-\frac{x(1-x)p_b^2-m_f^2}{x(1-x)p_b^2-xm+m_f^2}\right)\right\}.
\end{aligned}$$

The computation of the x-integration is straightforward. For example the he-

licity conserving part gives:

$$
\begin{aligned}
&\Phi_{TT}^{(++)}(q,k,l) \\
&= \alpha_s \sqrt{N_c^2-1} \sum_f C_f \frac{1}{\sqrt{\pi}} \int_0^1 d\alpha \left\{ [\alpha^2 + (1-\alpha)^2] \times \right. \\
&\times \left[\frac{p_a^2 - m + 2\,m_f^2}{2\,\Delta_a} \left(\log\left[\frac{-m - p_a^2 - \Delta_a}{-m - p_a^2 + \Delta_a} \right] - \log\left[\frac{-m + p_a^2 - \Delta_a}{-m + p_a^2 + \Delta_a} \right] \right) \right. \\
&- \left. \frac{p_b^2 - m + 2\,m_f^2}{2\,\Delta_b} \left(\log\left[\frac{-m - p_b^2 - \Delta_b}{-m - p_b^2 + \Delta_b} \right] - \log\left[\frac{-m + p_b^2 - \Delta_b}{-m + p_b^2 + \Delta_b} \right] \right) \right] \\
&- \frac{m_f^2}{\Delta_a} \left(\log\left[\frac{-m - p_a^2 - \Delta_a}{-m - p_a^2 + \Delta_a} \right] - \log\left[\frac{-m + p_a^2 - \Delta_a}{-m + p_a^2 + \Delta_a} \right] \right) \\
&+ \left. \frac{m_f^2}{\Delta_b} \left(\log\left[\frac{-m - p_b^2 - \Delta_b}{-m - p_b^2 + \Delta_b} \right] - \log\left[\frac{-m + p_b^2 - \Delta_b}{-m + p_b^2 + \Delta_b} \right] \right) \right\} , \qquad (2.92)
\end{aligned}
$$

This formula has to be used to the determination of the top-quark contribution, whereas the remaining α integration was done numerically. For all the other quarks the masses can be neglected. This limit $m_f \to 0$ preserves a significant simplification compared to the massive case. In this limit all integrations could be done analytically for the helicity conserving impact factor. After the integration in the Feynman parameter variable, one obtains in the zero quark mass limit of (2.91) for the separate helicity states:

$$
\begin{aligned}
\Phi_{TT}^{(++)}(q,k,l) &= \alpha_s \sqrt{N_c^2-1} \sum_f C_f \sqrt{4\pi} \int_0^1 \frac{d\alpha}{2\pi} \\
&\times [\alpha^2 + (1-\alpha)^2] \, \ln\left[\frac{p_a^2 - m}{p_b^2 - m} \right] \qquad (2.93) \\
\Phi_{TT}^{(--)}(q,k,l) &= \Phi_{TT}^{(++)}(q,k,l) \qquad (2.94) \\
\Phi_{TT}^{(+-)}(q,k,l) &= i\,\alpha_s \sqrt{N_c^2-1} \sum_f C_f \sqrt{4\pi} \int_0^1 \frac{d\alpha}{2\pi}\, 4\alpha(1-\alpha) \\
&\times \left\{ \frac{p_a^x p_a^y}{p_a^2} \left(1 + \frac{m}{p_a^2} \ln\left[\frac{p_a^2 - m}{-m} \right] \right) \right. \\
&- \left. \frac{p_b^x p_b^y}{p_b^2} \left(1 + \frac{m}{p_b^2} \ln\left[\frac{p_b^2 - m}{-m} \right] \right) \right\} \qquad (2.95) \\
\Phi_{TT}^{(-+)}(q,k,l) &= -\Phi_{TT}^{(+-)}(q,k,l)\,, \qquad (2.96)
\end{aligned}
$$

with $(p^x, p^y) = \mathbf{p}$. For the result with massive quarks a numerical integration has been performed. For the helicity conserving parts in the massless quark limit the remaining α integration was also performed analytically, giving the

result:

$$\begin{aligned}
\Phi_{TT}^{(++)}(q,k,l) &= \alpha_s\sqrt{N_c^2-1}\sum_f C_f\,\frac{1}{\sqrt{\pi}}\left\{2\left(x_1-x_1^2+x_2-x_2^2\right)\right.\\
&+ \left(2-3\,x_1+3\,x_1^2-2\,x_1^3\right)\log(1-x_1)\\
&+ \left(3\,x_1-3\,x_1^2+2\,x_1^3\right)\log(-x_1)+\\
&+ \left(2-3\,x_2+3\,x_2^2-2\,x_2^3\right)\log(1-x_2)\\
&+ \left(3\,x_2-3\,x_2^2+2\,x_2^3\right)\log(-x_2)+\\
&+ \frac{1}{3a^3}\left[d\,\left(-3\,a^2+3\,a\,d+2\,d^2\right)\,\log(\frac{d}{a})+\right.\\
&+ \left.\left.(a+d)\left(2\,a\,d-\left(2\,a^2+a\,d+2\,d^2\right)\,\log(1+\frac{d}{a})\right)\right]\right\}\,,
\end{aligned}\tag{2.97}$$

with

$$\begin{aligned}
a &= 4\,\mathbf{l}^2+M_Z^2+i\epsilon\\
b &= -4(\mathbf{l^2}+\mathbf{kl})-M_Z^2-i\epsilon\\
c &= (\mathbf{k}+\mathbf{l})^2\\
d &= -M_Z^2-i\epsilon\\
x_{1,2} &= \frac{-b\pm\sqrt{b^2-4ac}}{2a}.
\end{aligned}\tag{2.98}$$

In the same way one can calculate the scattering of real photons into longitudinal Z bosons and obtain:

$$\begin{aligned}
\Phi_{TL}^{(i)}(q,k,l) &= \alpha_s\sqrt{N_c^2-1}\sum_f C_f\,\frac{2}{\sqrt{\pi}}M_Z\int_0^1 d\alpha\,\alpha(1-\alpha)(1-2\alpha)\\
&\times \left\{\left[\frac{\boldsymbol{\epsilon}_i\cdot\mathbf{p_b}}{2\,p_b^2}\left(\frac{p_b^2-m}{\Delta_b}\left(\log\left[\frac{-m-p_b^2-\Delta_b}{-m-p_b^2+\Delta_b}\right]\right.\right.\right.\right.\\
&- \left.\left.\left.\left.\log\left[\frac{-m+p_b^2-\Delta_b}{-m+p_b^2+\Delta_b}\right]-\log\left[\frac{m_f^2-m}{m_f^2}\right]\right)\right)\right]\\
&- \left[\frac{\boldsymbol{\epsilon}_i\cdot\mathbf{p_a}}{2\,p_a^2}\left(\frac{p_a^2-m}{\Delta_a}\left(\log\left[\frac{-m-p_a^2-\Delta_a}{-m-p_a^2+\Delta_a}\right]\right.\right.\right.\\
&- \left.\left.\left.\left.\log\left[\frac{-m+p_a^2-\Delta_a}{-m+p_a^2+\Delta_a}\right]-\log\left[\frac{m_f^2-m}{m_f^2}\right]\right)\right)\right]\right\},
\end{aligned}\tag{2.99}$$

with

$$\begin{aligned}
\Delta_a &= \sqrt{(p_a^2-m)^2+4m_f^2\,p_a^2}\,,\\
\Delta_b &= \sqrt{(p_b^2-m)^2+4m_f^2\,p_b^2}\,,
\end{aligned}\tag{2.100}$$

Taking the limit $m_f \to 0$ this reduces to the simpler expression:

$$\Phi^{(i)}_{TL}(q,k,l) = \alpha_s \sqrt{N_c^2-1} \sum_f C_f \, 2\sqrt{4\pi}\, M_Z \int_0^1 \frac{d\alpha}{2\pi}\ \alpha(1-\alpha)(1-2\alpha) \times \\ \times \left\{ \frac{\boldsymbol{\epsilon}_i \cdot \mathbf{p_b}}{p_b^2} \ln\left[\frac{p_b^2 - m}{-m}\right] - \frac{\boldsymbol{\epsilon}_i \cdot \mathbf{p_a}}{p_a^2} \ln\left[\frac{p_a^2 - m}{-m}\right] \right\}. \tag{2.101}$$

In order to compute the two-gluon or the BFKL amplitude one has to substitute these expressions into (2.1) or (2.82, 2.86).

2.3.2 Numerical results

In this section we present numerical results on the QCD corrections for ZZ pair production in $\gamma\gamma$ collisions. Here we consider full circular polarisation of the incoming photons. In terms of the electroweak and QCD amplitudes (2.83,2.88) the cross section reads:

$$\frac{d\sigma}{dp_T^2} = \frac{1}{16\pi s^2} |A_{EW} + A_{QCD}|^2 \tag{2.102}$$

where $p_T = |2\,\mathbf{l}|$ is the exchanged transverse momenta. The angular distribution of the cross section is obtained by the relation:

$$dt = \frac{s}{2}\beta\ d\cos\theta\,, \tag{2.103}$$

with $\beta = \sqrt{1 - 4M_Z^2/s}$. The QCD part of the amplitude was calculated in the high-energy (Regge) approximation. Since in this approximation the helicity changing parts of the electroweak amplitude are suppressed by powers of s and thus are negligible, we need the full one loop result of the electroweak part. The corrections to the pure electroweak amplitude are dictated by the interference term.

The electroweak part of the amplitude was first computed in a full one loop calculation by Jikia [33] for Higgs masses over 300 GeV. In order to compute the above mentioned interference term, the results of [33] have been reproduced, however we used in this computation an up to date value of the top quark mass and a Higgs mass of $m_H = 115$ GeV. We adopted the definition of momenta and polarisation vectors from [36]. The Feynman diagrams were generated with *FeynArts* [35] and the resulting amplitudes were algebraically simplified using *FormCalc* [36]. To evaluate the one-loop integrals the package *LoopTools* [36, 37] was used. At small scattering angles the main contribution to the amplitude comes from the bosonic loop of the helicity conserving channel. These amplitudes are mainly imaginary and proportional to s in this kinematical limit, in agreement with the calculation of the high-energy approximation. For the helicity flip channels no contributions proportional to s survive, thus these

amplitudes are suppressed by one power of s compared to the helicity conserving cases. This results in the fact that the helicity flip parts of the cross section are for light Higgs masses about three orders of magnitude smaller than the helicity conserving parts and decrease further with growing s. If one of the Z bosons has transverse and the other longitudinal polarisation, the amplitude is vanishing at the forward point ($p_T = 0$) due to angular momentum conservation.

In the QCD part of the amplitude we have been discarding all quark masses apart from the top quark mass in the numerical calculation, since they are always accompanied by the Z mass and thus are negligible. The inclusion of the top quark mass reduces the QCD amplitude by 25%. For small scattering angles in the high-energy approximation the two incoming and two outgoing particles do not 'communicate' with each other because of the huge separation in rapidity. As a result, the amplitude with the helicity $++ \to ++$ is equal to the amplitude with helicity $+- \to +-$ etc. Since the helicity conserving amplitudes completely dominate the cross section, after the summation of outgoing helicities the result is the same for all the possibilities of incoming helicities, i.e. $++ \to$ TT is equal to $+- \to$ TT etc. In the following $\gamma\gamma \to Z_T Z_T$ stands for all these possibilities as well as for unpolarised scattering. In the same manner $++ \to$ LL is equal to $+- \to$ LL etc. The BFKL part of the amplitude will be also discussed as the pure QCD contribution alone. The mass of the Higgs boson was set to $m_H = 115$ GeV unless a different value is stated and the parameters $\alpha_W = \alpha/s_W^2$, $\alpha = 1/128$, $m_Z = 91.2$ GeV, $m_t = 174.3$ GeV and $\alpha_s(s_0)$ have been used throughout the numerical computations.

Let us consider the QCD corrections. In the Born analysis, from the naive counting of the couplings (see Fig. 2.1), one expects in the interference term a suppression, with respect to the one loop EW case, due to the factor α_s^2 and an additional suppression of a factor ≈ 4 due to the difference in the EW couplings. This would lead to corrections of less than a percent. At high energies in the Regge limit we expect an enhancement due to the appearance of some large logarithms, which may be resummed in the BFKL scheme. We stress that the resummed leading log QCD corrections at the lower energies we consider are overshooting what is expected from the real contribution, nevertheless they provide a first estimate. We remind, as discussed previously, that the BFKL resummation is evaluated in the saddle point approximation.

Fig. 2.8 displays the differential cross section at a centre of mass energy of $\sqrt{s_{\gamma\gamma}} = 1$ TeV. The upper plot displays the cross section versus $\cos\theta_Z$, where θ_Z is the scattering angle. The lower plot displays the cross section versus the exchanged transverse momenta. In the remaining plots we present the results always versus the exchanged transverse momenta. The transition between the two presentations is achieved via (2.103). At 1 TeV $p_T^2/M_Z^2 = 4$ corresponds to values of $\cos\theta$ (where θ is the scattering angle) of 0.90. The solid line is the pure electroweak cross section, and the dashed line is the one with the QCD corrections included, (2.102). The cross section has a slight rise approaching the forward region. This slight rise comes from the electroweak part since it completely dominates the amplitude. As in the following will become clear,

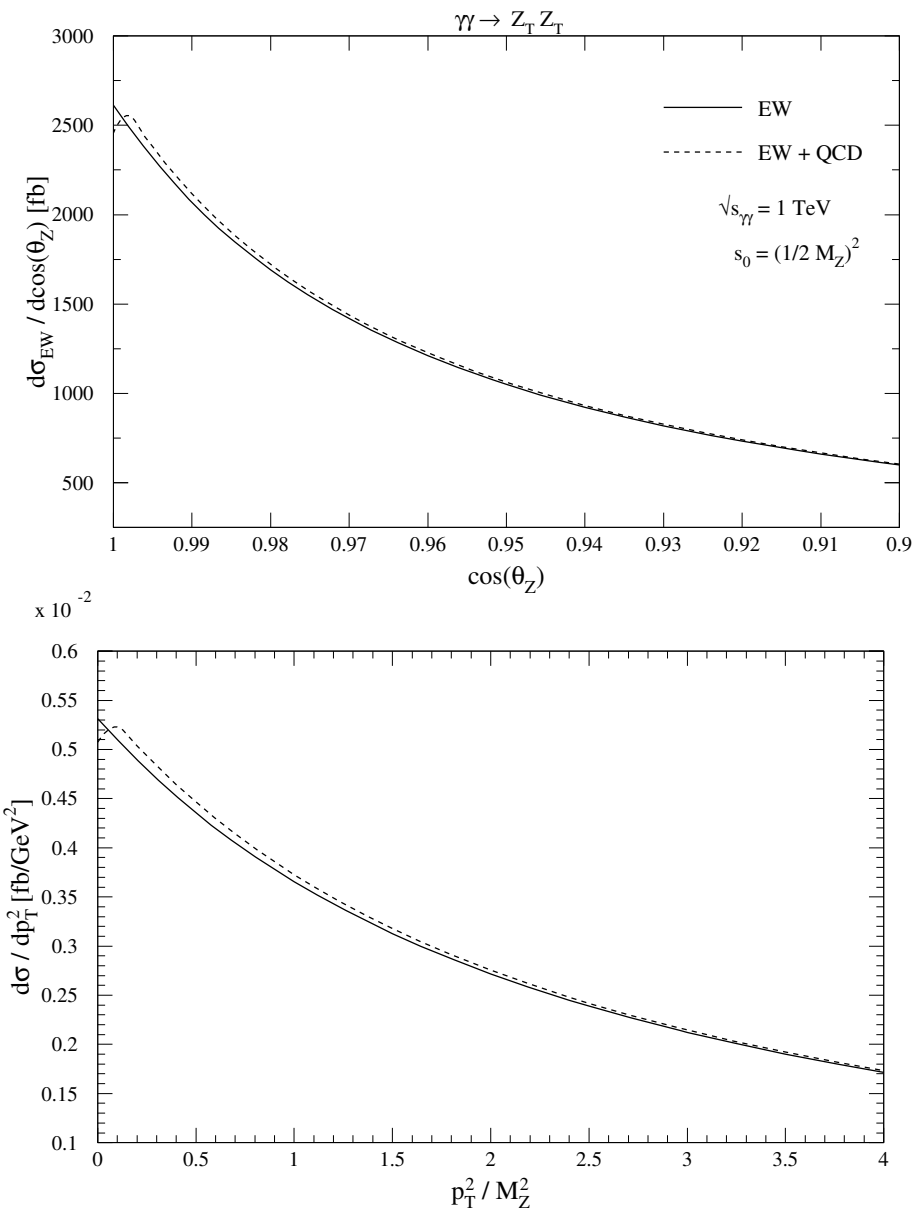

Figure 2.8: The pure EW differential cross section (solid line) and the one which include the QCD corrections (dashed line). In the upper plot the cross section is versus $\cos\theta_Z$, while in the lower one its versus the exchanged transverse momenta. For the BFKL contribution the scale $s_0 = (1/2M_Z)^2$ was used.

for the QCD part of the cross section the rise approaching the forward region is much stronger. Therefore the QCD corrections are enhanced close to the forward region.

This behaviour is shown in Fig. 2.9 and 2.10, where the QCD corrections to the differential cross section of transverse Z bosons relative to the pure electroweak contribution are plotted. This relative correction is defined as

$$\Delta = \left(\frac{d\sigma_{QCD+EW}}{dp_T^2} - \frac{d\sigma_{EW}}{dp_T^2} \right) \Big/ \frac{d\sigma_{EW}}{dp_T^2} \ , \tag{2.104}$$

and is plotted for centre of mass energies of 500 GeV, 800 GeV, 1.5 TeV and 3 TeV as functions of p_T^2/M_Z^2. At these energies $p_T^2/M_Z^2 = 4$ corresponds to values of $\cos\theta$ of 0.75, 0.90, 0.97 and 0.99 respectively. Thus, for rising energy the scattering angle will be continuously smaller for the same p_T values. For a TESLA detector it was proposed that the tracker system will reach values $\cos\theta < 0.993$, in this range one has a good measurement possibility [49]. Moreover, the decay products of the Z bosons will carry also transverse momenta, thus these particles can have bigger angles from the beam pipe.

Since for leading order BFKL the scale is not fixed, there is an uncertainty which affects the magnitude of the QCD corrections. The solid lines in Fig. 2.9 and 2.10 are results for the scale $s_0 = (1/2\ M_Z)^2$ while the dashed lines correspond to $s_0 = M_Z^2$. At the scale $s_0 = M_Z^2$ the minimal centre of mass energy $\sqrt{s}$, for which the saddle point approximation for the leading logarithmic calculations gives a reliable result, is 800 GeV. The electroweak amplitude is mainly imaginary, therefore, from the QCD amplitude it will be also the imaginary part which mainly accounts for the interference term. Corrections resulting from leading order BFKL contribution are at the percent level. For higher p_T they are about one percent and approaching the forward region (smaller p_T values) they rise and lead to corrections of a few percent. Close to the forward region the sign of the corrections is changing as a result of the fact that for small $\mathbf{l}$ the imaginary part of Φ_h (2.82) gets an enhancement. Fig. 2.9 and Fig. 2.10 summarise the dependencies of the corrections resulting from leading order BFKL calculations with respect to the centre of mass energy $\sqrt{s}$, the exchanged transverse momenta p_T and the scale s_0. For rising centre of mass energy the corrections increase. The solid lines ($s_0 = (1/2\ M_Z)^2$) in Fig. 2.9 and in Fig. 2.10 show that the corrections may rise in this regime by a factor of 2 if the energy increases from 500 GeV to 3 TeV. This is due to the leading log BFKL resummation and is dictated by the Pomeron intercept. The scale s_0 implicates also a strong dependence. In fact close to the forward region the corrections also grow by a factor of 2 if the scale is decreasing from $s_0 = M_Z^2$ to $s_0 = (1/2\ M_Z)^2$. The biggest dependence is coming from the exchanged momenta or equivalently from the scattering angle. The corrections have a strong rise with decreasing scattering angle or p_T and change sign close to the forward region.

Next we discuss the helicity breaking cross sections. The most important property of the helicity flip amplitudes is that the electroweak parts are not anymore

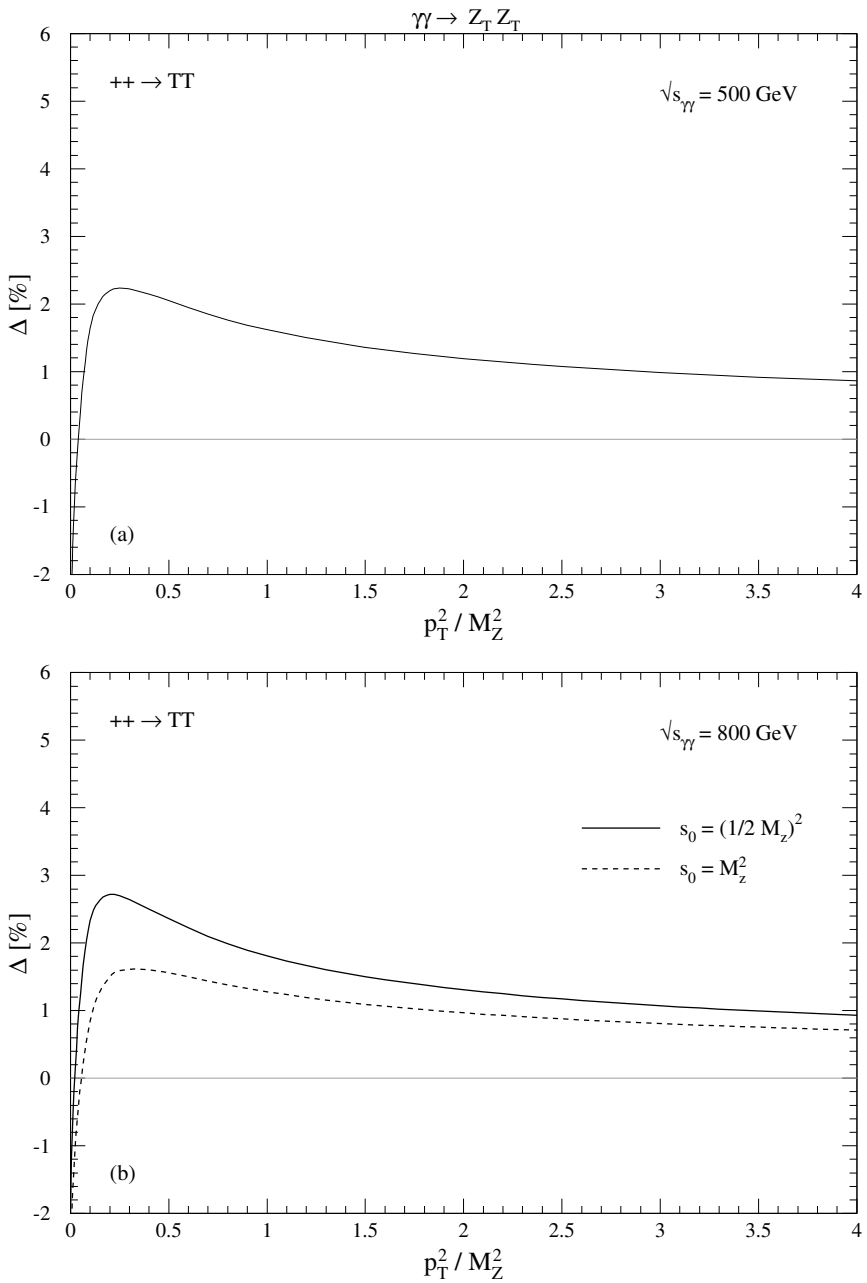

Figure 2.9: QCD corrections to the differential cross section relative to the pure EW contribution for different scales s_0 and centre of mass energies $\sqrt{s}$. The relative correction is defined as $\Delta = (\frac{d\sigma_{QCD+EW}}{dp_T^2} - \frac{d\sigma_{EW}}{dp_T^2})/\frac{d\sigma_{EW}}{dp_T^2}$.

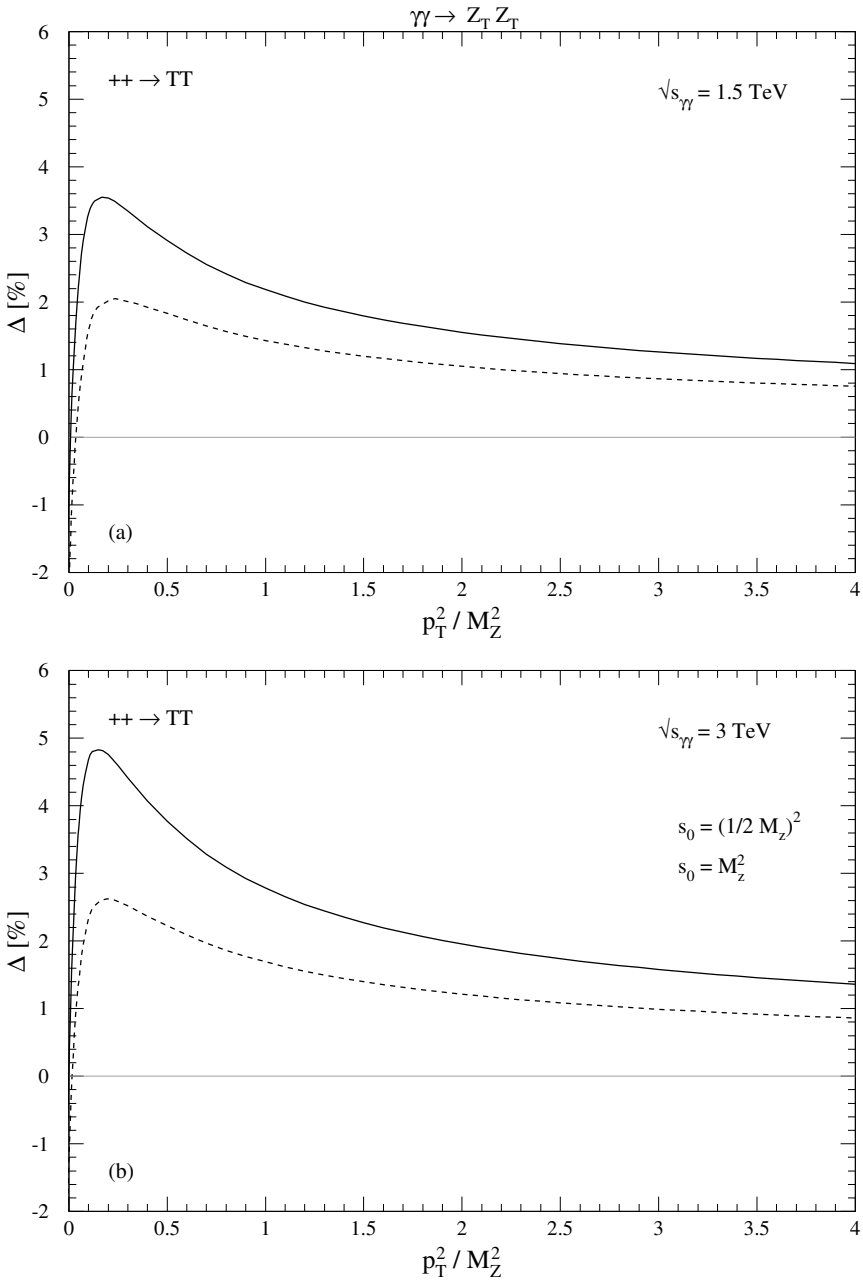

Figure 2.10: QCD corrections to the differential cross section relative to the pure EW contribution for different scales s_0 and centre of mass energies $\sqrt{s}$. The relative correction is defined as $\Delta = (\frac{d\sigma_{QCD+EW}}{dp_T^2} - \frac{d\sigma_{EW}}{dp_T^2})/\frac{d\sigma_{EW}}{dp_T^2}$.

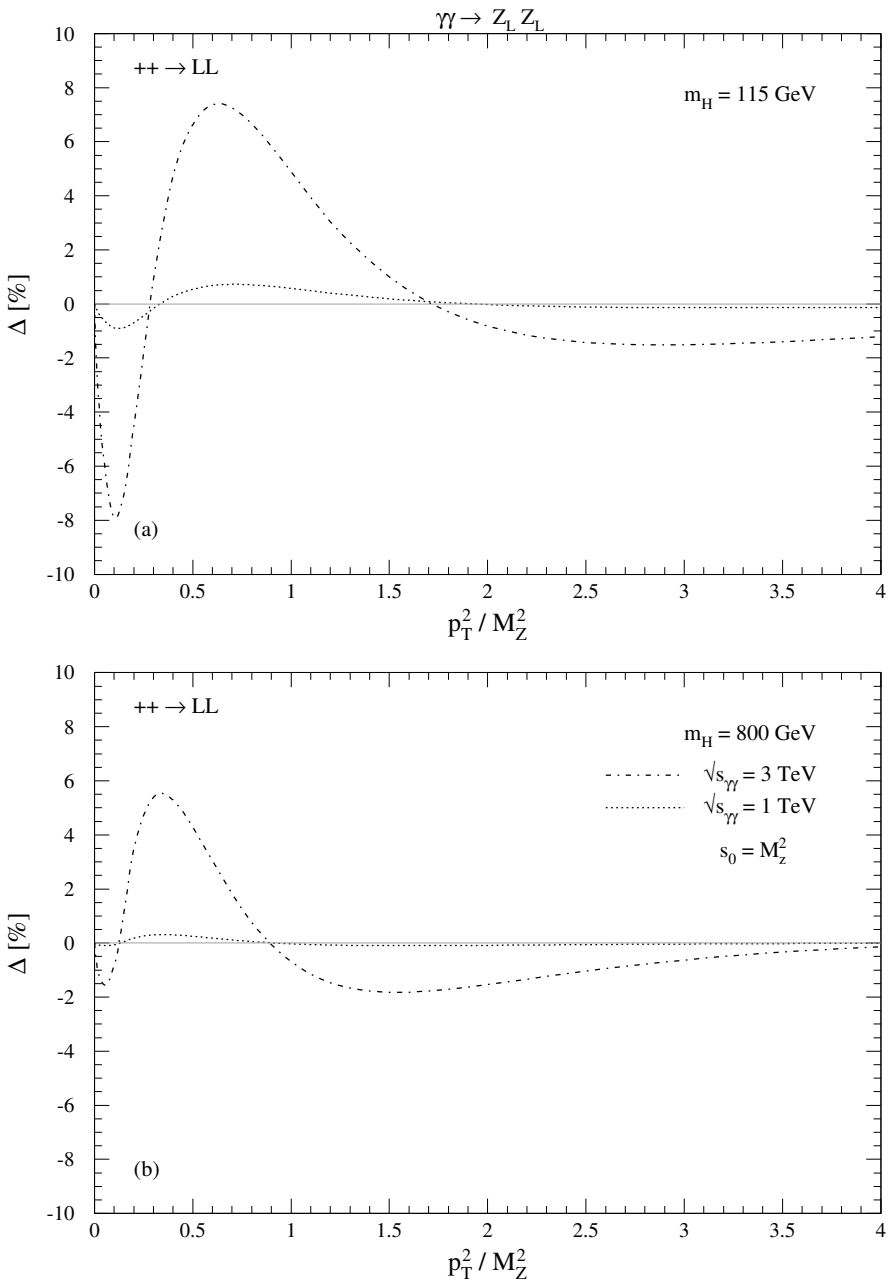

Figure 2.11: QCD corrections to the differential cross section relative to the pure EW contribution for different scales s_0 and centre of mass energies $\sqrt{s}$. The relative correction is defined as $\Delta = (\frac{d\sigma_{QCD+EW}}{dp_T^2} - \frac{d\sigma_{EW}}{dp_T^2})/\frac{d\sigma_{EW}}{dp_T^2}$.

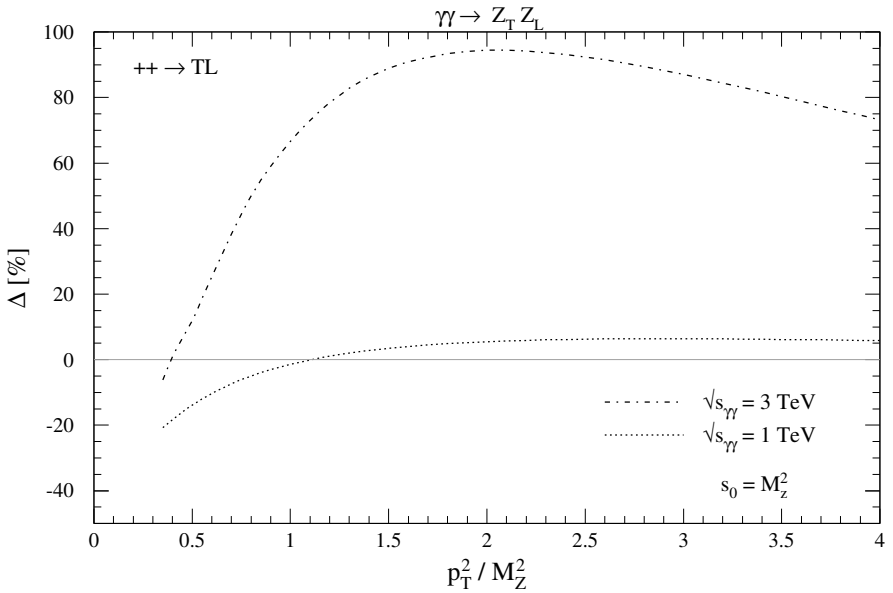

Figure 2.12: QCD corrections to the differential cross section relative to the pure EW contribution for different scales s_0 and centre of mass energies $\sqrt{s}$. The relative correction is defined as $\Delta = (\frac{d\sigma_{QCD+EW}}{dp_T^2} - \frac{d\sigma_{EW}}{dp_T^2})/\frac{d\sigma_{EW}}{dp_T^2}$.

proportional to s as the helicity conserving parts were, so they are suppressed by one power of s compared to the QCD part of the amplitude. As a consequence the QCD corrections in comparison to the electroweak part will increase rapidly with the scattering energy, they vanish only for $p_T = 0$. This appears in Fig. 2.11(a) where the relative QCD corrections are plotted for longitudinally polarised Z bosons. The dotted lines show corrections for a centre of mass energy of 1 TeV, while the dotted-dashed lines are corrections for 3 TeV. The scale s_0 was set in both cases as $s_0 = M_Z^2$. The corrections first rise when p_T is becoming smaller but they vanish for $p_T = 0$. For 1 TeV the corrections are less than 1%, but for 3 TeV they rise up to 8%. This strong rise is dominating by the different s dependence between the electroweak and QCD amplitude. The additional rise coming from the BFKL resummation is negligible compared to this effect. While the electroweak part of the amplitude was mainly imaginary in the helicity conserving cases, here real and imaginary parts are of the same order. The oscillations visible in the plot are coming entirely from the QCD part of the amplitude. There the real and imaginary parts of the helicity flip impact factors are oscillating with p_T but shifted in a way that the absolute value of the amplitude gives a smooth function (as we will see in Fig. 2.17). For higher Higgs masses the real part of the electroweak amplitude gets an enhancement from the Higgs pole contribution, thus the form of the corrections is changing. This is illustrated in Fig. 2.11(b) where the calculation was done

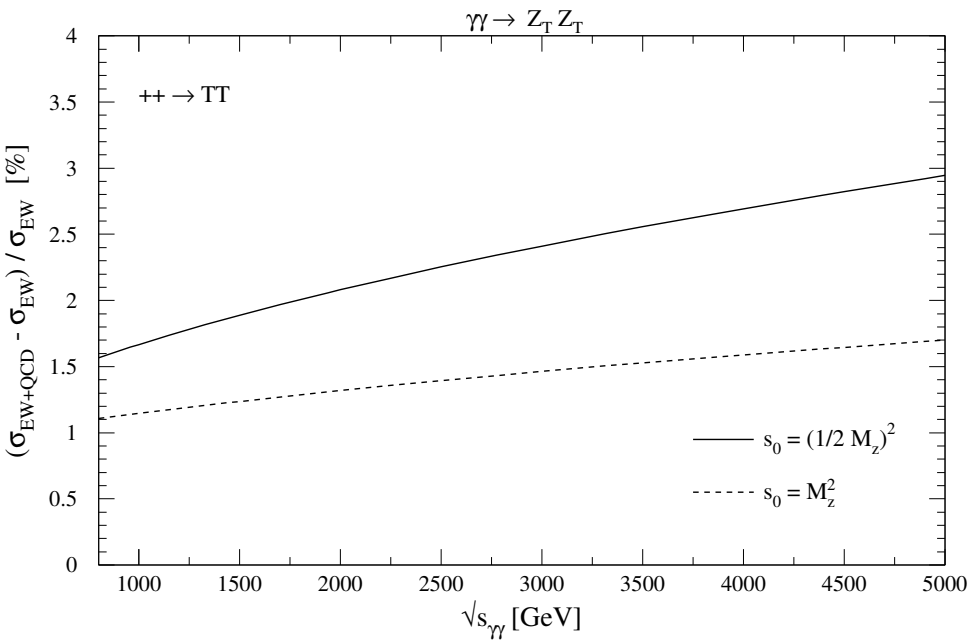

Figure 2.13: The QCD corrections to the integrated cross section relative to the pure EW contribution for different scales. The integration region was chosen as $0 < p_T < 4\,M_Z^2$.

for a Higgs mass of $m_H = 800$ GeV.

In Fig. 2.12 relative corrections are plotted where one of the Z bosons is transverse and the other longitudinally polarised. Again, the dotted lines are for $s = 1$ TeV while the dotted-dashed are for $s = 3$ TeV. The most striking property of these corrections is their magnitude, they can be as high as 100% already at $s = 3$ TeV. This is due to the fact that here the EW part of the amplitude is smaller but the QCD part is bigger in comparison with the case where both Z bosons are longitudinally polarised. The enhancement of the QCD part is coming from the helicity conserving impact factor Φ, which is separated by a huge rapidity gap from the suppressed helicity flip impact factor. On the other hand, the QCD part is vanishing for $p_T = 0$ since the helicity flip impact factor does. Because of the dominance of the helicity conserving impact factor, the oscillations coming from the helicity flip impact factor are not visible any more. We observe here again corrections which rise if p_T is getting smaller. Both, electroweak and QCD parts of the amplitude have to vanish for the case of forward scattering due to angular momentum conservation. Since the QCD part has its turning point for bigger p_T, approaching the forward point the corrections are decreasing. We did not plotted corrections up to $p_T = 0$, since (2.104) lacks of definition at the forward point, where both amplitudes are vanishing. Again, here the corrections rise strongly with s, since the electroweak amplitude is

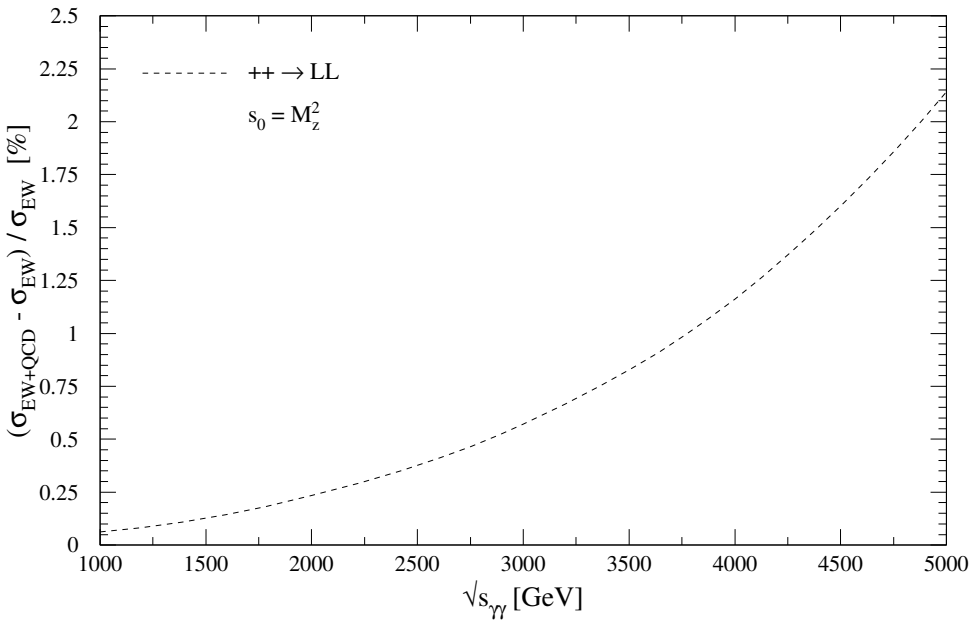

Figure 2.14: The QCD corrections to the integrated cross section relative to the pure EW contribution for different scales. The integration region was chosen as $0 < p_T < 4\,M_Z^2$.

suppressed by one power of s compared to the QCD one. The relative corrections are approximately one order of magnitude bigger if s grows from 1 to 3 TeV. The rise resulting from the BFKL resummation is again negligible in this context.

Next we display corrections to the integrated cross section. The high energy approximation on which the QCD calculation is based, is for a kinematical range where $s \gg -t$. Thus, for the corrections to the integrated cross section we integrated only up to $p_T^2 = 4M_Z^2$, since for high p_T the QCD calculation is loosing its validity. In Fig. 2.13 these relative corrections to the integrated cross section $(\sigma_{EW+QCD} - \sigma_{EW})/\sigma_{EW}$ are plotted as a function of the centre of mass energy for the helicity conserving case, i.e. transverse Z production. In this integration range the corrections are around one percent and they have a slight rise due to the BFKL resummation, since (up to powers of logarithms) electroweak and QCD amplitudes have the same behaviour in s. The magnitude of the corrections is again scale dependent and the rise is stronger for smaller scales, as expected. If one integrates over all scattering angles the corrections become less important, but since the main contribution of the cross section is coming from small scattering angles the result would not be strongly affected.

Fig. 2.14 displays the same relative integrated corrections but with two longitudinal Z bosons in the final state. In this helicity breaking part the electroweak

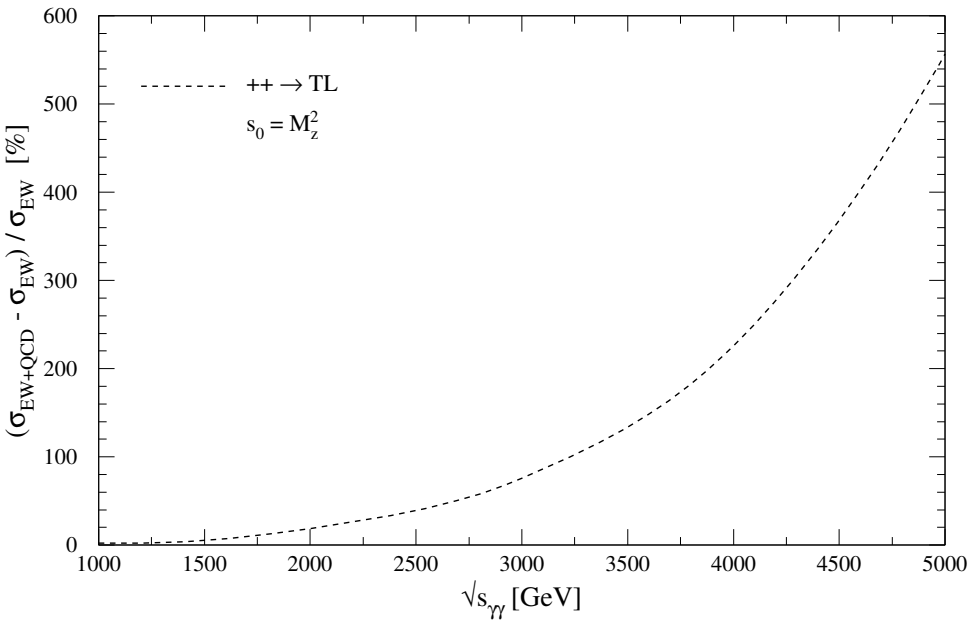

Figure 2.15: The QCD corrections to the integrated cross section relative to the pure EW contribution for different scales. The integration region was chosen as $1/4\, M_Z^2 < p_T < 4\, M_Z^2$.

amplitude is suppressed by one power of s in comparison to the QCD amplitude, so the corrections rise rapidly with the scattering energy. The rise from the BFKL resummation is negligible. The smallness of the corrections in the integrated cross section is due to the fact that the corrections to the differential cross section, Fig. 2.11, are changing sign with p_T varying, presenting an oscillating behaviour.

In Fig. 2.15 again corrections to the helicity flip cross section are plotted, but here one of the Z bosons is transverse polarised. Due to the different s behaviour of the amplitudes again a strong rise of the corrections with s is present. These are very big, for higher energies the QCD part of the amplitude completely dominates this part of the cross section. The magnitude of these corrections is mainly due to the helicity conserving impact factor Φ of the QCD amplitude. The integration was done down to $p_T^2 = 1/2M_Z^2$, because the relative corrections lose they meaning for $p_T = 0$, since both amplitudes are vanishing at the forward point.

In the following figures some properties of the pure QCD part of the amplitude are discussed. In Fig. 2.16 the absolute value of the QCD amplitudes is displayed for the helicity conserving case. The solid line is the BFKL (resummed) contribution while the dashed line is the Born (two-gluon) contribution. At $\sqrt{s} = 1$ TeV the gluon resummation is enhancing the pure QCD Born ampli-

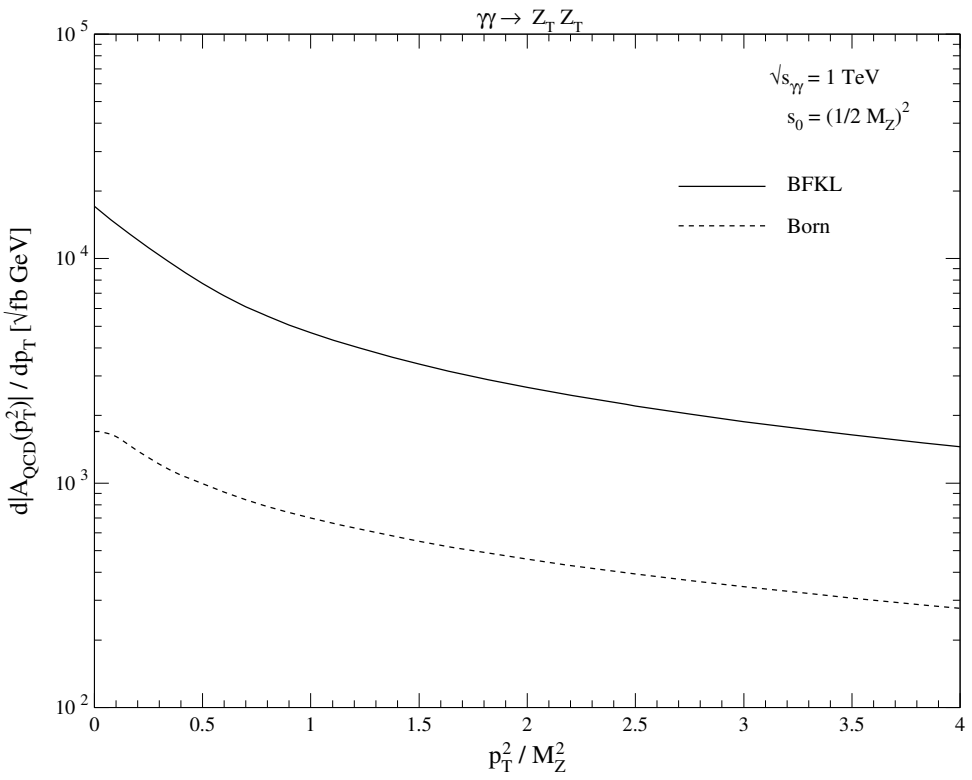

Figure 2.16: The pure QCD part of the amplitude versus the exchanged transverse momenta. The solid line is the BFKL contribution and the dashed line is the QCD Born approximation (two-gluon amplitude).

tude by one order of magnitude. The same enhancement is visible in the QCD corrections to the electroweak cross section. Both amplitudes are rising with decreasing p_T, whereas for higher energies the rise of the resummed amplitude will be stronger as the Born one.

In Fig. 2.17 the absolute value of the two helicity changing parts of the amplitude at $\sqrt{s} = 1$TeV are plotted. The most noticeable property is that the helicity changing parts are suppressed by more than two orders of magnitude with respect to the helicity conserving part. The $++ \to --$ cross section has, apart from its magnitude, properties similar to $++ \to ++$, for example its slope as a function of p_T. The $++ \to LL$ part is also rising when p_T is getting smaller but in the region of $p_T = 1/2\, M_Z$ it has an extremum and is steeply going to zero for $p_T = 0$. This behaviour comes from the different symmetry behaviour of the two involved impact factors, as discussed in chapter 2.1.

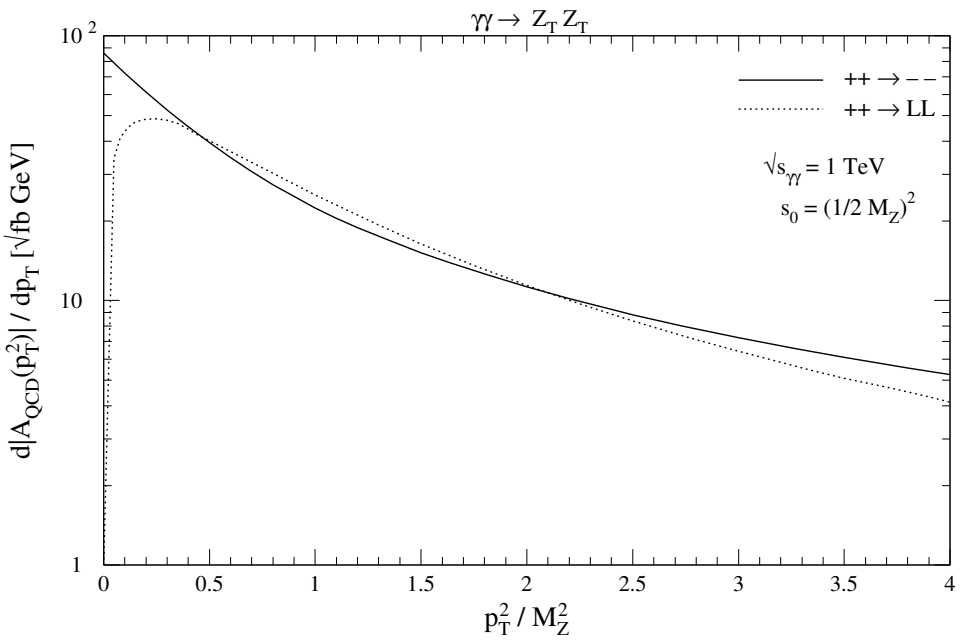

Figure 2.17: The same as Fig. 2.16 for the helicity changing parts of the BFKL contribution.

2.3.3 Summary of section 2.3

In summary, we have computed QCD corrections for $\gamma\gamma \to ZZ$ at high centre of mass energies in the kinematical region of small scattering angles. We have considered the exchange of BFKL gluon ladders which couple to the incoming photons via $\gamma \to Z$ impact factors. The electroweak part was computed in a full one loop calculation, and a complete analysis involving all helicity channels has been done.

In the helicity conserving channel the corrections are at the order of a few percent for $s = O(1\text{ TeV})$ and they show a moderate rise with the scattering energy. In the helicity flip channels the QCD corrections are at the same level for $s = O(1\text{ TeV})$. However, since in this channel the electroweak amplitudes are suppressed by one power of s compared to the QCD ones, the corrections rise much stronger with the scattering energy. Already for $s = O(3\text{ TeV})$ the QCD corrections are significant. Results presented in this section have been published in [47, 48].

Chapter 3

Electroweak amplitudes to all orders

In the first chapter we presented contributions of two loop corrections to $\gamma\gamma \to ZZ$ at small scattering angles. The results of the computations are corrections at the 10% level for 1 TeV. With rising scattering energies corrections rise as well. These results indicate that in order to achieve better accuracy at energies of several TeV one has to calculate corrections of higher-order, or preferably, resum corrections to any order in perturbation theory. Of course, this can be done only in some approximation, which will be the leading logarithmic approximation at the first stage. It was proved for $SU(2)$ theory [13] that higher-order resummed contributions are described with diagrams of ladder like topology built with reggeized particles. For the QCD corrections presented in the last chapter these have been reggeized gluons. In a resummed electroweak theory these will be reggeized particles of the electroweak sector. Thus the mechanism of reggeization in the electroweak sector will be a crucial point in order to resum corrections to all orders.

In an abelian gauge theory like quantum electrodynamics (QED) the spinor particle reggeizes, but the vector particle remains elementary [30]. In contrast, the reggeization of the Yang-Mills vector meson takes place in non-abelian gauge theories with spontaneously broken symmetry mediated by the Higgs mechanism. It was shown by direct calculation of the scattering amplitudes to sixth order of perturbation theory that for the gauge group $SU(2)$ the reggeization of the vector meson indeed takes place [22]. With effective vertices and the knowledge of the trajectory function of the reggeized vector meson it is possible to construct a general expression of the sum of all ladder diagrams contributing to the logarithmic approximation [13]. The Glashow-Salam-Weinberg theory of weak interactions is based on the direct product $SU(2)\times U(1)$ of the above mentioned group structures. $SU(2)$ is the non-abelian electroweak isospin group, to which three W gauge fields are associated and $U(1)$ is the abelian hypercharge group. The associated B field and the neutral component of the W triplet field mix to form the photon field A and the electroweak field Z. It is a priori not

clear if the new physical fields reggeize. In [32] it was computed up to sixth perturbative order that in the case of broken symmetries with abelian content there exist trajectories which cannot be associated with any physical vector meson. We will show that in the electroweak sector this trajectory is due to an appropriate mixing between the photon and Z fields and we will prove this result for all orders of perturbation theory. First we present higher-order calculations of the different isospin channels. The continuation in the future will be the derivation of integral equations on the basis of this results, which resum the contributions to all orders. The kernels of these integral equations are provided by our calculations. In this way, due to the high-energy factorisation, the resummed contributions to general electroweak processes can be described with the interaction decomposed to t-channel isospin states.

3.1 Elastic amplitudes in order g^2 and g^4

In the subsequent chapters we will make a decomposition of the amplitude in terms of t-channel isospin states. Our calculation will go up to sixth order of perturbation theory. First we present the ingredients of this calculation for arbitrary boson flavours. Similar calculations as will follow have been carried out in chapter 1 in the computation of $\gamma\gamma \to ZZ$ in the Regge kinematical region (1.3), where the scattering energy is much bigger than any other momentum scale in the theory. Thus contributions which are suppressed by powers of t/s can be neglected. Further, our computational method is based on the reconstruction of the asymptotic behaviour of the amplitudes by means of unitarity conditions in the s-channel. We restrict ourselves to the scattering of transverse bosons. To generalise the result to the scattering of longitudinal bosons as well is straight forward. Due to the high-energy factorisation, modifications in the result will arise only for the coupling of these bosons to the ladder like interaction. Since the s-channel helicity is conserved in the high-energy approximation we omit the helicity conservation factors $\delta_{\lambda_a \lambda_{a'}}$ throughout our computations.

Again, any 4-momentum is parametrised as:

$$k = \alpha p_1 + \beta p_2 + k_\perp \,. \tag{3.1}$$

The CMS we work in is defined by the momenta of the incoming bosons which are given (up to contributions suppressed by s) by the light cone vectors p_1 and p_2, thus the c.m. energy squared is

$$s = 2p_1 \cdot p_2 \tag{3.2}$$

and the momentum transfer squared is

$$t = q^2 = \alpha\beta s + q_\perp^2 \,. \tag{3.3}$$

As was stated in the first chapter, the main logarithmic contributions are coming from the kinematical region where all transverse momenta are at the same order

of magnitude and one has a strong ordering in the longitudinal parts of the exchanged momenta.

In the following we will make a decomposition of the amplitude in terms of t-channel isospin states. Our calculation will go up to sixth order of perturbation theory. First we will present the ingredients of this calculation for arbitrary boson flavours.

Retaining only the leading power of s the one boson exchange amplitude gives:

$$iA^{(0)}(k^2) = -ig^2 \frac{2s}{k_\perp^2 - M_i^2} \tag{3.4}$$

where the masses and couplings have to be replaced according to the Feynman diagram in consideration. The calculation of the vertices can be simplified with the eikonal approximation.

At the calculation to fourth order we will use unitarity conditions to obtain the amplitudes. The computation for example of the s-channel discontinuity gives the imaginary part of the s-channel contribution to the amplitude:

$$\mathrm{Im_s}\, A_{ab}^{(1)a'b'} = \frac{1}{2} \sum_i \int d\Pi_2 A_{ab\to i}^{(0)}(k^2) A_{i\to a'b'}^{(0)\dagger}((k-q)^2)\,. \tag{3.5}$$

Where all possible intermediate two-particle states i have to be taken into account. Since we restrict ourselves to the scattering of transverse bosons, these intermediate particles can only be bosons. The contribution from scalar particles is suppressed. For the scattering of longitudinal polarised bosons this is not the case. Additional diagrams with scalar Higgs intermediate particles are leading to a result which is consistent with the high-energy factorisation. The summation over the intermediate boson helicities has to be done by means of:

$$\sum_\lambda \epsilon_\lambda^\mu(k)\epsilon_\lambda^\nu(k) = -g^{\mu\nu} + \frac{k^\mu k^\nu}{M^2} \tag{3.6}$$

and the two-body phase space in Sudakov variables is:

$$\int d\Pi_2 = \frac{1}{8\pi^2 s} \int d^2k_\perp \tag{3.7}$$

With (3.4), (3.5) and (3.7), one gets for the imaginary part of the s-channel contribution:

$$\mathrm{Im_s}\, A_{ab}^{(1)a'b'} = s\, g^4 \int \frac{d^2k_\perp}{(2\pi)^2} \frac{1}{k_\perp^2 - M_i^2} \frac{1}{(k-q)_\perp^2 - M_j^2}\,, \tag{3.8}$$

where i and j are the two t-channel vector bosons. For future convenience we defined the function $\beta_{ij}(q^2)$ as:

$$\beta_{ij}(q^2) = g^2 \int \frac{d^2k_\perp}{(2\pi)^3} \frac{1}{k_\perp^2 - M_i^2} \frac{1}{(k-q)_\perp^2 - M_j^2}\,. \tag{3.9}$$

The u-channel part of the amplitude is obtained from the s-channel part by replacing s by u and taking into account the signature. The full amplitude is obtained thereafter via the dispersion relations of (1.21). We get:

$$A_{ab}^{(1)a'b'} = [-s\ln(-s) \pm \ln(-u)]\ g^2\, 2\beta_{ij}(q^2) \tag{3.10}$$

in the leading logarithmic approximation. The energy scale in the logarithm is arbitrary, it just has to be at the order of M_W^2. We will omit to write this scale in the following equations.

3.2 Elastic amplitudes in order g^6

The leading two loop contribution to the amplitude is again coming from spin-1 particles exchanged in the t-channel. Since we calculate the scattering of transverse bosons the dominant contributions are the exchange of a boson or the scalar Higgs particle within a boson loop. The momenta of the t-channel bosons are parametrised as (1.17) and the leading $\ln s$ contributions come from the kinematical regime of (1.18). We use unitarity relations in the calculation, hence one has to cut the above mentioned two loop diagrams in all possible ways. One loop graphs with self-energy or vertex corrections to the left or to the right of the cut are subdominant in $\ln s$. We divide the dominant contributions like in the first chapter into two groups, the two-particle intermediate state or virtual corrections and the tree-particle intermediate state or real corrections.

3.2.1 The two particle intermediate state

For the virtual radiative corrections, the imaginary part of the s-channel amplitude is given by

$$\begin{aligned} \mathrm{Im_s}\, A_{ab}^{(2)a'b'}(s,t) &= \frac{1}{2}\sum_i \int d\Pi_2 A_{ab\to i}^{(1)}(k_2^2) A_{i\to a'b'}^{(0)\dagger}((k_2-q)^2) \\ &+ \frac{1}{2}\sum_i \int d\Pi_2 A_{ab\to i}^{(0)}(k_1^2) A_{i\to a'b'}^{(1)\dagger}((k_1-q)^2)\,. \end{aligned} \tag{3.11}$$

We can make use of the results previously obtained. We note that for the amplitudes $A^{(1)}$ in (3.11) it suffices to retain only the terms with negative signature, since $\ln s$ cancels in states with positive signature. Especially in the decomposition in different t-channel isospin states, there will be flavour states where the s-channel (box) or u-channel (cross) contribution is absent, thus $\ln s$ cannot be cancelled. These states dominate over the ones where a cancellation

occurs. With the use of the results (3.4), (3.6), (3.7) and (3.8) we get:

$$\begin{aligned} \mathrm{Im_s}\, A^{(2)}_{virt}(s,t) &= s\ln(-s)\, g^6 \frac{1}{(2\pi)^5} \int d^2k_{1\perp} d^2k_{2\perp} \\ &\times \left\{ \frac{1}{((k_1-k_2)^2_\perp - M_m^2)(k^2_{1\perp} - M_i^2)((q-k_2)^2_\perp - M_l^2)} \right. \\ &+ \left. \frac{1}{((k_1-k_2)^2_\perp - M_m^2)(k^2_{2\perp} - M_j^2)((q-k_1)^2_\perp - M_k^2)} \right\}. \end{aligned} \tag{3.12}$$

After reconstructing the real part with unitarity relations and adding the u-channel contribution we have:

$$A^{(2)}_{virt}(s,t) = \left[-s\ln^2(-s) \pm u\ln^2 u\right] \left(\gamma_{iml}(q^2) + \gamma_{jmk}(q^2)\right), \tag{3.13}$$

defining the function $\gamma_{imj}(q^2)$ as

$$\gamma_{imj}(q^2) = \frac{g^6}{(2\pi)^6} \int \frac{d^2k_{1\perp} d^2k_{2\perp}}{((k_1-k_2)^2_\perp - M_m^2)(k^2_{1\perp} - M_i^2)((q-k_2)^2_\perp - M_j^2)} \tag{3.14}$$

where $\gamma_{imj} = \gamma_{mij} = \gamma_{ijm} = \gamma_{jmi}$.

3.2.2 The three particle intermediate state

Next we consider the three-particle intermediate state to the s-channel discontinuity. The intermediate particle with momenta $k_1 - k_2$ can be either a vector boson or the Higgs particle. In the kinematical region of (1.18), the on-shellness of this particle m implies:

$$\alpha_1\beta_2 s = (k_1-k_2)^2_\perp - M_m^2, \tag{3.15}$$

with M_m being the mass of the emitted particle and the transverse momenta are all of the same order of magnitude.

First, we consider the emission of bosons. There are always three possible type of diagrams, these depend on the flavour of bosons under consideration. Examples are shown in Fig. 3.1. The boson with momenta $k_1 - k_2$ can be emitted by the t-channel boson or by the upper or lower s-channel boson. The contribution of the sum of these three Feynman diagrams can always written in the form of:

$$iA^\rho_{2\to 3} = \pm i4\, g^6\, \frac{p_1^\nu}{k^2_{1\perp} - M_i^2}\, \Gamma^\rho_{\nu\mu}\, \frac{p_2^\mu}{k^2_{2\perp} - M_j^2} \tag{3.16}$$

which is described by the first Feynman diagrams of Fig. 3.1. There are two t-channel propagators and an effective vertex summarising the contributions from the three corresponding Feynman diagrams. The relative sign of the expression depends on the boson flavours and the effective vertex $\Gamma^\rho_{\nu\mu}$ is depending on the boson flavours ijm

$$\Gamma^\rho_{\nu\mu} = \frac{2\, p_1^\mu p_2^\nu}{s}\, C^\rho \tag{3.17}$$

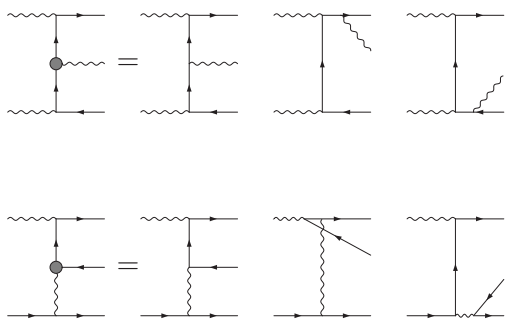

Figure 3.1: Examples for effective vertices. Solid lines are W bosons with the arrow indicating the charge flow and the curly lines can be either a Z boson or a photon.

with

$$C^\rho = \left(\alpha_1 - \frac{2(k_{1\perp}^2 - M_i^2)}{\beta_2 s}\right) p_1^\rho + \left(\beta_2 - \frac{2(k_{2\perp}^2 - M_j^2)}{\alpha_1 s}\right) p_2^\rho - (k_1 + k_2)_\perp^\rho . \quad (3.18)$$

This expression is universal for all the possible flavour combinations independently where the boson with momenta $k_1 - k_2$ couples. Sign changes coming from different propagators are always cancelled with the sign of the according couplings. As an example one may compare the two cases of Fig. 3.1.

Using unitarity relations, the real corrections with only bosons in the intermediate states gives:

$$\mathrm{Im}_s\, A_{real}^{(2)}(s,t) = \frac{1}{2}\int d\Pi_3\, A_{\sigma\, 2\to 3}(k_1,k_2) A_{2\to 3}^{\sigma\dagger}(q-k_1, q-k_2)\,, \quad (3.19)$$

where an appropriate summation over the boson helicities (3.6) is implied. Using (1.17), (1.18) and (3.15) the three-body phase space is

$$\int d\Pi_3 = \frac{1}{4(2\pi)^5 s}\, \ln\left(\frac{s}{M_W^2 - t}\right) \int d^2k_{1\perp} d^2k_{2\perp}\,. \quad (3.20)$$

Calculating the real corrections to the imaginary part of the amplitude (3.19) it is necessary to know the scalar product of the vectors (3.18) with different momenta:

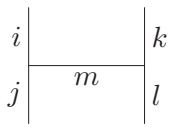

$$C_\sigma(k_1,k_2)C^{\sigma\dagger}(k_1-q,k_2-q) = \tag{3.21}$$

$$2q_\perp^2 + M_m^2 - M_i^2 - M_j^2 - M_k^2 - M_l^2 + \frac{(M_j^2-M_i^2)(M_l^2-M_k^2)}{M_m^2} -$$
$$-\frac{2(k_{1\perp}^2 - M_i^2)((q-k_2)_\perp^2 - M_l^2)}{(k_1-k_2)_\perp^2 - M_m^2} - \frac{2(k_{2\perp}^2 - M_j^2)((q-k_1)_\perp^2 - M_k^2)}{(k_1-k_2)_\perp^2 - M_m^2}$$

where we have made use of the relation (3.15). The last term in the second line comes from the second term of (3.6) and is absent for equal boson masses. Substituting (3.16) and (3.20) into (3.19), making use of the product (3.21) and finally reconstruct the real part and add the similar u-channel contribution we end up with:

$$\begin{aligned} A^{(2)}_{real}(s,t) &= \pm[-s\ln(-s) \pm u\ln(-u)]\left\{\frac{g^2}{2}\Big(2q_\perp^2 + M_m^2 - M_i^2 - M_j^2\right. \\ &- M_k^2 - M_l^2 + \frac{(M_j^2-M_i^2)(M_l^2-M_k^2)}{M_m^2}\Big)\beta_{ij}(q^2)\beta_{kl}(q^2) \\ &- \left.\gamma_{iml}(q^2) - \gamma_{jmk}(q^2)\right\}. \end{aligned} \tag{3.22}$$

We see that the γ functions may cancel with the virtual corrections given in (3.13) if the appropriate overall sign is given. For $SU(2)$ this is the case for the isospin-1 channel [28].

For the real corrections we also have to take into account the exchange of a Higgs boson. As argued in the first chapter these are contributing only to the three-particle intermediate state, and for the scattering of transverse bosons only when the Higgs boson is radiated from the t-channel vector boson. The elastic amplitude is given thereafter by the product:

$$\mathrm{Im}\, A^H_{real}(s,t) = \frac{1}{2}\int d\Pi_3\, A^H_{2\to3}(k_1,k_2)A^H_{2\to3}(q-k_1,q-k_2)\,. \tag{3.23}$$

With the kinematics (1.17), (1.18) and (3.15) and retaining only the leading power of s, the Higgs exchange amplitude gives:

$$iA^H_{2\to3} = -is\ 2\ g^3\,\frac{M_W}{(k_{1\perp}^2 - M_i^2)(k_{2\perp}^2 - M_j^2)}. \tag{3.24}$$

Writing this result in a similar way as (3.16) for the case of the emission of the scalar particle, the effective vertex for Higgs emission reduces to:

$$\Gamma^H_{\nu\mu} = \frac{-2\,p_1^\nu p_2^\mu}{s} M_W \tag{3.25}$$

and the square of the vertex will contain in place of the product (3.21) simply the factor M_W^2. Thus the amplitude for the exchange of a Higgs boson gives in the high-energy approximation:

$$A^H(s,t) = [-s\ln(-s) \pm u\ln(-u)]\, g^2 M_W^2\, \beta_{ij}(q^2)\beta_{kl}(q^2)\,. \tag{3.26}$$

With this expressions we are able to calculate any 2→2 vector boson scattering process up to two loop in the leading logarithmic approximation.

3.3 Decomposition into t-channel isospin states

With this presented building blocks we can start with a decomposition of the amplitude in different t-channel isospin states. In this way a clear structure will appear in the high-energy asymptotics of the amplitudes. The proper decomposition is dictated by the usual sum rules combining two spin one states. In the $SU(2)$ calculation of [28] the different third components of the t-channel isospin states gave the same result, since all bosons are identical. In the Glashow-Salam-Weinberg theory this will be no longer the case. In the usual definition of the charged vector bosons

$$|W^+\rangle = \frac{1}{\sqrt{2}}(|W^1\rangle - i|W^2\rangle) \qquad |W^-\rangle = \frac{1}{\sqrt{2}}(|W^1\rangle + i|W^2\rangle) \tag{3.27}$$

the relative phase for $|W^+\rangle$ is opposite to the usual convention of eigenstates of $SU(2)$. An accordant modification of the tabulated Clebsch-Gordan-Coefficients has to be considered to couple such anti-particle states to particle isospin states [50]. In the following calculations we use the electroweak coupling $g^2 = 4\pi\alpha_{em}/s_w^2$. In the Feynman graphs which will be presented the solid lines are W bosons with the arrow indicating the charge flow. The curly lines can be either a Z boson or a photon, except when it couples to a Higgs particle, then it is always a Z boson.

3.3.1 Isospin-1 t-channel states

We begin with the calculation of the isospin-1 t-channel states. Only these are contributing to the Born approximation. We will use the notation A_{jm} and $|jm\rangle$ where j is the isospin and m the third component of the isospin projected in the t-channel.

Charged channel

First, we project to the quantum numbers of the W bosons, thus we have to calculate the amplitude $A_{11} = \langle 11|11\rangle$. The involved amplitudes with the appropriate Clebsch-Gordan coefficients give the decomposition:

$$\langle 11|11\rangle = \frac{1}{2}\Big(\langle 11;10|11;10\rangle - \langle 11;10|10;11\rangle - \langle 10;11|11;10\rangle + \langle 10;11|10;11\rangle\Big) \tag{3.28}$$

Since in the Born approximation the t-channel particle can only be a W boson the contributing Feynman diagrams are leading to the result:

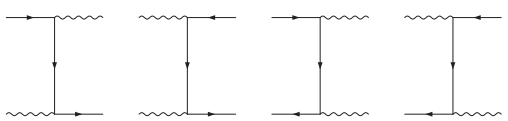

$$A_{11}^{(0)} = -4sg^2(c_w + s_w)^2 \frac{1}{q_\perp^2 - M_W^2}\,. \tag{3.29}$$

The calculation of the corresponding one loop contribution is leading to the $\beta_{ij}(q^2)$ functions. The neutral particle propagator (curly line) can be either a Z boson or a photon, thus we define:

$$\beta_{wz}(q^2) = g^2 \int \frac{d^2k_\perp}{(2\pi)^3} \frac{1}{k_\perp^2 - M_W^2} \frac{1}{(k-q)_\perp^2 - M_Z^2} \tag{3.30}$$

and

$$\beta_{w\gamma}(q^2) = g^2 \int \frac{d^2k_\perp}{(2\pi)^3} \frac{1}{k_\perp^2 - M_W^2} \frac{1}{(k-q)_\perp^2}\,. \tag{3.31}$$

Taking into account all possible combinations with the Z boson and photon, the one loop contribution is given as:

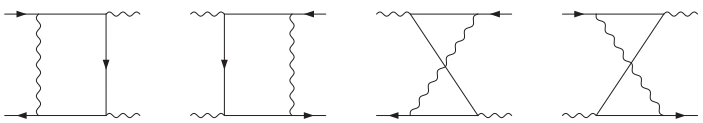

$$A_{11}^{(1)} = [-s\ln(-s) + u\ln(-u)]\, g^2(c_w + s_w)^2\, 2\left\{c_w^2\, \beta_{wz}(q^2) + s_w^2\, \beta_{w\gamma}(q^2)\right\} \tag{3.32}$$

We see that, as in the pure $SU(2)$ case, the spin-1 state has negative signature. This follows from the fact that due to the Clebsch-Gordan-Coefficients the crossed graphs (u-channel contribution) gain a minus sign.

Next we are calculating the virtual contributions to the two loop amplitude. We get these from the Born and one loop amplitudes via unitarity relations outlined in the previous chapter. There are plenty of Feynman graphs according to the decomposition (3.28) but it suffices to retain only those one loop amplitudes where the u- or s-channel contribution is absent. Otherwise $\ln s$ cancels, giving non-leading terms in the logarithmic approximation. The remaining Feynman graphs contributing to the s-channel imaginary part are:

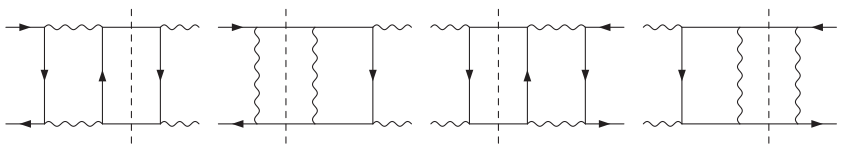

Together with the corresponding u-channel contribution we get:

$$\begin{aligned} A_{11,virt}^{(2)} &= [-s\ln^2(-s) + u\ln^2(-u)]\,(c_w + s_w)^2 \\ &\times \left\{\gamma_{www}(q^2) + c_w^4\gamma_{zwz}(q^2) + s_w^4\gamma_{\gamma w\gamma}(q^2) + 2s_w^2c_w^2\gamma_{\gamma wz}(q^2)\right\}. \end{aligned} \tag{3.33}$$

γ_{ijk} was defined in (3.14). Calculating the real corrections:

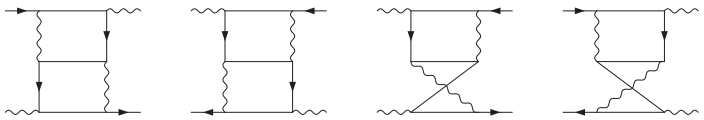

we need the product (3.21) giving:

$$
\begin{aligned}
& [-s\ln^2(-s)+u\ln^2(-u)]\,\frac{1}{2}(c_w+s_w)^2 \qquad (3.34)\\
\times\ & \Big\{c_w^4\Big[(2q_\perp^2-M_W^2-2M_Z^2-\frac{(M_W^2-M_Z^2)^2}{M_W^2})\,g^2\beta_{wz}^2(q^2)\\
-\ & 2\gamma_{www}(q^2)-2\gamma_{zwz}(q^2)\Big]\\
+\ & s_w^4\Big[(2q_\perp^2-2M_W^2)\,g^2\beta_{w\gamma}^2(q^2)-2\gamma_{www}(q^2)-2\gamma_{\gamma w\gamma}(q^2)\Big]\\
+\ & 2s_w^2c_w^2\Big[(2q_\perp^2-2M_W^2)\,g^2\beta_{wz}(q^2)\beta_{w\gamma}^2(q^2)-2\gamma_{www}(q^2)-2\gamma_{\gamma wz}(q^2)\Big]\Big\}.
\end{aligned}
$$

Adding also the Higgs contribution:

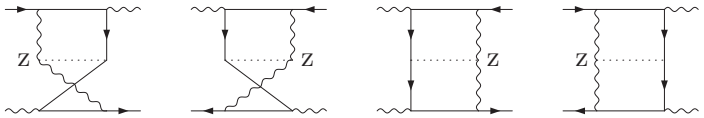

we arrive at:

$$
\begin{aligned}
A_{11,real}^{(2)} &= [-s\ln^2(-s)+u\ln^2(-u)]\,(c_w+s_w)^2 \qquad (3.35)\\
&\times \Big\{g^2(q_\perp^2-M_W^2)\Big[c_w^2\,\beta_{wz}(q^2)+s_w^2\,\beta_{w\gamma}(q^2)\Big]^2\\
&- \gamma_{www}(q^2)-c_w^4\gamma_{zwz}(q^2)-s_w^4\gamma_{\gamma w\gamma}(q^2)-2s_w^2c_w^2\gamma_{\gamma wz}(q^2)\Big\}.
\end{aligned}
$$

The result has a part which is proportional to the square of the one loop contribution and a part with several two loop integrals. Comparing (3.35) with (3.33) we see that in the leading logarithmic approximation the virtual contribution of the amplitude at the two loop level get exactly cancelled by part of the real corrections. Adding together the contributions obtained up to two loop and factorising out the Born contribution, we get for the amplitude to sixth-order of perturbation theory:

$$
\begin{aligned}
A_{11} &= \frac{-2s}{q_\perp^2-M_W^2}\,g^2(c_w+s_w)^2 \qquad (3.36)\\
&\times \Big\{1+(q_\perp^2-M_W^2)\Big[c_w^2\,\beta_{wz}(q^2)+s_w^2\,\beta_{w\gamma}(q^2)\Big]\ln(-s)\\
&+ (q_\perp^2-M_W^2)^2\Big[c_w^2\,\beta_{wz}(q^2)+s_w^2\,\beta_{w\gamma}(q^2)\Big]^2\,\frac{\ln^2(-s)}{2!}\Big\}-\{s\to u\}\Big\}.
\end{aligned}
$$

Due to the additional logarithm and the factor 2 which was obtained in the two loop result this expression marks the beginning of an exponential series. Thus the result of this calculation suggests that the amplitude of the charged isospin-1 channel, for arbitrary orders of perturbation theory in the leading logarithmic approximation, equals:

$$A_{11} = \Gamma_1 \frac{(-s)^{1+(q_\perp^2 - M_W^2)(c_w^2\,\beta_{wz}(q^2)+s_w^2\,\beta_{w\gamma}(q^2))} - (s \to u)}{q_\perp^2 - M_W^2}\,\Gamma_2\,. \tag{3.37}$$

We replaced here the coupling constant of the presented tree level contributions with general couplings Γ_i, which depend on the scattering process under consideration. Due to the high-energy factorisation the resummed interaction will be independent of them. This is explicitly shown here in the calculations of vector boson scattering (where we summed the photon and Z contributions). In the higher order corrections (3.32), (3.33) and (3.35) the same tree level couplings always factorise out. The same Regge form of the amplitude is naturally also given for A_{1-1}. Thus the trajectory of the W bosons is given by:

$$j_w(q^2) = 1 + (q_\perp^2 - M_W^2)\Big[c_w^2\,\beta_{wz}(q^2) + s_w^2\,\beta_{w\gamma}(q^2)\Big] \tag{3.38}$$

The trajectory passes through the boson spin 1 at the W mass. From this result follows that the W boson reggeize. A reggeized particle is a particle with a propagator which is modified in the following way:

$$\frac{1}{q^2 - M^2} \to \frac{1}{q^2 - M^2}\left(\frac{s}{s_0}\right)^{\alpha(t)}\,. \tag{3.39}$$

Higher order corrections to the exchange of the particle quantum numbers are resulting in the factor $s^{\alpha(t)}$. In the analytic continuation of the t-channel partial wave expansion of amplitudes it can be shown that in the Regge limit the amplitude is always proportional to s to the power of the spin of the exchanged t-channel particle. Thus the exchange of a reggeized particle means the exchange of a particle with the angular momentum $1 + \alpha(t)$. Though the presented perturbative calculations are only valid in the region where the trajectory is close to one, we can do an analytic continuation of the result. At integer values of the trajectory the amplitude describes the exchange of a resonance, thus a reggeized particle has the features of a manifestly composite system. The W reggeization was strongly expected since the electroweak mixing does not effect the charged degrees of freedom. Here we explicitly see that the Z boson and the photon are mixing in a proper way to build the W boson trajectory.

Neutral channel

With $\langle 10|10\rangle$ there is another isospin-1 t-channel state which has to be calculated. A similar decomposition as (3.28) leads to amplitudes with W bosons in the initial and final state. For the Born contribution we have:

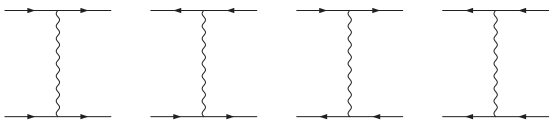

$$A_{10}^{(0)} = -4s\, g^2 \left(\frac{c_w^2}{q_\perp^2 - M_Z^2} + \frac{s_w^2}{q_\perp^2} \right) \tag{3.40}$$

where the two terms in the bracket corresponds to the Z and photon exchange.

In the calculation of the one loop amplitude the Feynman graphs with Z or photon in the t-channel can be neglected, $\ln s$ cancels out in these contributions and terms with β_{zz}, $\beta_{\gamma z}$ etc. are absent in the result:

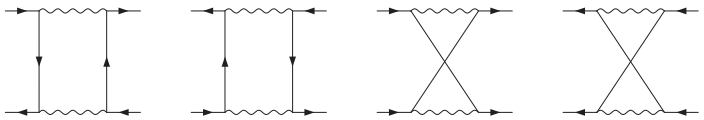

$$A_{10}^{(1)} = [-s\ln(-s) + u\ln(-u)]\, g^2\, 2\, \beta_{ww}(q^2) \tag{3.41}$$

The calculation of the virtual contribution to the two loop amplitude is similar to what was outlined in the previous case. Amplitudes with three neutral particles in the t-channel can be neglected. The remaining Feynman diagrams are:

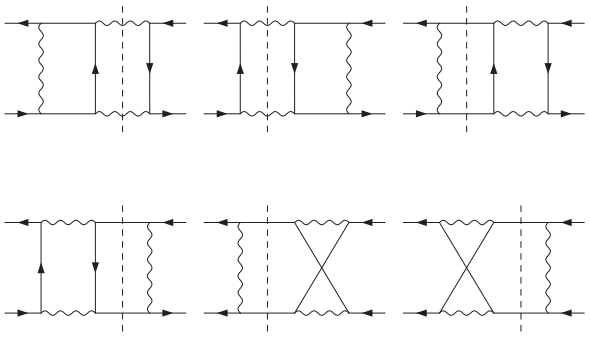

and same diagrams with the charge flow in the opposite direction. After cancellations due to the Clebsch-Gordan coefficients we arrive at:

$$A_{10,virt}^{(2)} = [-s\ln^2(-s) + u\ln^2(-u)]\, 2\Big\{ c_w^2 \gamma_{zwz}(q^2) + s_w^2 \gamma_{\gamma w\gamma}(q^2) \Big\}\,. \tag{3.42}$$

In the real corrections graphs with Z boson or photon in the t-channel are suppressed as well, $\ln s$ cancels in these states and we are left with:

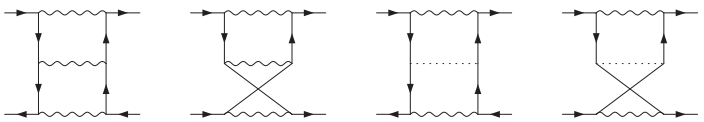

and with the corresponding graphs with the charge flow in the opposite direction. We note that, in contrast to the previous case of $\langle 11|11\rangle$, the overall sign of (3.22) is positive in this particular flavour configuration. Together with the Higgs contribution the real part is:

$$\begin{aligned} A^{(2)}_{10,real} &= [-s\ln^2(-s) + u\ln^2(-u)] \\ &\times \left\{ g^2(q_\perp^2 - M_W^2)\beta_{ww}^2(q^2) - 2c_w^2\gamma_{wzw}(q^2) - 2s_w^2\gamma_{w\gamma w}(q^2) \right\} \end{aligned} \tag{3.43}$$

again cancelling the virtual contributions. With the identity $q_\perp^2 - M_W^2 = s_w^2 q_\perp^2 + c_w^2(q_\perp^2 - M_Z^2)$ the amplitude A_{10} to sixth-order of perturbation theory can be written in the form:

$$\begin{aligned} A_{10} &= -2s\,g^2 \frac{c_w^2}{q_\perp^2 - M_Z^2} \Big\{ 1 + (q_\perp^2 - M_Z^2)\beta_{ww}(q^2)\ln(-s) \\ &+ (q_\perp^2 - M_Z^2)^2\,\beta_{ww}^2(q^2)\,\frac{\ln^2(-s)}{2!} \Big\} - \{s \to u\} \Big\} \\ &- 2s\,g^2 \frac{s_w^2}{q_\perp^2} \Big\{ 1 + q_\perp^2\beta_{ww}(q^2)\ln(-s) + q_\perp^4\,\beta_{ww}^2(q^2)\,\frac{\ln^2(-s)}{2!} \Big\} - \{s \to u\} \Big\}. \end{aligned} \tag{3.44}$$

At first sight, this form of the amplitude suggests a trajectory for the Z boson and a trajectory for the photon as well. However the non-cancelled part of the real corrections shows that the calculations of higher order are leading to contributions proportional to:

$$[-s\ln^n(-s) + u\ln^n(-u)]\,g^2(q_\perp^2 - M_W^2)^{n-1}\beta_{ww}^n(q^2) \tag{3.45}$$

which does not support the existence of a photon or Z boson trajectory. We assume that the result to all orders of perturbation theory can be again written in an exponential from. We also have to take into account, that on one hand the Born contribution (3.40) contains the Z boson and photon pole and on the other hand the leading term of the exponential form will give the Born exchange of a W boson which is absent in this channel, thus this contribution has to be subtracted. Considering these arguments, we make the conjecture that the neutral isospin-1 amplitude to all orders has to be written in the from of:

$$\begin{aligned} A_{10} &= 2\,g^2 \frac{(-s)^{1+(q_\perp^2 - M_W^2)\beta_{ww}(q^2)} - (s \to u)}{q_\perp^2 - M_W^2} \\ &- 4s\,g^2 \left(\frac{c_w^2}{q_\perp^2 - M_Z^2} + \frac{s_w^2}{q_\perp^2} - \frac{1}{q_\perp^2 - M_W^2} \right). \end{aligned} \tag{3.46}$$

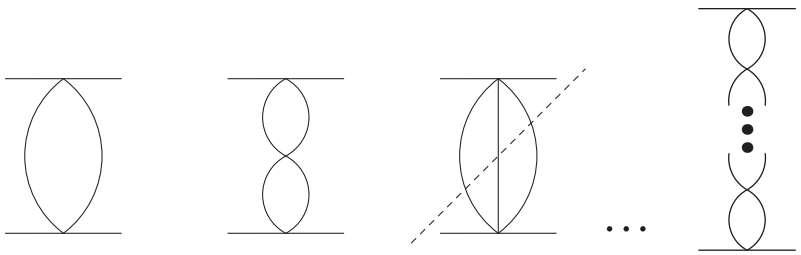

Figure 3.2: General structure in the isospin-1 channels. Contributions with higher loop integrals cancel order by order. The result to any orders is proportional to the nth power of the one loop result.

Here we find the third trajectory emerging in the theory:

$$j_{\gamma-z} = 1 + (q_\perp^2 - M_W^2)\beta_{ww}(q^2) \tag{3.47}$$

The trajectory passes through the boson spin 1 at the W mass, thus reflecting the quantum numbers of the neutral $SU(2)$ particle W^3 present before the electroweak mixing. Again, the appropriate mixing of photon and Z boson was necessary to couple two t-channel W bosons with opposite charge flow to form the neutral trajectory.

The general structure of the isospin-1 channels is depicted in Fig. 3.2. From direct calculations it follows that in the two loop contributions two loop integrals γ_{ijk} cancel. We expect that higher loop integrals will cancel order by order as well, leading to a result which is to any orders proportional to the nth power of the one loop result. This conjecture is strongly supported by corresponding $SU(2)$ results [13], though we have a different configuration. The direct product of the Abelian $U(1)$ group and the non-Abelian $SU(2)$ group is leading to a Regge propagator in the neutral channel. Such a trajectory which cannot be associated with a physical particle was found in [32] as well. This neutral trajectory has a pole in momentum space at the W mass. However, when the trajectory is vanishing at the W mass, only the Z boson and photon poles survive.

The presented investigations suggest that the electroweak sector has three trajectories, merging at the W mass and restoring the old symmetry at this point. For the existence of these trajectories it was necessary that the contribution of the photon is considered as well. The statement that the electroweak vector bosons W and Z reggeize while the photon remains elementary, would be incorrect in the Standard Model. The reggeization of the particles to all orders can be proved with the bootstrap equations. This will be the subject of the next section. At last we note that all of the presented results agree with [28] in the limit where the Weinberg mixing angle is going to zero. Especially, the expressions in this limit resulting from $\langle 11|11\rangle$ equal to the corresponding expressions of $\langle 10|10\rangle$, since in the $SU(2)$ theory all three bosons are identical.

3.3.2 Bootstrap condition for the neutral isospin-1 channel

In the $SU(2)$ calculations [13] it was proved, that the virtual contributions are included by the replacement of the particles by reggeons with the trajectory $j = 1 + \alpha_w(t)$. We will make the same multi-Regge ansatz for the n-particle production amplitude, which we will write in the factorised form with effective vertices and reggeized boson propagators. In the calculation presented for the amplitude $\langle 10|10\rangle$ we saw that at the one and two loop level the diagrams that survived in the logarithmic approximation have been those with only W bosons in the t-channel. We assume that this will be the case for all orders and the reggeized particles in the t-channel are reggeized W bosons. The n-particle production amplitude associated with the neutral channel is thus:

$$A_{2\to 2+n} = s\,\Gamma_{aa'}\frac{(s_1/M_W^2)^{\alpha_w(t_1)}}{t_1 - M_W^2}\,C_{12}^{ww}\frac{(s_2/M_W^2)^{\alpha_w(t_2)}}{t_2 - M_W^2}\,\cdots$$
$$\cdots\frac{(s_{n+1}/M_W^2)^{\alpha_w(t_{n+1})}}{t_{n+1} - M_W^2}\,\Gamma_{bb'}\,, \qquad s_k = (p_{k-1} + p_k)^2\,. \tag{3.48}$$

where the trajectory function of the charged channel α_w is defined as:

$$\alpha_w(q^2) = (q_\perp^2 - M_W^2)[c_w^2\,\beta_{wz}(q^2) + s_w^2\,\beta_{w\gamma}(q^2)] \tag{3.49}$$

and $C_{ij}^{ww}(k_i, k_j)$ is the effective vertex of the emission of photon, Z boson or Higgs particle from the t-channel W boson. Applying for expression (3.48) the unitarity condition and integrating over the n-particle phase space we can calculate the elastic amplitudes to all orders. In this case we do not have the unitarity condition for a scattering process, but for the t-channel exchange of a definite isospin configuration. We get:

$$\begin{aligned}\mathrm{Im}_s A_{10}(s,t) &= -\frac{1}{2}\pi s\sum_{n=0}^{\infty}\left(\frac{g^2}{8\pi^3}\right)^{n+1}\int\prod_{i=1}^{n}\frac{d\alpha_i}{\alpha_i} \\ &\times\int\prod_{l=1}^{n+1}\frac{d^2k_{l\perp}}{(k_{l\perp}^2 - M_W^2)((q-k_l)_\perp^2 - M_W^2)}\left(\frac{s_l}{M_W^2}\right)^{\alpha_w(k_l^2)+\alpha_w((q-k_l)^2)} \\ &\times\quad K_{1,2}^w\cdot K_{2,3}^w\cdot\ldots\cdot K_{n,n+1}^w\end{aligned} \tag{3.50}$$

for the neutral channel. K^w is the product (3.21) of the effective vertices C^{ww} up to a factor $2g^2$ which was extracted. It includes the emission of a Z boson, photon and Higgs from the t-channel W bosons. The nested integrations over α_i can be disentangled by taking the Mellin transform of the amplitude (3.50) and using the convolution property of the Mellin transforms. We obtain:

$$\begin{aligned}F_{\omega,10}(q^2) &= \sum_{n=0}^{\infty}\left(\frac{g^2}{8\pi^3}\right)^{n+1}\int\left(\prod_{l=1}^{n+1}\frac{d^2k_{l\perp}}{(k_{l\perp}^2 - M_W^2)((q-k_l)_\perp^2 - M_W^2)}\right) \\ &\times\quad\frac{K_{1,2}^w\cdot K_{2,3}^w\cdot\ldots\cdot K_{n,n+1}^w}{\omega - \alpha_w(k_l^2) - \alpha_w((q-k_l)^2)}\end{aligned} \tag{3.51}$$

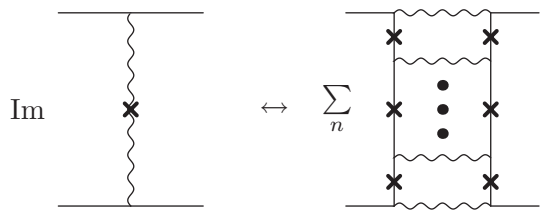

Figure 3.3: Diagrammatical representation of the bootstrap relation. The asterix on the vertical particle lines indicate that they are reggeized particles.

for the Mellin transformed amplitude after solving the α_i integrals. The elastic amplitude for the neutral isospin-1 channel to all orders in perturbation theory is obtained through the Watson-Sommerfeld transformation:

$$\begin{aligned} A_{10}(s,t) &= -s\int\frac{d\omega}{i}\left(\frac{s}{M_W^2}\right)^{\omega}\frac{1+e^{-i\pi\omega}}{\sin\pi\omega}F_{\omega,10}(q^2) \\ &- 4s\,g^2\left(\frac{c_w^2}{q_\perp^2-M_Z^2}+\frac{s_w^2}{q_\perp^2}-\frac{1}{q_\perp^2-M_W^2}\right), \end{aligned} \tag{3.52}$$

where the last term is a contribution to the partial wave amplitude which is non-analytic with respect to ω, but it ensures the emergence of the Born term (3.40). If in (3.51) we separate now the last integration and define the Bethe-Salpeter amplitude:

$$F_{\omega,10}(q^2)=\frac{g^2}{8\pi^3}\int\frac{d^2k_\perp}{(k_\perp^2-M_W^2)((q-k)_\perp^2-M_W^2)}f_{\omega,10}(k,q-k)\,, \tag{3.53}$$

the sum of all ladder contributions built with reggeized W bosons can be described by the integral equation:

$$\begin{aligned} &[\omega-\alpha_w(k^2)-\alpha_w((q-k)^2)]f_{\omega,10}(k,q-k)=g^2 \\ &+ \frac{g^2}{8\pi^3}\int\frac{d^2k'_\perp\;f_{\omega,10}(k',q-k')}{(k_\perp'^2-M_W^2)((q-k')_\perp^2-M_W^2)}\left\{(q_\perp^2-M_W^2)\right. \\ &- \left[(k_\perp^2-M_W^2)((q-k')_\perp^2-M_W^2)+(k_\perp'^2-M_W^2)((q-k)_\perp^2-M_W^2)\right] \\ &\times \left.\left(\frac{c_w^2}{(k-k')_\perp^2-M_Z^2}+\frac{s_w^2}{(k-k')_\perp^2}\right)\right\}. \end{aligned} \tag{3.54}$$

The solution of this integral equation gives us the resummed contribution to all orders in the neutral isospin-1 channel. Here the virtual contributions cancel out exactly with a part of the kernel. Thus the solution is independent of k and we have simply:

$$f_{\omega,10}(q^2)=\frac{g^2}{\omega-(q_\perp^2-M_W^2)\beta_{ww}(q^2)} \tag{3.55}$$

for the neutral isospin-1 channel. This solution is exactly the Regge pole of the neutral channel. Inserting it into (3.53) and (3.52) we get again the amplitude for the exchange of the reggeized neutral particle. This presented relation is depicted in Fig. 3.3 and is called bootstrap relation. The bootstrap relation is a necessary fulfilment of the unitarity condition, i.e. the sum of all intermediate states has to give the imaginary part of the elastic amplitude. Our perturbative calculation and conjecture is fulfilled in this non-linear relation which follows from S-matrix unitarity. This proves the reggeization in the neutral channel for all orders of perturbation theory in the leading log approximation. The trajectory of the $W^{\pm}$, obtained in the calculation of A_{11}, was essential in the resummation of the amplitude A_{10}.

A similar bootstrap relation has to be derived for the charged channel. The first step towards this relation are the n-particle production amplitudes corresponding to the charged channel. The virtual corrections are again included with the implementation of the isospin-1 t-channel states to all orders. These can be the charged as well as the neutral ones. With our conjectures of the last section, cf. (3.37) and (3.46), these amplitudes are of the form of:

$$\begin{aligned} A_{2\to 2+n} \quad &= \quad s\,\Gamma_{aa'}\frac{(s_1/M_W^2)^{\alpha_w(t_1)}}{t_1-M_W^2}\,C_{12}^{ww}\,\frac{(s_2/M_W^2)^{\alpha_w(t_2)}}{t_2-M_W^2}\,C_{23}^{w3} \\ &\times \quad \left[\frac{(s_3/M_W^2)^{\alpha_3(t_3)}}{t_3-M_W^2}+\frac{c_w^2}{t_3-M_Z^2}+\frac{s_w^2}{t_3}+\frac{-1}{t_3-M_W^2}\right]\cdots \\ &\cdots \quad \frac{(s_{n+1}/M_W^2)^{\alpha_w(t_{n+1})}}{t_{n+1}-M_W^2}\,\Gamma_{bb'}\,, \qquad s_k=(p_{k-1}+p_k)^2\,. \end{aligned} \tag{3.56}$$

where the trajectory function of the neutral channel α_3 is defined as:

$$\alpha_3(q^2)=(q_\perp^2-M_W^2)\beta_{ww}(q^2)\,. \tag{3.57}$$

and α_w was already defined in (3.49). $C_{ij}^{w3}(k_i,k_j)$ is the effective vertex for the emission of a W boson and $C_{ij}^{ww}(k_i,k_j)$ is the effective vertex for the emission of a Higgs boson. With the unitarity condition the n-particle production amplitudes lead to the elastic amplitude of the charged isospin-1 channel. We have to sum over all possible intermediate states of the kind of (3.56) and integrate over the n-particle phase space. These investigations will lead to an integral eqaution which is similar to (3.54), but written in a matrix form. The kernel of this integral equation is provided by the two-loop calculations presented in the last section. The solution and the bootstrap scheme will prove the reggeization of the W boson in the electroweak sector and the appearance of the fixed poles of the neutral channel. The reggeization of the vector boson was already proved to all orders in $SU(2)$ theory [13] and, as previously stated, the electroweak mixing does not effect the charge degrees of freedom.

3.3.3 The isospin-2 t-channel states

In this chapter we present the result of the isospin-2 t-channel states without giving much details of the calculation, which is similar to the cases presented in the last chapter. Again, we restrict ourselves to the case of scattering of transverse bosons. Basic differences to the isospin-1 case will be the absence of the Born contributions and a positive signature. To the amplitude of $\langle 22|22\rangle$ only diagrams with an exchange of isospin-2 in the t-channel contribute. The one loop result is:

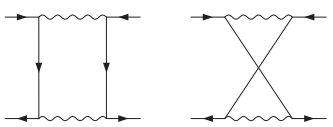

$$A_{22}^{(1)} = [-s\ln(-s) - u\ln(-u)]\, g^2\, 2\, \beta_{ww}(q^2) \tag{3.58}$$

having positive signature. Virtual corrections to the two loop contribution are:

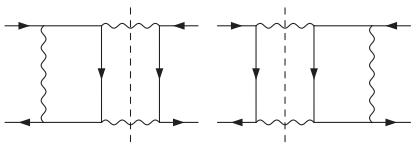

$$A_{22,virt}^{(2)} = [-s\ln^2(-s) - u\ln^2(-u)]\, 2\Big\{c_w^2\gamma_{zwz}(q^2) + s_w^2\gamma_{\gamma w\gamma}(q^2)\Big\}\,. \tag{3.59}$$

Apart from the signature the results are the same as for the A_{10} amplitudes. In both cases for the three particle intermediate state there are only W bosons in the t-channel in the leading log approximation. However, the flavour configuration in the isospin-2 state leads to a different sign in (3.22) giving together with the Higgs contribution:

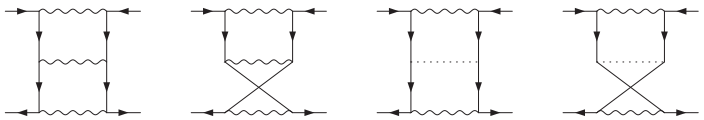

$$\begin{aligned} A_{22,real}^{(2)} &= [-s\ln^2(-s) - u\ln^2(-u)] \\ &\times \Big\{g^2(-q_\perp^2 + 2M_W^2)\beta_{ww}^2(q^2) + 2c_w^2\gamma_{wzw}(q^2) + 2s_w^2\gamma_{w\gamma w}(q^2)\Big\}\,. \end{aligned} \tag{3.60}$$

Due to the flavour configuration, in the sum the virtual contributions are not cancelled by part of the real corrections and we have:

$$\begin{aligned} A_{22}^{(2)} &= [-s\ln^2(-s) - u\ln^2(-u)] \\ &\times \Big\{g^2(-q_\perp^2 + 2M_W^2)\beta_{ww}^2(q^2) + 4c_w^2\gamma_{wzw}(q^2) + 4s_w^2\gamma_{w\gamma w}(q^2)\Big\}\,. \end{aligned} \tag{3.61}$$

The decomposition of the state $\langle 21|21\rangle$:

$$\langle 21|21\rangle = \frac{1}{2}\Big(\langle 11;10|11;10\rangle + \langle 11;10|10;11\rangle + \langle 10;11|11;10\rangle + \langle 10;11|10;11\rangle\Big) \tag{3.62}$$

is similar to (3.28) with the significant difference having only positive Clebsch-Gordan coefficients which leads to the positive signature and to the total cancellation of the Feynman graphs at Born level. The Feynman graphs contributing here are the same as for the case $\langle 11|11\rangle$. The one loop amplitude:

$$A_{21}^{(1)} = [-s\ln(-s) - u\ln(-u)]\, g^2(c_w + s_w)^2\, 2\Big\{c_w^2\,\beta_{wz}(q^2) + s_w^2\,\beta_{w\gamma}(q^2)\Big\} \tag{3.63}$$

and the virtual contribution to the two loop amplitude:

$$\begin{aligned} A_{21,virt}^{(2)} &= [-s\ln^2(-s) - u\ln^2(-u)]\,(c_w + s_w)^2 \\ &\times \Big\{\gamma_{www}(q^2) + c_w^4\gamma_{zwz}(q^2) + s_w^4\gamma_{\gamma w\gamma}(q^2) + 2s_w^2c_w^2\gamma_{\gamma wz}(q^2)\Big\} \end{aligned} \tag{3.64}$$

are the same as for A_{11} but with positive signature. However, the only positive Clebsch-Gordan coefficients lead to a different result in the real contribution:

$$\begin{aligned} A_{21,real}^{(2)} &= [-s\ln^2(-s) - u\ln^2(-u)]\,(c_w + s_w)^2 \\ &\times \Big\{g^2(-q_\perp^2 + M_W^2)\Big[c_w^2\,\beta_{wz}(q^2) + s_w^2\,\beta_{w\gamma}(q^2)\Big]^2 \\ &+ M_W^2\beta_{wz}(q^2) + \gamma_{www}(q^2) + c_w^4\gamma_{zwz}(q^2) \\ &+ s_w^4\gamma_{\gamma w\gamma}(q^2) + 2s_w^2c_w^2\gamma_{\gamma wz}(q^2)\Big\} \end{aligned} \tag{3.65}$$

and the complete two loop amplitude is:

$$\begin{aligned} A_{21}^{(2)} &= [-s\ln^2(-s) - u\ln^2(-u)]\,(c_w + s_w)^2 \\ &\times \Big\{g^2(-q_\perp^2 + M_W^2)\Big[c_w^2\,\beta_{wz}(q^2) + s_w^2\,\beta_{w\gamma}(q^2)\Big]^2 \\ &+ M_W^2\beta_{wz}(q^2) + 2\gamma_{www}(q^2) + 2c_w^4\gamma_{zwz}(q^2) \\ &+ 2s_w^4\gamma_{\gamma w\gamma}(q^2) + 4s_w^2c_w^2\gamma_{\gamma wz}(q^2)\Big\}\,. \end{aligned} \tag{3.66}$$

The virtual part has not been cancelled. A_{2-2} is equal to A_{22} and A_{2-1} to A_{21}. The one loop graphs corresponding to the amplitude A_{20} are the following:

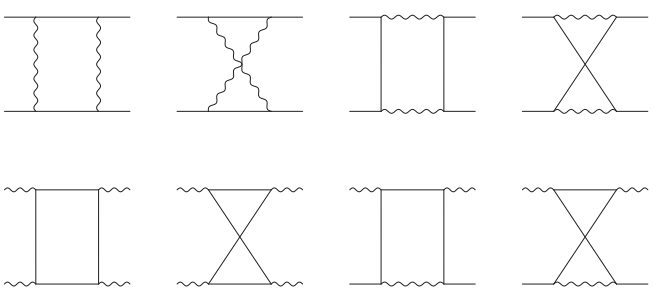

where arrows on the solid lines (charge flow of the W boson) can be any combination giving total charge or isospin zero in the t-channel. Adding all contributions, the result is:

$$\begin{aligned} A_{20}^{(1)} &= [-s\ln(-s) - u\ln(-u)]\,\frac{2}{3}g^2\Big\{c_w^4 2\beta_{ww}(q^2) + s_w^4 2\beta_{\gamma\gamma} + 4c_w^2 s_w^2\beta_{z\gamma} \\ &+ \beta_{ww}(q^2) + (s_w+c_w)^4 4\beta_{ww}(q^2) - (s_w+c_w)^2 4\beta_{ww}(q^2)\Big\}. \end{aligned} \tag{3.67}$$

The graphs for the two loop contribution of the s-channel discontinuity are:

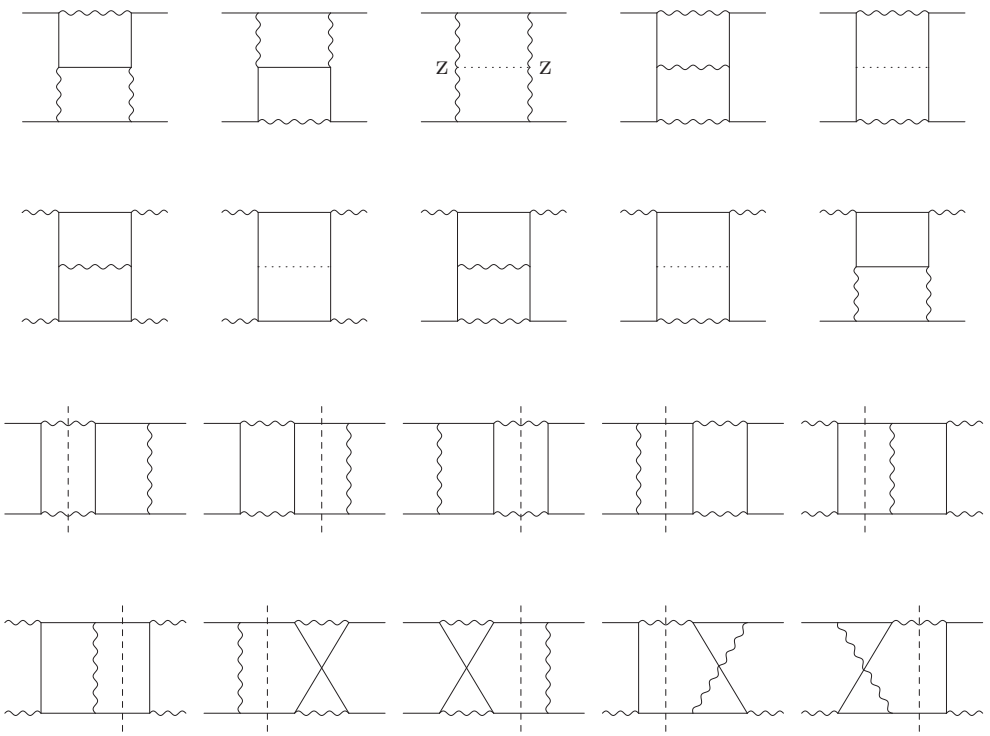

Again, the charge flow can be any combination giving total charge or isospin zero in the t-channel. Together with the corresponding u-channel contributions we have:

$$\begin{aligned} A_{20}^{(2)} &= [-s\ln^2(-s) - u\ln^2(-u)]\,\frac{1}{6}\Big\{g^2[4-8(s_w+c_w)^2]\Big[(2q_\perp^2 - 4M_Z^2)c_w^4\beta_{ww}\beta_{zz} \\ &+ M_W^2\beta_{ww}\beta_{zz} + 2q_\perp^2 s_w^4\beta_{ww}\beta_{\gamma\gamma} + (2q_\perp^2 - 2M_Z^2)2s_w^2c_w^2\beta_{ww}\beta_{\gamma z}\Big] + 2g^2M_W^2\beta_{zz}^2 \\ &+ g^2[1+4(s_w+c_w)^4 - 4(s_w+c_w)^2]\Big[(2q_\perp^2 - 2M_W^2)\beta_{ww}^2\Big] \\ &+ [32(s_w+c_w)^2 - 8]\Big[c_w^2\gamma_{wwz} + s_w^2\gamma_{ww\gamma}\Big]\Big\} \end{aligned} \tag{3.68}$$

at two loops. Which, as well as the other expressions with different third isospin quantum numbers, equals the SU(2) result [28]:

$$A_{I=2}^{(2)} = [-s\ln(-s) - u\ln(-u)]\Big[g^2(-q_\perp^2 + 2M^2)\beta^2(q^2) + 4\gamma(q^2)\Big] \tag{3.69}$$

in the limit $c_w \to 1$.

3.3.4 The t-channel exchange of vacuum quantum numbers

For the exchange of vacuum quantum numbers the same Feynman graphs contribute as in the projection to $\langle 20|20\rangle$ but all Clebsch-Gordan coefficients are positive. The calculation of the isospin-0 channel gives:

$$\begin{aligned} A_{00}^{(1)} &= [-s\ln(-s) - u\ln(-u)]\,\frac{2}{3}g^2\Big\{2(c_w^4 2\beta_{ww}(q^2) + s_w^4 2\beta_{\gamma\gamma} + 4c_w^2 s_w^2 \beta_{z\gamma}) \\ &+ 2\beta_{ww}(q^2) + (s_w + c_w)^4 2\beta_{ww}(q^2) + (s_w + c_w)^2 4\beta_{ww}(q^2)\Big\} \end{aligned} \tag{3.70}$$

at one loop and

$$\begin{aligned} A_{00}^{(2)} &= [-s\ln^2(-s) - u\ln^2(-u)]\,\frac{1}{3}\Big\{g^2[4 + 4(s_w + c_w)^2]\Big[(2q_\perp^2 - 4M_Z^2)c_w^4\beta_{ww}\beta_{zz} \\ &+ M_W^2\beta_{ww}\beta_{zz} + 2q_\perp^2 s_w^4\beta_{ww}\beta_{\gamma\gamma} + (2q_\perp^2 - 2M_Z^2)2s_w^2c_w^2\beta_{ww}\beta_{\gamma z}\Big] + 2g^2M_W^2\beta_{zz}^2 \\ &+ g^2[1 + (s_w + c_w)^4 + 2(s_w + c_w)^2]\Big[(2q_\perp^2 - 2M_W^2)\beta_{ww}^2\Big] \\ &- [16(s_w + c_w)^2 + 8]\Big[c_w^2\gamma_{wwz} + s_w^2\gamma_{ww\gamma}\Big]\Big\} \end{aligned} \tag{3.71}$$

at two loops. Giving the SU(2) result [28]:

$$A_{I=0}^{(2)} = [-s\ln(-s) - u\ln(-u)]\,4\Big[g^2(2q_\perp^2 - \frac{5}{2}M^2)\beta^2(q^2) - 2\gamma(q^2)\Big] \tag{3.72}$$

in the limit $c_w \to 1$.

There are basic differences between the isospin-1 channels and the other channels under consideration. For the vacuum and isospin-1 channels the tree level contribution is absent. Naturally, one gauge boson cannot exchange the vacuum or isospin-2 quantum numbers. The only channel with negative signature is the isospin-1 channel. In the vacuum and the isospin-2 channels the leading logs in energy are cancelled, and the contributions are subleading with respect to the isospin-1 channel. The general structure of the vacuum and isospin-2 channels is similar to that of the isospin-1 channel, depicted in Fig.3.2. However, the higher loop integrals do not cancel here, thus there is obviously no exponentiation in these channels. Nevertheless, one can calculate n-particle production amplitudes and include the virtual corrections with the same ansatz as in the isospin-1 channel using reggeized propagators. This will lead to similar integral equations as presented in the isospin-1 channel. These integral equations resum the contributions to all orders. The appropriate kernels are provided by the presented two loop calculations.

With the solution of these integral equations the resummed electroweak corrections can be computed to any process. This is possible due to the high-energy factorisation, which states that the interaction is process independent. Thus if

we write the solution of the integral equations as a 4-point Green's function, we only have to compute the couplings of the scattering particles to these Green's functions. The same procedure was used in the calculation of the QCD corrections presented in the previous chapter. Thereafter any amplitude can be written as the linear combination of t-channel isospin amplitudes:

$$A = c_{00}A_{00} + c_{11}A_{11} + ... \tag{3.73}$$

As it is proved by the Pomeranchuk theorem, the main contribution in the high-energy asymptotics will come from the vacuum channel.

3.4 Summary of chapter 3

In this chapter we have calculated electroweak amplitudes up to the order of g^6 in the leading log approximation. The result was decomposed into t-channel isospin states. The isospin-1 states have negative signature and due to the cancellation among real and virtual corrections the result exponentiates. We derived an integral equation for the neutral isospin-1 channel to iterate the result up to any orders of perturbation theory. We have demonstrated a bootstrap scheme, in which the infinite sum of ladder amplitudes gives the propagator of the neutral reggeized particle itself. The vacuum and isospin-2 channels have positive signature, thus the leading logarithms cancel. There is no obvious exponentiation in these channels. We found three trajectories emerging in the electroweak sector. Two are due to reggeized W bosons and the third one corresponds to the neutral channel vanishing at the W mass. Here the appropriate mixing between the Z boson and photon is leading to a reggeized particle. Results presented in this chapter will be published in [51].

Summary and outlook

We investigated higher-order corrections to vector boson scattering. These have been resummed QCD and electroweak corrections. In particular the process $\gamma\gamma \to ZZ$ was considered in detail. We reanalysed the full one loop contribution and compared it with the result on the high-energy approximation. We showed that the high-energy approximation is quite accurate. We computed two loop corrections in the high-energy approximation as well. Leading logarithmic two loop corrections are at the order of 10% at 1 TeV.

QCD corrections emerge since, like the photon, all vector bosons fluctuate into quark-antiquark pairs, which are strongly interacting colour dipoles. First, we computed the nonforward boson impact factors. These describe the probability that the boson fluctuates into a quark-antiquark dipole.

Concerning QCD corrections, we presented expressions for the Born and the leading logarithmic resummed (BFKL) contributions for an arbitrary process of elastic scattering of vector bosons. For numerical studies we switched to the definite process of $\gamma\gamma \to ZZ$ and we computed the QCD part of the amplitude in the high-energy approximation. The electroweak part was computed in a full one loop calculation, and a complete analysis involving all helicity channels was done. The results are displayed for the differential and integrated cross sections, comparing QCD corrections relative to the one loop electroweak result. We discussed some properties of the pure QCD part of the cross section as well.

In the helicity conserving channel the corrections are at the order of a few percent for $s = O(1 \text{ TeV})$ and they show a moderate rise with the scattering energy. In the helicity flip channels the QCD corrections are at the same level for $s = O(1 \text{ TeV})$. However, since in these channels the electroweak amplitudes are suppressed by one power of s compared to the QCD ones, the relative corrections rise much stronger with the scattering energy. Already for $s = O(3$ TeV) the QCD part of the amplitude may lead to 100% corrections for helicity non-conserving parts of the cross section. The results of our study indicate that in the analysis of the measurements QCD corrections cannot be neglected. The same reasoning is valid for the integrated cross sections, since the biggest contribution to the cross section comes from scattering at small angles.

As a sideline of our calculations, we presented our result on the impact factors in the colour dipole picture. For the elastic scattering of two colour dipoles we

found that the dipole cross section depends on the transverse distance between the ends of the two dipoles, and not between the centres of the two quark-antiquark pairs. This result also holds for diffractive vector production. For open $q\bar{q}$-production, we confirmed the well-known result of the forward direction: the integrated (over the transverse size of the produced quark-antiquark pair) cross section is described by the square of the elastic dipole cross section.

We believe that our findings may provide some guidance in modelling the b-dependence of the dipole cross section. As indicated in the introduction, the b-dependence represents the mayor challenge in understanding the transition from the region of perturbative to non-perturbative QCD, and our formula may provide a starting point along these lines.

Concerning the QCD corrections we stress that the leading log BFKL contribution contains a noticeable scale dependence. For a more precise analysis one has to use the next-to-leading BFKL Green's function and next-to-leading impact factors. One also has to look at the full SM two loop contribution, in order to achieve a better precision at this order of the calculation.

On the experimental side the separation of longitudinal and transverse final state Z bosons clearly presents a demanding challenge. Only a statistical analysis of the angular distribution of the decay products of the Z bosons allows to discriminate between the different polarisations. However, as discussed at the beginning of this thesis, a careful measurement of the process $\gamma\gamma \to ZZ$ with all its different helicity configurations is important and should be pursued.

The above described experimental challenge will be absent at the production of Higgs particles via photon fusion, e.g. $\gamma\gamma \to HH$ or $\gamma\gamma \to ZH$. For this processes resummed QCD corrections can be investigated as well. These will have features similar to the ones for the production of longitudinal Z bosons, which are presented in this thesis. The cross section is helicity breaking, thus the relative QCD corrections will gain a strong rise with the scattering energy. If QCD corrections became relevant, they should be measurable, since there are no problematic backgrounds. We expect the biggest corrections to $\gamma\gamma \to ZH$, since this process is similar to the production of one longitudinal and one transverse Z boson.

The fact that two loop corrections at small scattering angles to $\gamma\gamma \to ZZ$ are at the order of 10% at 1 TeV, indicates that electroweak corrections of higher-order have to be taken into account. The first approach is a resummation of leading logarithms in the Regge kinematical region. We started a resummation program of the electroweak sector in this thesis. Such a resummation program has already been developed for $SU(N)$ theories [13, 28]. However, in the electroweak sector the group structure is different. The electroweak sector is based on the direct product of $SU(2) \times U(1)$, which are the abelian hypercharge group $U(1)$ and the non-abelian electroweak isospin group $SU(2)$.

The first step in our approach was the computation of electroweak amplitudes up to the order of g^6. We decomposed the result into t-channel isospin states.

We found that the isospin-1 states have a negative signature and due to the cancellation among real and virtual corrections the result exponentiates. The vacuum and isospin-2 channels have a positive signature, thus the leading logarithms cancel. There is no obvious exponentiation in these channels.

The projection to the isospin-1 channels is equivalent to the projection of the quantum numbers of the vector bosons contained in the theory. The procedure of reggeization in the electroweak sector is a key point for further investigations. Higher-order resummed contributions are described with diagrams of ladder like topology built with reggeized particles of the electroweak sector. In an abelian gauge theory the vector particle remains elementary [30]. On the other hand, the reggeization of the Yang-Mills vector meson takes place in $SU(2)$ theory [28]. We found three trajectories emerging in the electroweak sector. Two are due to reggeized W bosons and the third one corresponds to the neutral channel vanishing at the W mass. This trajectory cannot be associated with a physical particle of the theory in agreement with [32]. Here the appropriate mixing between the Z boson and photon was a crucial point for the results.

The results on the different isospin channels can be iterated up to any order in perturbation theory with the help of Bethe-Salpeter equations. We derived an integral equation for the neutral isospin-1 channel. We demonstrated a bootstrap scheme, in which the infinite sum of ladder amplitudes gives the propagator of the neutral reggeized particle itself. The fulfilment of this bootstrap scheme proved the reggeization in the neutral channel to any orders of perturbation theory. It shows the self-consistency of our perturbative calculation and confirms the conjecture of the resummation to all orders.

The next obvious step will be to define the integral equation and to prove the bootstrap scheme for the charged isospin-1 channel as well. After this, the integral equations can be formulated in a safe way for all the other isospin channels. Our two loop calculation for the different isospin channels provide the appropriate kernels. Having all these integral equations, the leading logarithmic resummation of the electroweak sector in the Regge kinematical region is formally described. Due to the high-energy factorisation, every electroweak amplitude can be written as a linear combination of the different t-channel isospin states.

In order to present numerical results on scattering processes one has to find the solution of these integral equations. Solving these integral equations will not be straight forward as it was the case in the isospin-1 channels. This is due to the fact that the virtual part of the equation will not be cancelled by part of the kernel. In particular, the solution of the vacuum channel equation in QCD relies on the conformal invariance of the equation [44]. This conformal invariance will be broken in a theory with massive gauge bosons. For the computation of cross sections, however, the integral equations can be solved numerically. Numerical investigations of this kind have been done recently for the NLL BFKL equation [52]. One may also iterate the equations to get contributions to a desired order in perturbation theory. This will be sufficient

for energies of the next generation of colliders. At last, an analytic solution for the limit of the forward case should be possible.

Last but not least, calculations investigating the Regge properties of the Higgs boson are of interest. The reggeization of the Higgs particle is possible due to the existence of the massive electroweak vector bosons. Higher-order corrections from vector boson contributions may lead to a reggeized scalar particle. Though the Higgs mechanism predicts the existence of a scalar particle, it predicts only a few of its properties. Investigating the reggeization of the Higgs may provide us with information not inmediately visible in the Lagrangian. Reggeization would give first hints to a possible composite nature of the Higgs particle.

Bibliography

[1] M. Baillargeon, G. Belanger and F. Boudjema, `hep-ph/9405359`

[2] G. Bélanger and F. Boudjema, Phys. Lett. **B 288** (1992) 210; K. A. Peterson and S. Godfrey, hep-ph/9302297; O. J. P. Éobli, M. C. Gonzaléz-García and S. F. Novaes, Nucl. Phys. **B 411** (1994) 381, hep-ph/9306306; O. J. P. Éobli, M. B. Magro, P. G. Mercandante and S. F. Novaes, Phys.Rev. **D 52** (1995) 15, hep-ph/9503432; S. Godfrey, hep-ph/9505252; G. J. Gounaris, F. M. Renard, Z. Phys. **C 69** (1996) 513, hep-ph/9505429; G. J. Gounaris, J. Layssac, F. M. Renard, Z. Phys. **C 69** (1996) 505, hep-ph/9505430; M. Baillargeon, G. Bélanger and F. Boudjema, Nucl.Phys. **B 500** (1997) 224, hep-ph/9701372; E. Boos. et. al., hep-ph/0103090

[3] I.F. Ginzburg, preprint 28(182) INP Novosobirsk (1990); G.J. Gounaris, J. Layssac, F.M. Renard, *Z. Phys.* **C 65** (1995) 505; G.J. Gounaris, F.M. Renard, *Z. Phys.* **C 65** (1995) 513; A. T. Banin, I. F. Ginzburg and I. P. Ivanov, *Phys. Rev.* **D 59** (1999) 115001

[4] F. Boudjema, in Physics and Experiments with Linear e^+e^- Colliders, Waikoloa, Hawaii, 1993, Ed. F.A. Harris *et al.*, Word Sci., vol.II, p. 712

[5] G.J. Gounaris, J. Layssac, P.I. Porfyriadis and F.M. Renard, *Eur. Phys. J.* **C 13** (2000) 79

[6] B. Bajc, *Phys. Rev.* **D 48** (1993) 1907

[7] J.L. Hewett and F.J. Petriello, *Phys. Rev.* **D 64** (2001) 095017

[8] T. G. Rizzo, Phys. Rev. **D 60** (1999) 115010; K. Cheung, Phys. Rev. **D61** (2000) 015005; H. Davoudiasl, Phys. Rev. **D 60** (1999) 084022; Phys. Rev. **D 61** (2000) 044018

[9] B.W. Lee, C. Quigg and H.B. Thacker, *Phys. Rev.* **D 16** (1977) 1519

[10] E. E. Boos and G. V. Jikia, *Phys. Lett.* **B 275** (1992) 164

[11] A. Dobado and M.J. Herrero, *Phys. Lett.* **B 228** (1989) 495; **233** (1989) 505; J.F. Donoghue and C. Ramirez, *Phys. Lett.* **B 234** (1990) 361

[12] A. Denner, S. Dittmaier and T. Hahn, *Phys. Rev.* **D 56** (1997) 117; A. Denner and T. Hahn, *Nucl. Phys.* **B 525** (1998) 27; A. Denner, S. Dittmaier and R. Schuster, *Nucl. Phys.* **B 452** (1995) 80

[13] E.A. Kuraev, L.N. Lipatov, V.S.Fadin, *Sov. Phys. JETP* **44** (1976) 443, ibid. **45** (1977) 199, Ya.Ya. Balitskii, L.N. Lipatov, *Sov. J. Nucl. Phys.* **28** (1978) 822

[14] N. N. Nikolaev and B. G. Zakharov, *Z. Phys.* **C 49** (1991) 607; *Z. Phys* **C 53** (1992) 331

[15] A. H. Mueller, *Nucl. Phys.* **B 415** (1994) 373; *Nucl. Phys.* **B 437** (1995) 107

[16] K. Golec-Biernat and M. Wüsthoff, *Phys. Rev.* **D 59** (1999) 014017; *Phys. Rev.* **D 60** (1999) 114023; *Eur. Phys. J.* **C 20** (2001) 313

[17] J. R. Forshaw, G. Kerley and G. Shaw, *Phys. Rev* **D 60** (1999) 074012, *Nucl. Phys.* **A 675** (2000) 80

[18] E. Gotsman, E. M. Levin, U. Maor and E. Naftali, *Eur. Phys. J.* **C 10** (1999) 689

[19] M. McDermott, L. Frankfurt, V. Guzey and M. Strikman, *Eur. Phys. J.* **C 16** (2000) 641

[20] J. Bartels, K. Golec-Biernat and H. Kowalski, *Phys. Rev.* **D 66** (2002) 014001

[21] H. Cheng and T. T. Wu, *Phys. Rev.* **182** (1969) 1852, 1868, 1873, 1899

[22] L. N. Lipatov and G. V. Frolov, *Yad. Fiz.* **13** (1971) 588

[23] D. Yu. Ivanov and M. Wusthoff, *Eur.Phys.J.* **C 8** (1999) 107

[24] N. G. Evanson and J. R. Forshaw, *Phys. Rev.* **D 60** (1999) 0340161

[25] D. Yu. Ivanov and R. Kirschner, *Phys.Rev.* **D 58** (1998) 114026; D. Yu. Ivanov, R. Kirschner, A. Schafer and L. Szymanowski, *Phys.Lett.* **B 478** (2000) 101

[26] M. G. Ryskin, *Z. Phys.* **C 57** (1993) 89

[27] S. Gieseke and C. F. Qiao, *Phys.Rev.* **D 61** (2000) 074028

[28] L.N. Lipatov, *Sov. J. Nucl. Phys.* **23** (1976) 338

[29] M. Gell-Mann and M. L. Goldberger, *Phys. Rev. Lett.* **9** (1962) 275, *Phys. Lett.* **4** (1963) 265

[30] S. Mandelstam, *Phys. Rev.* **137 B** (1965) 949

[31] M. T. Grisaru and H.J. Schnitzer, *Phys. Rev.* **D20** (1979) 784

[32] L. Lukaszuk and L. Szymanowsky, *Nucl. Phys.* **B159** (1979) 316

[33] G. Jikia, *Nucl. Phys.* **B 405** (1993) 24

[34] I.F. Ginzburg, G.L. Kotkin, S.L. Panfil and V.G. Serbo, *Nucl. Phys.* **B 228** (1983) 285

[35] J. Küblbeck, M. Böhm, and A. Denner, *Comp. Phys. Commun.* **60** (1990) 165; T. Hahn, `hep-ph/0012260`

[36] T. Hahn and M. Pérez-Victoria, *Comp. Phys. Commun.* **118** (1999) 153

[37] G.J. van Oldenborgh and J.A.M. Vermaseren, *Z. Phys.* **C 46** (1990) 425; G.J. van Oldenborgh, *Comp. Phys. Commun.* **66** (1991) 1

[38] E.W.N. Glover and J.J. van der Bij, *Nucl. Phys.* **B321** (1989) 561

[39] S.J. Brodsky, F. Hauptmann and D.E. Soper, *Phys. Rev.* **D 56** (1997) 6957

[40] J. B. Kogut and D. E. Soper, *Phys.Rev.* **D 1** (1970) 2901

[41] D. E. Soper, *Phys.Rev.* **D 15** (1977) 1141

[42] J. R. Forshaw and D. A. Ross, *Quantum Chromodynamics and the Pomeron*, Cambridge University Press, Cambridge, England, 1996

[43] J. Bartels, K. Golec-Biernat and K. Peters, *Acta Phys. Pol.* **B 34** (2003) 3051

[44] L.N. Lipatov, *Sov. Phys. JETP* **63** (1986) 94

[45] J. Bartels, M. A. Braun, D. Colferai and G. P. Vacca, *Eur.Phys.J.C* **20** (2001) 323

[46] L.N. Lipatov, *Pomeron in quantum chromodynamics*, in "Perturbative QCD", pp. 411-489, ed. A. H. Mueller, World Scientific, Singapore, 1989; Phys. Rep. **286** (1997) 131

[47] K. Peters and G.P. Vacca, *Eur. Phys. J.* **C 30** (2003) 435

[48] G. Chachamis and K. Peters, *Phys. Lett.* **B 580** (2004) 169

[49] T. Behnke, S. Bertolucci, R. D. Heuer and R. Settles, "TESLA Technical design report. Pt. 4: A detector for TESLA," DESY-01-011

[50] A.D. Martin and T.D. Spearman, *Elementary Particle Theory*, North Holland, 1970

[51] J. Bartels, L.N. Lipatov and K. Peters,
"Reggeization and the Pomeranchuk Singularity in the Electroweak Sector"
in preparation

[52] J. R. Andersen and A. Sabio Vera, *Phys. Lett.* **B 567** (2003) 116

Acknowledgements

First of all, I would like to thank my supervisor Prof. Jochen Bartels for countless discussions, his continuous support and patience. I have always benefited from his clear view of investigating physics problems and presentations.

I am very grateful for Gian Paolo Vacca for a fruitful and pleasant collaboration and especially for his important support which he still gave me after he had leaving our institute. I would like thank G. Chachamis, K. Golec-Biernat and L.N. Lipatov for fruitful and pleasant collaborations as well.

My understanding of physics during the last three years was greatly enhanced by useful and enjoyable conversations with A. Brandenburg, D. Colferai, M. Diehl, S. Dittmaier, V. Fadin, S. Gieseke, K. Kutak, A. Kyrieleis, M. Lublinsky, T. Prüstel, A. Sabio-Vera, F. Schwennsen, M. Steinhauser.

I am thankful to the members of the II. Institute of Theoretical Physics and the DESY Theory Group for a pleasant atmosphere.

This work was supported by the Graduiertenkolleg 'Zukünftige Entwicklungen in der Teilchenphysik'.

Finally, I would like to thank my parents for constant support and encouragement during all the years.